

GAS CONDENSATE DAMAGE IN HYDRAULICALLY FRACTURED WELLS

A Thesis

by

REZA ROSTAMI RAVARI

Submitted to the Office of Graduate Studies of
Texas A&M University
in partial fulfillment of the requirements for the degree of

MASTER OF SCIENCE

August 2004

Major Subject: Petroleum Engineering

GAS CONDENSATE DAMAGE IN HYDRAULICALLY FRACTURED WELLS

A Thesis

by

REZA ROSTAMI RAVARI

Submitted to Texas A&M University
in partial fulfillment of the requirements
for the degree of

MASTER OF SCIENCE

Approved as to style and content by:

Robert A. Wattenbarger
(Co-Chair of Committee)

David S. Schechter
(Co-Chair of Committee)

John R. Moroney
(Member)

Stephen A. Holditch
(Head of Department)

August 2004

Major Subject: Petroleum Engineering

ABSTRACT

Gas Condensate Damage in Hydraulically Fractured Wells. (August 2004)

Reza Rostami Ravari, B.S., Sharif University of Technology

Co-Chairs of Advisory Committee: Dr. Robert A. Wattenbarger

Dr. David S. Schechter

This project is a research into the effect of gas condensate damage in hydraulically fractured wells. It is the result of a problem encountered in producing a low permeability formation from a well in South Texas owned by the El Paso Production Company. The well was producing from a gas condensate reservoir. Questions were raised about whether flowing bottomhole pressure below dewpoint would be appropriate. Condensate damage in the hydraulic fracture was expected to be of significant effect.

In the most recent work done by Adedeji Ayoola Adeyeye, this subject was studied when the effects of reservoir depletion were minimized by introduction of an injector well with fluid composition the same as the original reservoir fluid. He also used an infinite conductivity hydraulic fracture along with a linear model as an adequate analogy. He concluded that the skin due to liquid build-up is not enough to prevent lower flowing bottomhole pressures from producing more gas.

This current study investigated the condensate damage at the face of the hydraulic fracture in transient and boundary dominated periods when the effects of reservoir depletion are taken into account. As a first step, simulation of liquid flow into the fracture was performed using a 2D 1-phase simulator in order to help us to better understand the results of gas condensate simulation. Then during the research, gas condensate models with various gas compositions were simulated using a commercial simulator (CMG). The results of this research are a step forward in helping to improve the management of gas condensate reservoirs by understanding the mechanics of liquid build-up. It also provides methodology for quantifying the condensate damage that impairs linear flow of gas into the hydraulic fracture.

DEDICATION

This work is dedicated to my parents. Only through their love, invaluable advice, motivation and support have I been able to progress in my professional and personal life. This work is also dedicated to my brothers for their help, encouragement and the great moments we spent together.

ACKNOWLEDGEMENTS

I would like to express my gratitude and appreciation to those who significantly contributed to this work. Only through their support and invaluable advice have I been able to complete the task.

I'm deeply thankful to Dr. Robert Wattenbarger, co-chair of my advisory committee, for his support, guidance and continued help throughout my research. It was great to work with him.

I wish to express my sincere gratitude and appreciation to Dr. David S. Schechter, co-chair of my advisory committee, for his active participation and guidance during my investigation.

I would like to thank Dr. John R. Moroney for serving as a member of the advisory committee.

Finally, I would like to thank NIOC for providing the financial support during my graduate studies at Texas A&M University.

TABLE OF CONTENTS

	Page
ABSTRACT	iii
DEDICATION	iv
ACKNOWLEDGEMENTS	v
TABLE OF CONTENTS	vi
LIST OF FIGURES.....	viii
LIST OF TABLES	xi
 CHAPTER	
I INTRODUCTION	1
1.1 Problem description	1
1.2 Gas condensate reservoirs	2
1.3 Use of hydraulic fractures	7
II SINGLE-PHASE DAMAGE ANALYSIS.....	10
2.1 Model description.....	11
2.2 Fracture face skin	13
2.3 Constant rate fracture face skin.....	14
2.4 Constant well pressure fracture face skin.....	17
2.5 Damaged zone permeability effect.....	29
2.6 Rate and cumulative production analysis.....	30
III GAS CONDENSATE DAMAGE ANALYSIS	33
3.1 Reservoir description.....	33
3.2 Case study 1: condensate damage analysis for a lean gas condensate reservoir (SPE3).....	36
3.3 Case study 2: condensate damage analysis for a rich gas condensate reservoir.....	44

CHAPTER	Page
IV SIMULATION OF CONDENSATE DAMAGE IN A 2D-MODEL	52
4.1 Reservoir description.....	52
4.2 Simulation results	54
V DISCUSSION AND CONCLUSIONS.....	61
5.1 Discussion	61
5.2 Conclusions	62
5.3 Recommendations for future work.....	63
NOMENCLATURE.....	64
REFERENCES	66
APPENDIX A LINEAR FLOW MODELING.....	71
APPENDIX B GASSIM DATA FILES.....	78
APPENDIX C ANALYTICAL SOLUTIONS TO CLOSED, LINEAR RESERVOIRS	81
APPENDIX D ARTIFACT WELLBORE STORAGE	102
APPENDIX E CMG DATA FILES	108
VITA	127

LIST OF FIGURES

FIGURE	Page
2.1 Quarter model for 80 acre drainage area (from Ref. 1).....	13
2.2 Permeability reduction normal to fracture face (from Ref. 1).....	14
2.3 Constant rate s_{ff} in transient period.....	15
2.4 Constant rate s_{ff} in p_{ss} period	16
2.5 Type-curve plot for a single-phase undamaged linear reservoir with p_{wf} at 3,600 psi	18
2.6 Infinite-acting flow curve for a single-phase undamaged linear reservoir with p_{wf} at 3,600 psi.....	19
2.7 Boundary-dominated flow curve for a single-phase undamaged linear reservoir with p_{wf} at 3,600 psi.....	20
2.8 Pressure profiles for a single-phase undamaged linear reservoir with p_{wf} at 3,600 psi	21
2.9 Comparison of simulated pressures with calculated pressures for a single-phase undamaged linear reservoir with p_{wf} at 3,600 psi.....	22
2.10 Pressure profile for a single-phase damaged linear reservoir with p_{wf} at 3,600 psi	23
2.11 Comparison of simulated pressures with calculated pressures for a single-phase damaged linear reservoir with p_{wf} at 3,600 psi.....	24
2.12 Type-curve for a single-phase damaged linear reservoir with p_{wf} at 3,600 psi	25
2.13 Transient flow curve for a single-phase damaged linear reservoir with p_{wf} at 3,600 psi.....	26
2.14 Boundary-dominated flow curve for single-phase damaged linear reservoir with p_{wf} at 3,600 psi.....	26
2.15 Type-curve for a single-phase damaged linear reservoir with $k_s=5E-05$ md produced at 3,600 psi	27
2.16 Transient flow curve for a single-phase linear reservoir with $k_s=5E-05$ md produced at 3,600 psi	28
2.17 Boundary-dominated flow curve for single-phase linear reservoir with $k_s=5E-05$ md produced at 3,600 psi	28

FIGURE	Page
2.18 Comparison between production behavior of undamaged case with that of damaged linear reservoir with $k_s=0.001$ md produced at 3,600 psi	31
3.1 Schematic of the 1D linear model in CMG	35
3.2 Gas-liquid relative permeability curves	36
3.3 Constant-volume depletion test after SPE3 ⁵	38
3.4 Gas rate plots for case study 1 (SPE3) at different p_{wf}	39
3.5 Cumulative gas production plots for case study 1 (SPE3) at different flowing bottomhole pressures	40
3.6 Gas relative permeability profiles for case study 1 (SPE3) with p_{wf} at 1,000 psi	41
3.7 Oil saturation profiles for case study 1 (SPE3) with p_{wf} at 1,000 psi	41
3.8 Gas saturation profiles for case study 1 (SPE3) with p_{wf} at 1,000 psi	42
3.9 Gas-liquid relative permeability curves for undamaged SPE3 case	43
3.10 Comparison between the damaged case gas rate and undamaged case one for case study 1 with p_{wf} at 1,000 psi	43
3.11 Comparison between the damaged case cumulative production and undamaged case one for case study 1 with p_{wf} at 1,000 psi	44
3.12 <i>PVT</i> match between experimental relative volumes and calculated ones for case study 2	46
3.13 <i>PVT</i> match between experimental volume percent liquid and calculated one for case study 2	46
3.14 <i>PVT</i> match between experimental Gas Z-factor and calculated one for case study 2	47
3.15 Gas rate plots for case study 2 at different p_{wf}	48
3.16 Cumulative gas production plots for case study 2 at different p_{wf}	48
3.17 Gas relative permeability profiles for case study 2 with p_{wf} at 1,000 psi	49
3.18 Oil saturation profiles for case study 2 with p_{wf} at 1,000 psi	50

FIGURE	Page
3.19 Gas saturation profiles for case study 2 with p_{wf} at 1,000 psi	50
4.1 Schematic of a 2D-areal model with hydraulic fracture.....	53
4.2 Schematic of a 2D-areal model with data modification.....	54
4.3 Gas production rates for a 2D-model with $x_e/x_f=2$ at different p_{wf}	56
4.4 Cumulative gas productions for a 2D-model with $x_e/x_f=2$ at different p_{wf}	56
4.5 Gas production rates for a 2D-model with $x_e/x_f=10$ at different p_{wf}	57
4.6 Cumulative gas productions for a 2D-model with $x_e/x_f=10$ at different p_{wf}	57
4.7 Gas production rates for a 2D-model with $x_e/x_f=100$ at different p_{wf}	58
4.8 Cumulative gas productions for a 2D-model with $x_e/x_f=100$ at different p_{wf}	58
4.9 Comparison of gas production rates for a 2D-model with p_{wf} at 1,000 psi and with different fracture lengths.....	59
4.10 Comparison of cumulative gas productions for a 2D-model with p_{wf} at 1,000 psi and with different fracture lengths	59

LIST OF TABLES

TABLE		Page
2.1	Reservoir and liquid properties of the model used in GASSIM.....	11
2.2	Reservoir properties of the first gridblock used in GASSIM.....	12
2.3	Transient and <i>pss</i> fracture face skins for each damaged linear model.....	29
2.4	Analytical fracture face skins for each damaged linear model	30
3.1	Main characteristics of the reservoir model	34
3.2	Characteristics of the first gridblock (well cell).....	34
3.3	Case study 1 (SPE3) condensate fluid model.....	37
3.4	Case study 2 condensate fluid model	45
4.1	Main characteristics of the 2D reservoir model	53
4.2	Main fracture parameters used in each case for 2D model	55

CHAPTER I

INTRODUCTION

1.1 Problem description

The pressure and flow rate behavior of a gas condensate is distinctly different from the behavior of a two-phase reservoir. The producing rate is not only affected by the pressure gradient but is also a more complex function of the actual value of the flowing bottomhole pressure. The value of the bottomhole pressure controls the amount and distribution of liquid condensate accumulation near the well with an unavoidable relative permeability reduction which leads to a significant loss in well productivity ¹.

This work is a result of a problem encountered in producing Smith #1, a hydraulically fractured well owned by El Paso Production Company. The well was producing a tight gas condensate reservoir and the flow rate behavior did not behave as expected. In other words, the more flowing bottomhole pressure was lowered, the higher gas rate was observed.

Most previous work has tackled the problem from a radial model perspective. Since in many tight gas wells, long-term linear flow occurs during depletion and long-term production is more nearly a constant pressure condition ², this work will use a linear model representing the linear flow of fluid from the formation into the hydraulic fracture and it will be simulated at constant flowing bottomhole pressure. The constant pressure equations as well as constant rate equations were derived and presented in Appendix C.

This thesis follows the style of the *SPE Reservoir Evaluation & Engineering*.

The rest of this chapter presents a comprehensive review of the theory and latest investigations regarding the most important aspects of gas condensate reservoirs and hydraulic fracturing.

In Chapter II, the results of simulation are compared to analytical solutions for skin in a single-phase system. The Well Cell method was used in constructing the linear model to properly predict the linear flow at constant pressure conditions. The detailed discussion of the Well Cell method is presented in Appendix A. This chapter also helps to quantify fracture face skin in infinite-acting and boundary-dominated flow periods.

Chapter III covers the compositional simulation of a gas condensate reservoir for two different fluids. The first fluid which is a lean gas condensate³ was taken from CMG's data file collection and was adapted for use of this study, and the second one which is relatively rich was taken from Ref. 4. It also covers the construction of the 1D linear model used in simulation, including the definition of reservoir dimensions and grid-size. The 1D linear model is quite analogous to the hydraulic fracture case for an infinite conductivity fracture. For the purposes of this research, it is used to investigate the effect of condensate build-up near hydraulic fractures, as the reservoir pressure depletes and near wellbore pressure falls below the dewpoint pressure. The goal is to quantify the damage that results from the condensate build-up and note its effect on pressure drawdown, which eventually translates into gas production.

Chapter IV studies the flow impairment in a gas condensate reservoir with infinite conductivity fracture which partially penetrates the reservoir. The simulations are done by making 2D gas condensate models in CMG.

1.2 Gas condensate reservoirs

A gas condensate is, by definition, a naturally occurring hydrocarbon mixture found at reservoir temperature greater than the critical temperature of the petroleum mixture and

less than the cricondentherm. The most common feature of a gas condensate is retrograde condensation resulting from isothermal pressure decline. As reservoir pressure decreases, the retrograde gas exhibits a dew point. As pressure is reduced, liquid condenses from the gas to form a free liquid in the reservoir⁵. The amount of liquid increases as the pressure in the reservoir decreases until a certain value at which further reduction of the pressure causes the liquid to re-vaporize. This region is called the retrograde condensation zone and reservoirs experiencing this phenomenon are known as gas condensate reservoirs¹.

1.2.1 Gas condensate reservoir fluid modeling

In compositional simulation of oil and gas reservoirs equation-of-state (*EOS*) methods are seeing increasing usage over more traditional *K*-value methods for phase equilibrium calculations. An equation-of-state is an equation which expresses the relationship between pressure, temperature and volume of a gas or liquid. These equations are usually of cubic form. Two *EOS* widely used in the petroleum industry today are the Peng-Robinson⁶ (*PR*) and Soave-Redlich-Kwong⁷ (*SRK*) *EOS*.

It has been found by several authors that equations-of-state are, in general not able to accurately predict reservoir fluid behavior using theoretical *EOS* parameters. It has been found that tuning the *EOS* (by modifying the *EOS* parameters) is required to adequately match laboratory derived *PVT* data.

A number of studies⁸⁻¹⁶ report comparisons of cubic *EOS* and laboratory *PVT* results for a wide variety of reservoir fluids and conditions. Most of these studies emphasize the C_{7+} characterization as the key element in attaining agreement between *EOS* and laboratory results. Coats *et al.*¹⁷ mentioned that the *EOS* is generally not predictive and extensive splitting of the C_{7+} fraction to match laboratory data is generally unnecessary.

Fevang *et al.*¹⁸ studied a variety of fluids ranging from medium rich gas condensate to near critical fluids using black-oil and compositional models. They simulated production for both injection and natural depletion production schemes and compared the results obtained with both models. They concluded that gas condensate produced by gas cycling above the dewpoint could be simulated accurately with a black-oil simulator. However, they also found for the case of rich gas condensate where permeability increases with depth, that black-oil simulators significantly over-predict oil recovery owing to compositional effects that are not properly treated in a black-oil model. They concluded that the black-oil model consistently over-predicts oil production because oil vaporization is over-estimated.

Fevang *et al.*¹⁸ recommended the use of compositional simulation models for gas injection studies and limited the use of black-oil model only for reservoir fluids with minimal vaporization, and lean gas condensate reservoirs undergoing cycling injection above the dewpoint pressure.

1.2.2 Relative permeability

It has been recognized in the literature that relative permeability does impact the degree of productivity loss below the dew point. Hinchman and Barree¹⁹ showed how the choice between imbibition and drainage relative permeability curves could dramatically alter the productivity forecast below the saturation pressure for gas condensate reservoirs.

Productivity above the dew point pressure is controlled by the reservoir permeability and thickness, and by the viscosity of the gas. Below the dew point, the degree of productivity reduction will be controlled by the critical condensate saturation and the shape of the gas and condensate relative permeability curves²⁰.

Whitson *et al.*²¹ showed that relative permeability effects in gas condensate reservoirs can be classified into three categories: (1) near-well steady-state gas/oil flow where saturation hysteresis is severe throughout the life of a well; (2) in the bulk of the reservoir far-removed from the wells, an imbibition process occurs throughout the life of the reservoir, where liquid mobility is (practically) zero and gas flows at a somewhat reduced permeability; and (3) water encroachment, where gas and/or retrograde condensate are trapped in quantities from 15-40 saturation percent, and water permeability can be significantly reduced. In terms of reservoir well performance, the near-well relative permeability behavior is the dominant factor. The far-removed region of condensate accumulation has somewhat reduced gas relative permeability, but this effect is generally a second-order or negligible effect. Trapped saturations and reduced water relative permeability can be important for reservoir performance, but has no direct effect on well performance prior to water breakthrough.

Gringarten *et al.*²² found that when reservoir pressure around a well drops below the dew point pressure, retrograde condensation occurs and three regions are created with different liquid saturations. Away from the well, an outer region has the initial liquid saturation; next, there is an intermediate region with a rapid increase in gas relative permeability. Liquid in that region is immobile. Closer to the well, an inner region forms where the liquid saturation reaches a critical value, and the effluent travels as a two-phase flow with constant composition (the condensate deposited as pressure decreased is equal to that flown towards the well). There may also exist a fourth region in the immediate vicinity of the well where low interfacial tensions at high rates yield a decrease of the liquid saturation and an increase of the gas relative permeability.

1.2.3 Condensate blocking

Wells in gas condensate reservoirs often experience rapid decline when the near wellbore pressure goes below the dewpoint pressure. Radial compositional simulation

models were often used to investigate the problem of productivity loss^{19, 23-27}. These models clearly show that the loss in productivity was due to liquid dropout near the wellbore. This so-called condensate blocking (increase in condensate saturation around the wellbore) reduces the effective permeability to gas and results in a rapid decline in well productivity once the near wellbore pressure drops below the dewpoint. Due to the large volume of gas passing through a relatively small, low pressure region around the well, the condensate saturation can buildup rapidly and exceed the critical saturation required for two-phase flow. As the average reservoir pressure continues to decline, the entire reservoir will fall below the dew point pressure. This will result in liquid hydrocarbon saturation throughout the reservoir. Depending on the amount of liquid condensation and the critical liquid saturation, there may or may not be two-phase flow in the entire reservoir.

The effect of condensate blocking is more evident in low permeability reservoirs. Barnum *et al.*²⁰ showed that the recovery factor of gas condensate radial wells is only affected by condensate blocking if the well's kh is less than 1,000 md-ft. For higher quality reservoirs, productivity loss is not very severe.

El-Banbi *et al.*²⁸ showed that the well productivity of vertical wells in a moderately rich gas condensate reservoir initially decreased rapidly and then increased as the reservoir was depleted. This phenomenon was explained by compositional simulation. Initially, when the wells go below the dewpoint, the productivity decreases because of the high condensate saturation in the ring (areas around the wellbore), which severely reduces the effective permeability to gas, thereby reducing gas productivity. However, the wells showed approximately stable gas production after the period of an initial decline and a subsequent increase in gas production rate. The gas flowing into the ring became leaner causing the condensate saturation in the ring to decrease. This increased the effective permeability of the gas and caused the gas productivity to increase as was observed in field data.

1.3 Use of hydraulic fractures

Hydraulic fracturing has been proven to be one of the most effective techniques for improving the productivity of dry gas reservoirs. Acid fracturing and hydraulic fracturing have also found to be effective in improving the productivity of gas condensate reservoirs²⁹⁻³⁴. Hydraulic fracturing in gas condensate reservoirs also has additional advantages: stimulation reduces the pressure drawdown and thus leads to less liquid dropout. On top of that, non-Darcy effects are reduced and the well will suffer lower productivity decrease when liquid blocking occurs. Distribution of the liquid condensate around the fracture, whose length can be several hundred feet for low-permeability reservoirs but only tens of feet for high-permeability reservoirs, can alleviate or greatly soften the impact of hydraulic fracturing on gas production. This flow impairment along the fracture surface in the reservoir is commonly referred to as fracture face skin effect.

Settari *et al.*³⁰ conducted a study on the effect of condensate blockage on productivity index of hydraulically fractured wells in a complex, highly heterogeneous reservoir, containing rich gas condensate. The study using a 2-component black oil simulation model was performed for the Smorbukk field, offshore, Norway. They found that the proppant fracturing was effective in mitigating the effect of condensate blockage on *PI*. The effectiveness depended primarily on the reservoir heterogeneity, fracture length and fracture conductivity.

Sognesand³¹ examined the effect of retrograde condensate blockage on long-term well performance of vertically fractured gas condensate wells. He presented a method to correct the effect of condensate blockage using the concept of time-dependent skin factor. He also documented the difference in productivity loss due to condensate blockage for non-fractured and fractured wells. He found by simulation study that considerable difference in long-term productivity results between stimulated and non-stimulated gas condensate wells. The author made the argument that moderate permeability wells, which otherwise would not require stimulation, might be prime

candidates for stimulation to reduce or eliminate the effect of condensate blockage. Stimulation of such wells would be justified mainly on the analysis of the percentage of well pressure losses that are caused by reservoir and near-wellbore effects, relative to total pressure losses including flow through tubing. Also, he concluded that the retrograde condensate buildup in the vicinity of a vertically fractured gas condensate wells can be modeled as a skin factor.

Carlson *et al.*³³ studied the effects of retrograde liquid condensation on single well productivity in a low permeability reservoir by using radial compositional modeling of a hydraulic fracture. They concluded that a well assuming a radial flow into a wellbore, there would be significant productivity impairment by condensate dropout in the immediate wellbore area. A hydraulic fracture treatment reduces the amount of drawdown in the well and results in a less concentrated condensate precipitation significant impairment does not occur during the first ten years of production. They recommended research on the effect of retrograde liquid condensate on single well productivity at higher level of condensate dropout and also on the effect of factors like *IFT* and wettability on gas-condensate permeability curves.

Indriati *et al.*¹ proposed a model that predicts the performance of hydraulically fractured gas condensate reservoirs (quantifying the effects of gas permeability reduction), adjusts fracture treatment design, calculates the optimum fracture morphology and presents guidelines for the calculation of the optimum pressure drawdown during production to maximize well performance. They concluded that for a given mass of proppant to be injected, the fracture length would need to be larger than the zero-fracture-face-skin optimum, in some cases considerably large, or to put it differently, for every flowing bottomhole pressure there exists an optimum fracture geometry that maximize the dimensionless productivity index. They also showed that for rich gas condensate reservoirs there exists an optimum flowing bottomhole pressure in which the lowest bottomhole pressure no longer provides the highest production. On the other hand for lean gas condensate reservoirs, the optimum flowing bottomhole pressure

is generally the lowest bottomhole pressure that can be tolerated by operational constraints.

Al-Hashim and Hashmi ³⁵ showed that hydraulic fracturing is effective in improving the productivity index (PI) of gas condensate wells both above and below the dewpoint pressure by about three times as compared to the non-fractured wells. Hydraulic fractures are also found to extend cumulative production above the dew point pressure. As dimensionless fracture conductivity increases, the long-term performance of the gas condensate reservoir is improved, and the improvement is more pronounced for longer fractures. Once the dewpoint is reached, the flowing bottomhole pressure drops sharply to the specified minimum flowing bottomhole pressure in fractured and non-fractured wells. However, the drop is less severe in the fractured case. The sharp drop in the flowing bottomhole pressure, results in reduction in the productivity of gas condensate wells.

CHAPTER II

SINGLE-PHASE DAMAGE ANALYSIS

The concept of skin factor or damage due to skin has been very useful in the quantification of impediment to flow in oil and gas production. The most common is damage around the wellbore, denoted by skin factor, s . In the case of hydraulic fractures the analogy to wellbore skin, is the fracture face skin, s_{ff} , which is a permeability reduction normal to the face of the fracture.

From the literature we know that in a radial model, the skin factors obtained from infinite-acting solution, Eq. 2.1, and pseudo-steady state solution, Eq. 2.4, are identical for both constant rate and constant p_{wf} cases.

$$p_D = \frac{1}{2} \ln t_D + 0.4045 + s \dots\dots\dots (2.1)$$

Where:

$$\text{Dimensionless pressure, } p_D = \frac{kh(p_i - p_{wf})}{141.2qB\mu} \dots\dots\dots (2.2)$$

$$\text{Dimensionless time, } t_D = \frac{0.00633kt}{\phi\mu c_i r_w^2} \dots\dots\dots (2.3)$$

$$q = \frac{kh}{141.2B\mu} \left(\frac{1}{\ln \frac{r_e}{r_w} - \frac{3}{4} + s} \right) \dots\dots\dots (2.4)$$

In other words, for a radial model, the calculated skin factor for a well produced under constant rate is the same as that produced under constant p_{wf} .

In the current work, since we are assuming an infinite conductivity fracture which propagates the entire drainage boundary of the well ($x_e/x_f=1$), the flow pattern from the formation into the hydraulic fracture is linear. So, the objective of this chapter is to analyze the production impairment in a linear model when a single phase fluid (liquid) is flowing for both constant rate and constant p_{wf} . The simulations are done using GASSIM,

a 2D, single-phase simulator used for single-phase fluid (liquid or gas). Then, the results of simulation are compared to analytical solution.

2.1 Model description

This chapter uses a simple linear model including liquid as the reservoir fluid to illustrate the damage effect at the face of the fracture. The case study is an 80-acre tight gas reservoir with reservoir properties given in **Table 2.1**. For analysis, one-quarter of the reservoir was modeled. x_e and x_f are both equal to 933.381 ft. The grid set-up for the simulation is illustrated in **Fig. 2.1**. In order to precisely model the linear flow of liquid into the fracture, the well cell method was used whose detailed discussion is given in Appendix A. This method specifies high permeability and very low porosity in the first gridblock to make the cell pressure equal to the flowing bottomhole pressure. The model includes 100 gridblocks in x-direction when the properties of the first gridblock have been tabulated in **Table 2.2** (See Appendix B for data files).

Table 2.1— Reservoir and liquid properties of the model used in GASSIM

Reservoir Characteristic	Values
Reservoir Half Length (x_e), ft	933.381
Reservoir Half Length (y_e), ft	933.381
Thickness (h), ft	50
Absolute permeability (k_x), md	0.05
Absolute permeability (k_y), md	0.05

Table 2.1— Continued

Reservoir Characteristic	Values
Porosity (ϕ), fraction	0.13
Formation Volume Factor (B_o), RB/STB	1
Viscosity (μ), cp	0.7
Total Compressibility (c_g), psi ⁻¹	0.00001
Initial Pressure (p_i), psi	3,900

Table 2.2— Reservoir properties of the first gridblock used in GASSIM

Reservoir Characteristic	Values
Absolute Permeability (k_x), md	50,000
Absolute Permeability (k_y), md	50,000
Porosity (ϕ), fraction	0.00001

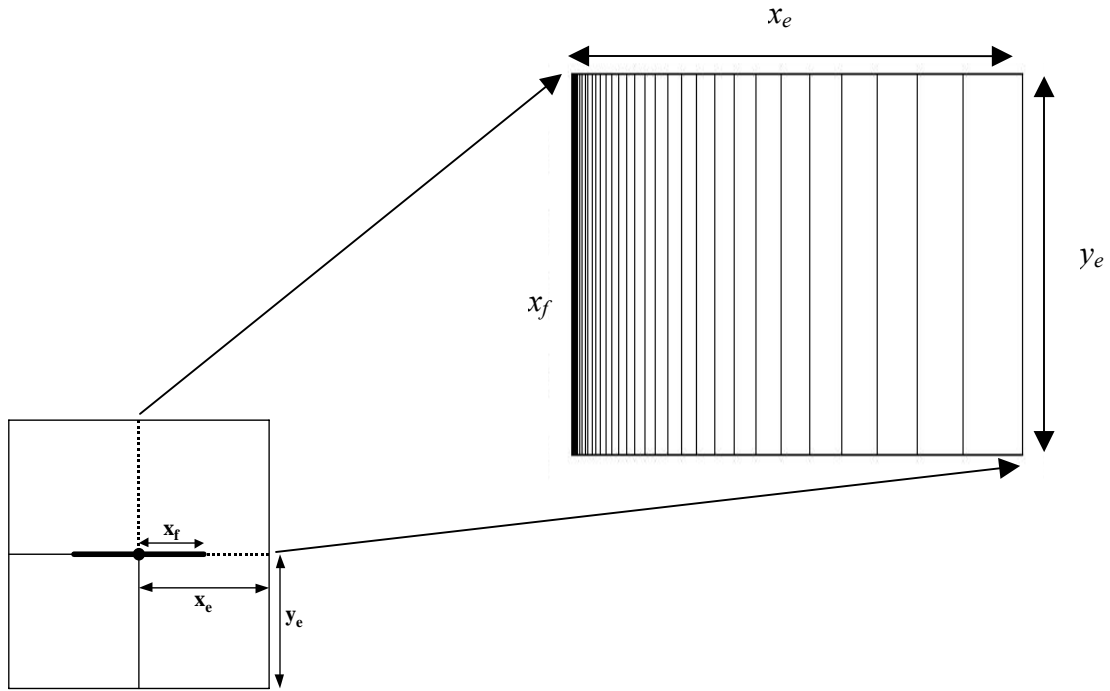


Fig. 2.1 – Quarter model for 80 acre drainage area.

2.2 Fracture face skin

Most wells drilled in low permeability formations need hydraulic fracturing to be able to produce with economic viability. With continued production, there is a permeability reduction normal to the face of the fracture, shown in **Fig. 2.2**, and there is a need for this skin to be quantified. Cinco and Samaniego³⁶ provided an expression of the fracture face skin effect that becomes additive to the dimensionless pressure for the finite conductivity fracture performance.

$$\text{Fracture face skin, } s_{ff} = \frac{\pi w_s}{2x_f} \left(\frac{k}{k_s} - 1 \right) \dots\dots\dots (2.5)$$

For single phase fluid, skin effects on the face of a fracture are simulated, and the simulation results are compared to the analytical solution, Eq. 2.5.

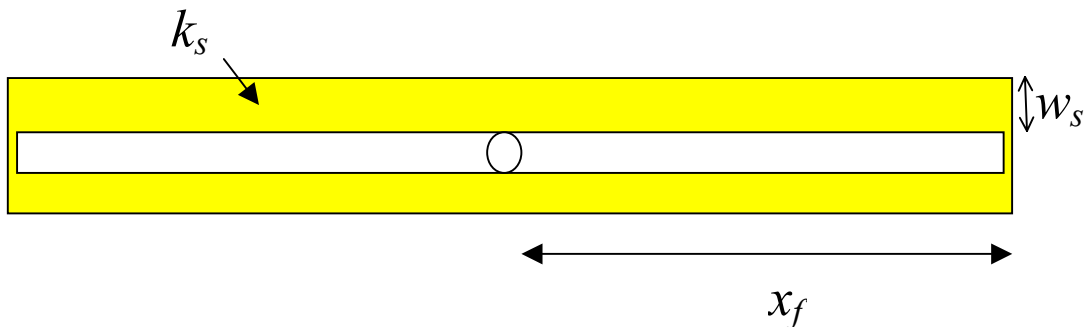


Fig. 2.2 — Permeability reduction normal to fracture face.

2.3 Constant rate fracture face skin

In this section, we use the linear model mentioned earlier to evaluate the fracture face skin. We apply a small pressure drop by specifying a low flow rate (1 STBD) to lessen the non-linearity effects due to liquid compressibility change. Later we use the simulation results of this basic or undamaged case to compare to that of the damaged case (See Appendix B for data file). Then, in order to make a damaged zone in the model, we specified a reduced permeability which is 50 times smaller than the original permeability to 14 gridblocks starting from 2nd gridblock and ending at 15th. We ran these two cases on GASSIM and compared the simulation results with the analytical solutions. The analytical solutions to the closed, linear reservoirs have been detailed in Appendix C.

Eq. 2.6 is the infinite-acting linear solution for constant rate production from a closed linear reservoir and Eq. 2.7 is the approximation for closed reservoir for constant rate in dimensionless forms ².

$$p_{wD} = \sqrt{\pi t_{Dx_e}} \dots\dots\dots (2.6)$$

$$p_{wD} = \frac{\pi}{2} \left(\frac{x_e}{y_e} \right) t_{Dx_e} + \frac{\pi}{6} \left(\frac{y_e}{x_e} \right) \dots\dots\dots (2.7)$$

In Eqs. 2.6 and 2.7 the dimensionless variables are represented by:

$$p_{wD} = \frac{k h (p_i - p_{wf})}{141.2 q_o B_o \mu_o} \dots\dots\dots (2.8)$$

$$t_{Dxe} = \frac{0.00633 kt}{\phi \mu c_t x_e^2} \dots\dots\dots (2.9)$$

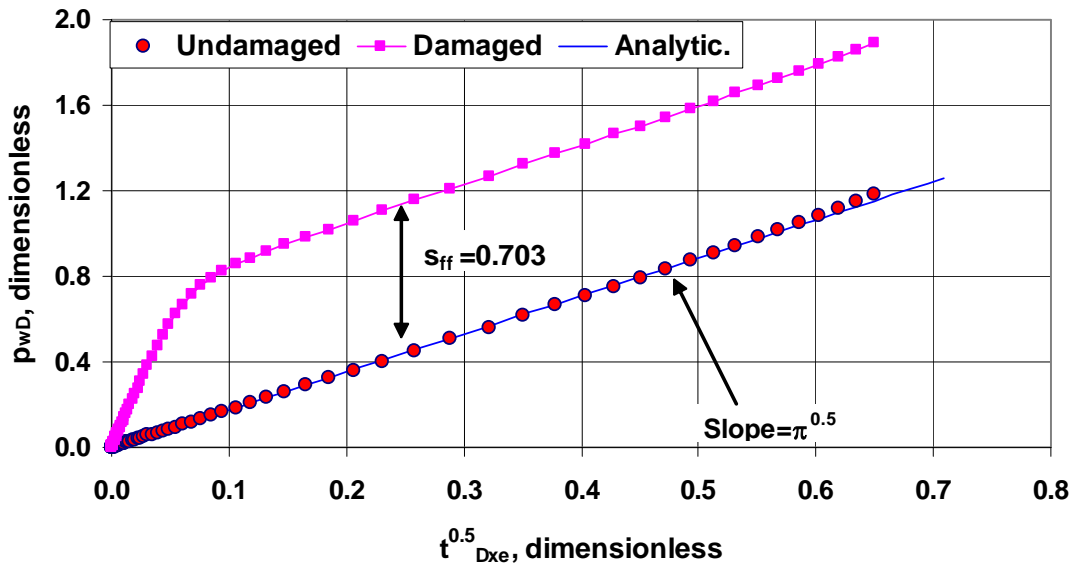


Fig. 2.3 — Constant rate s_{ff} in transient period.

Fig. 2.3 shows that a plot of p_{wD} against square root of t_{Dxe} gives a straight line with slope of $\pi^{0.5}$ for an undamaged case which agrees with the analytical solution, Eq. 2.6. For the damaged case, p_{wD} departs from the straight line at very early times and then becomes parallel to the analytical solution. The difference between two cases, damaged and undamaged, is about 0.703 which is very close to the value obtained from Eq. 2.5. Knowing that $k=0.05$ md, $k_s=0.001$ md, $x_f=933.381$ ft and $w_s=8.7279$ ft, we get:

$$s_{ff} = \frac{\pi(8.7279)}{2(933.381)} \left(\frac{0.05}{0.001} - 1 \right) \dots\dots\dots (2.10)$$

$$s_{ff} = 0.72 \dots\dots\dots (2.11)$$

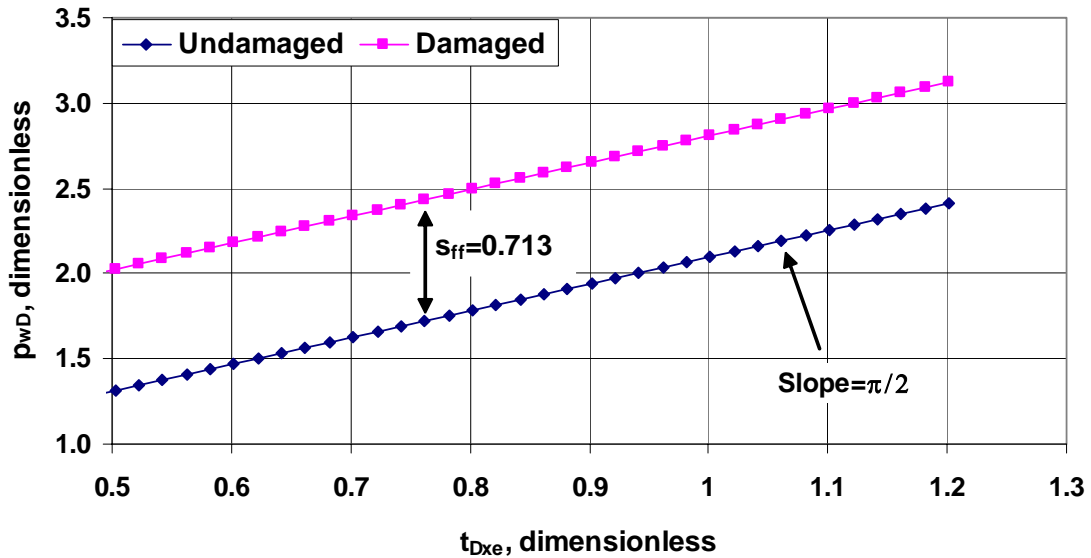


Fig. 2.4 — Constant rate s_{ff} in pss period.

Fig. 2.4 shows a different approach for the simulation results analysis. It is a plot of p_{wD} against t_{Dxe} on Cartesian plot, and it shows that in pss period, simulation runs for both the damaged and undamaged cases have parallel straight lines with slope of $\pi/2$, which differ by s_{ff} . Again, the obtained skin factor closely matches the calculated one using Eq. 2.5.

So, simulation of a single phase flow in a closed, linear reservoir at constant rate indicates that analytical solutions, Eqs. 2.6 and 2.7 can precisely enough estimate the fracture face skin. It also shows that the calculated skin by using these two equations

agree with the one by using Eq. 2.5. Therefore, the finalized form of Eqs. 2.6 and 2.7 are as follow:

$$p_{wD} = \sqrt{\pi t_{Dx_e}} + s_{ff} \dots\dots\dots (2.12)$$

$$p_{wD} = \frac{\pi}{2} \left(\frac{x_e}{y_e} \right) t_{Dx_e} + \frac{\pi}{6} \left(\frac{y_e}{x_e} \right) + s_{ff} \dots\dots\dots (2.13)$$

2.4 Constant well pressure fracture face skin

In the previous section we studied the effect of fracture face skin in a closed, linear reservoir produced at constant rate. This section uses the same model to illustrate the fracture face skin effect when the reservoir is produced at constant p_{wf} . In order to minimize the nonlinearities, a small pressure drop ($\Delta p = 300$ psi) was applied. The undamaged case was run on GASSIM and the results were compared to the simulation results of the damaged case which includes the same damaged zone and reduced permeability (See Appendix B for data file). The analytical solutions to closed, linear reservoir produced at constant p_{wf} have been discussed in Appendix C. Eqs. 2.14 and 2.15 are the infinite-acting solution and boundary-dominated approximation for a closed, linear reservoir produced at constant pressure respectively ².

$$\frac{1}{q_D} = \frac{\pi}{2} \sqrt{\pi t_{Dx_e}} \dots\dots\dots (2.14)$$

$$\frac{1}{q_D} = \frac{\pi}{4} \left(\frac{y_e}{x_e} \right) \exp \left[\frac{\pi^2}{4} \left(\frac{x_e}{y_e} \right)^2 t_{Dx_e} \right] \dots\dots\dots (2.15)$$

Where:

$$\frac{1}{q_D} = \frac{kh(p_i - p_{wf})}{141.2q_o B_o \mu_o} \dots\dots\dots (2.16)$$

$$t_{Dx_e} = \frac{0.00633kt}{\phi \mu c_t x_e^2} \dots\dots\dots (2.9)$$

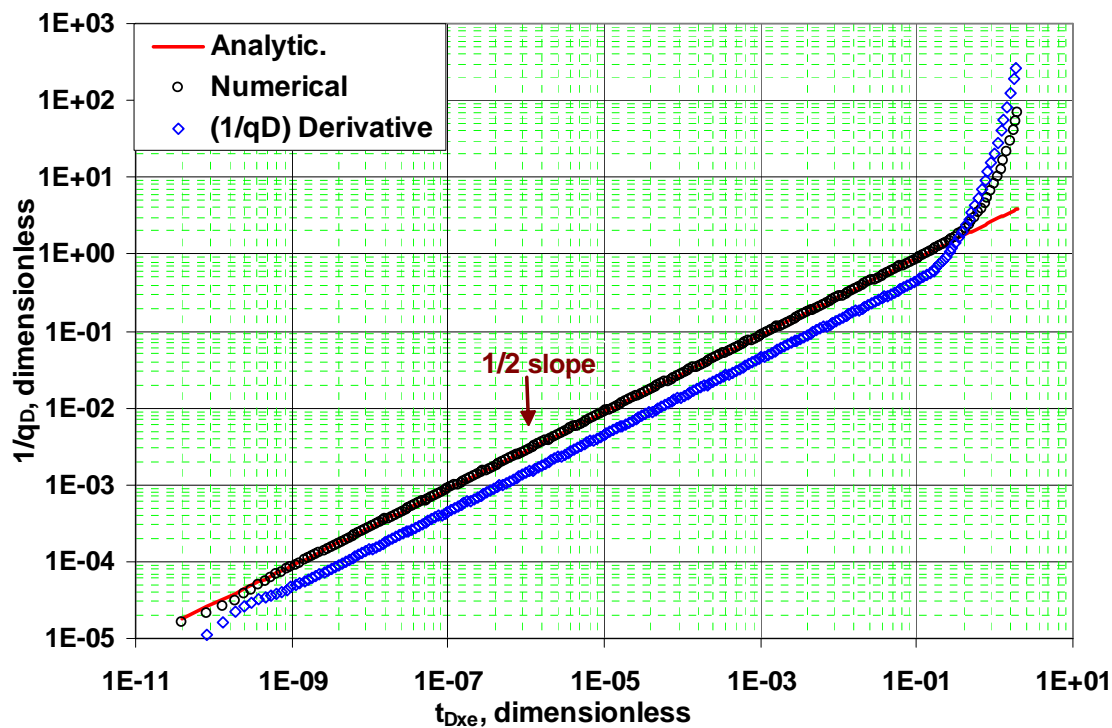


Fig. 2.5 — Type-curve plot for a single-phase undamaged linear reservoir with p_{wf} at 3,600 psi.

The plot in **Fig. 2.5** shows the type-curve analysis for an undamaged linear reservoir produced at constant flowing bottomhole pressure. The simulation results agree with the analytical solution, Eq. 2.14, in transient period represented by a $\frac{1}{2}$ -slope on the diagnostic plot. At very early times, there is a departure from $\frac{1}{2}$ -slope which is due to early simulation error and is denoted as artifact wellbore storage. This simulation error can be improved by using more refined grids specially refinement of the very few grids near the producing well. The derivative plot indicates that there is only one $\frac{1}{2}$ -slope and the reservoir is not damaged, otherwise we would have seen another $\frac{1}{2}$ -slope followed by the first one.

Figs. 2.6 and 2.7 illustrate the skin effect analysis in transient and boundary-dominated flow separately.

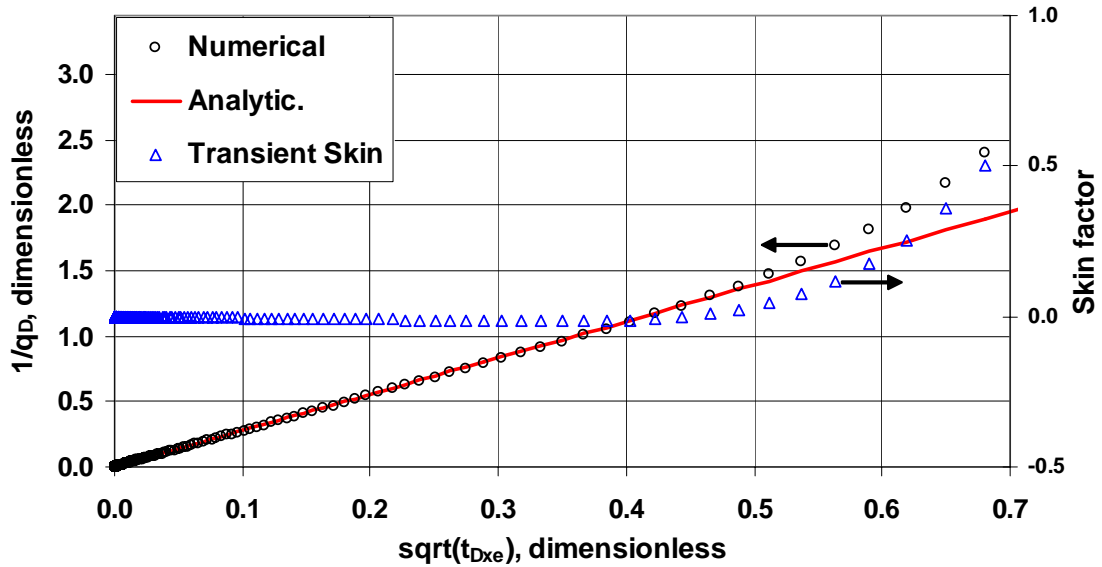


Fig. 2.6 – Infinite-acting flow curve for a single-phase undamaged linear reservoir with p_{wf} at 3,600 psi.

The plot in **Fig. 2.6** shows that for an infinite-acting reservoir with no damaged zone, a plot of $1/q_D$ against square root of t_{Dxe} gives a straight line which matches to the analytical solution, Eq. 2.14. If we rewrite Eq. 2.14 in terms of skin, and express Eq. 2.15 as stabilized flow⁴, we will be given with the following equations:

$$\frac{1}{q_D} = \frac{\pi}{2} \sqrt{\pi t_{Dxe}} + s_{ff} \dots\dots\dots (2.17)$$

$$q_o = \frac{kh(\bar{p} - p_{wf})}{141.2 B_o \mu_o \left[\frac{2}{\pi} \left(\frac{y_e}{x_e} \right) + s_{ff} \right]} \quad \dots\dots\dots (2.18)$$

The calculated skin using Eq. 2.17 gives the value of zero in transient period and starts going up as soon as the infinite-acting flow ends.

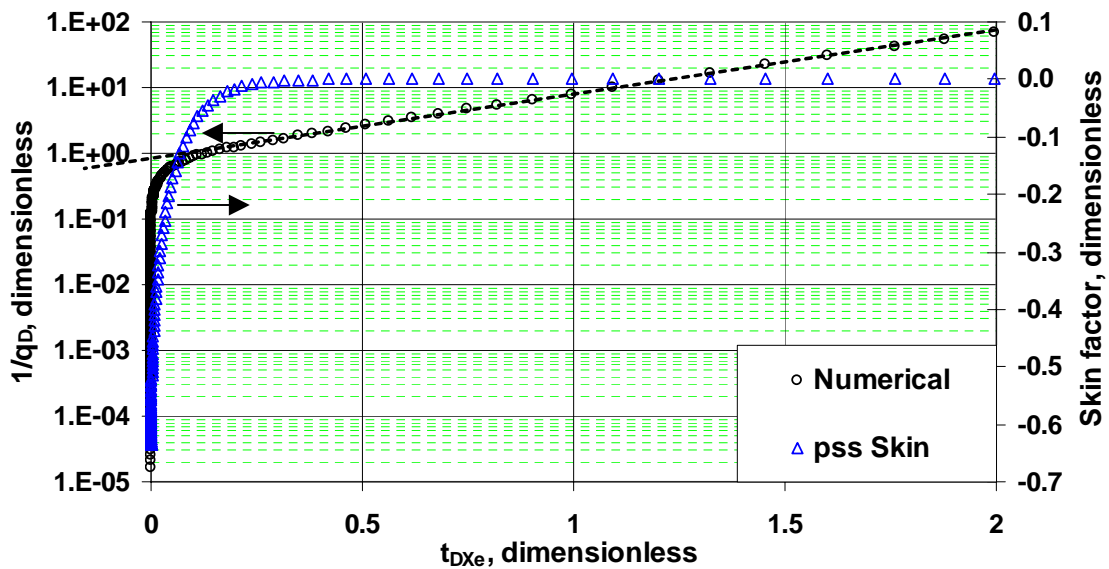


Fig. 2.7 — Boundary-dominated flow curve for a single-phase undamaged linear reservoir with p_{wf} at 3,600 psi.

Fig. 2.7 shows the same analysis for boundary-dominated flow period. It is a semi-log plot of $1/q_D$ against t_{Dxe} representing no damage in linear reservoir as the plot of calculated skin illustrates.

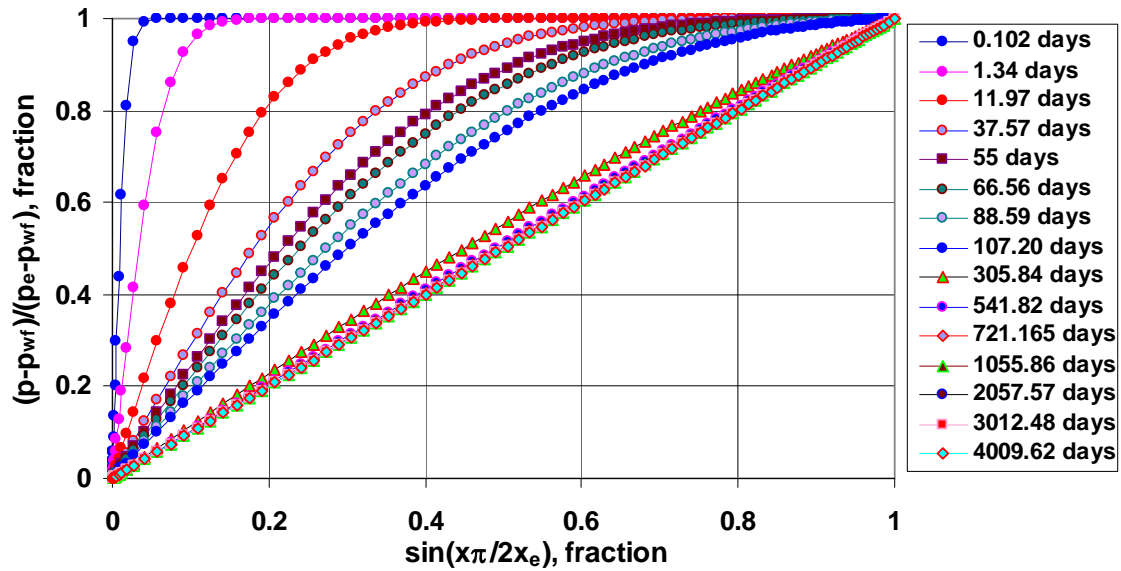


Fig. 2.8 — Pressure profiles for a single-phase undamaged linear reservoir with p_{wf} at 3,600 psi.

The plots in **Figs. 2.8** and **2.9** verify the results of skin analysis in transient and *pss* periods. **Fig. 2.8** shows that the plot of normalized pressure drop, $\frac{P - P_{wf}}{P_e - P_{wf}}$, against normalized distance from the producer, $\sin\left(\frac{\pi x}{2x_e}\right)$, gives a 45-degree straight line for undamaged linear reservoir acting in boundary-dominated flow period. Basically, the pressure profile versus distance, x , for boundary-dominated flow equation, Eq. 2.18, has a shape that is proportional to $\sin\left(\frac{\pi x}{2y_e}\right)$ function at late times³⁷. Eqs. 2.19 and 2.20 are the pressure profile equation at early time and the complete pressure profile equation for a closed, linear reservoir produced at constant p_{wf} (see Appendix C).

$$p = p_i \operatorname{erf}\left(\frac{x}{2x_e \sqrt{t_{Dx_e}}}\right) + p_{wf} \operatorname{erfc}\left(\frac{x}{2x_e \sqrt{t_{Dx_e}}}\right) \dots\dots\dots (2.19)$$

$$p = p_{wf} + \frac{4}{\pi}(p_i - p_{wf}) \sum_{n=odd}^{\infty} \frac{1}{n} \exp\left[-\frac{n^2 \pi^2}{4} t_{Dx_e} \left(\frac{x_e}{y_e}\right)^2\right] * \sin\left[\frac{n \pi x}{2 y_e}\right] \dots\dots\dots (2.20)$$

Eq. 2.19 shows that the pressure profile in infinite-acting period has a shape that is proportional to $erf\left(\frac{x}{2x_e\sqrt{t_{Dx_e}}}\right)$ function and consequently, doesn't give a straight line on

Fig. 2.8.

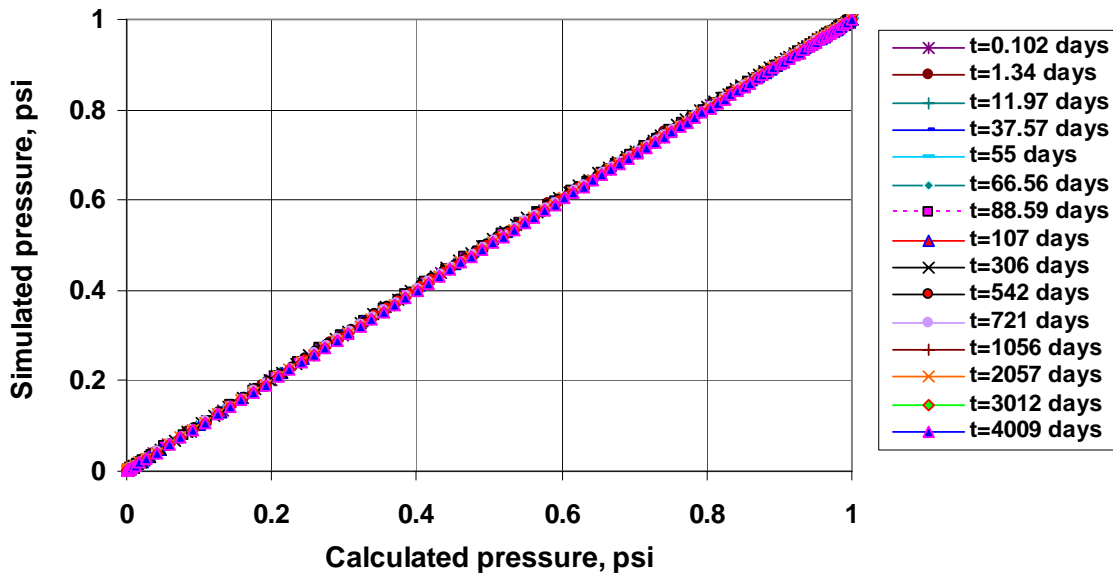


Fig. 2.9 — Comparison of simulated pressures with calculated pressures for a single-phase undamaged linear reservoir with p_{wf} at 3,600 psi.

Fig. 2.9 is a plot of simulated pressures against the calculated pressures by using Eq. 2.20, and it shows that for a linear reservoir with no damage, the simulation results agree with the analytical solutions. In other words, having a 45-degree line on this plot means there is no damage in the model.

The damaged case was simulated by introduction of a damaged zone with 8.7279 ft length and with 0.001 md reduced permeability into the basic (undamaged) case (See Appendix B for data file). **Fig. 2.10** shows that when the linear reservoir is damaged, the pressure profile at boundary-dominated flow period is far away from the 45-degree line. The schematic in **Fig. 2.11** illustrates the simulated pressures against the calculated pressures by using the analytical solutions, and it shows that at early times the simulated pressures are much higher than the calculated pressures. As time progresses, this difference becomes smaller until the boundary-dominated flow begins (after 541 days). At this time up to the end of the simulation, the difference remains almost constant indicating a constant skin during the p_{ss} period.

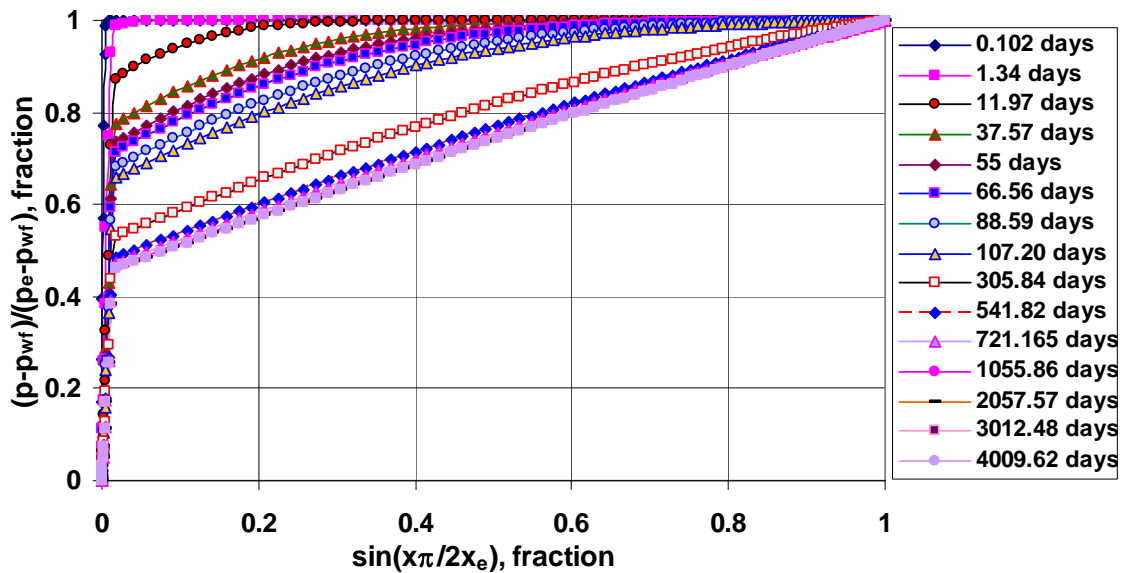


Fig. 2.10 — Pressure profile for a single-phase damaged linear reservoir with p_{wf} at 3,600 psi.

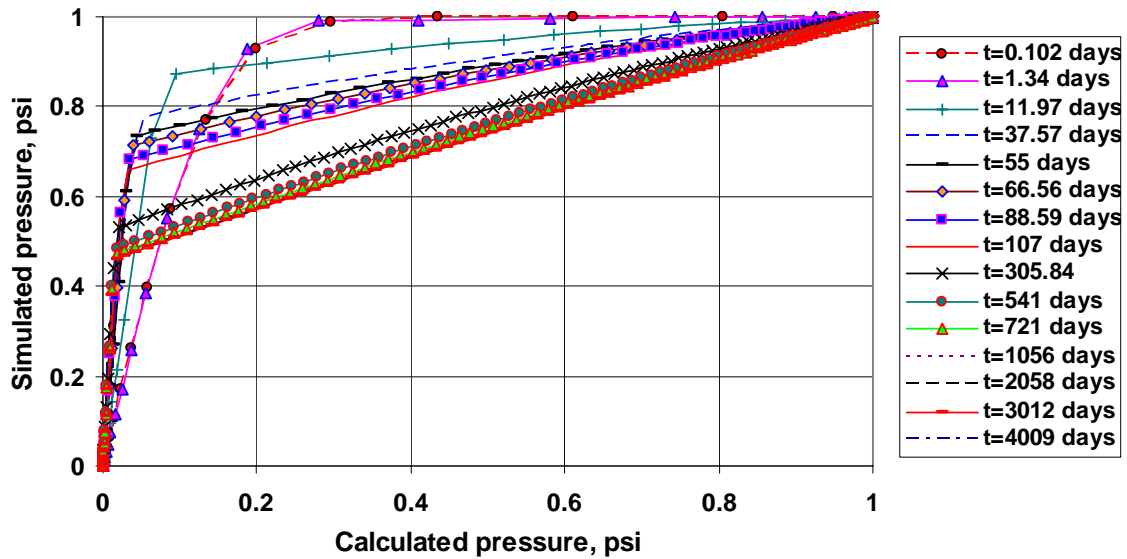


Fig. 2.11 — Comparison of simulated pressures with calculated pressures for a single-phase damaged linear reservoir with p_{wf} at 3,600 psi.

The schematic in **Fig. 2.12** shows that the type-curve plot of a damaged linear reservoir in transient period gives a $\frac{1}{2}$ - slope straight line. It also shows the departure from the analytical solution, Eq. 2.14, which is the first indication of the skin effect. The derivative plot illustrates two $\frac{1}{2}$ -slopes separated by a transition and the p_{ss} period following the second $\frac{1}{2}$ -slope. The first $\frac{1}{2}$ -slope appears at early times when the pressure drop in undamaged region is zero and the infinite-acting behavior is occurring in the damaged zone. Eq. 2.14 is used to calculate the pressure drop in the damaged zone when the damaged zone permeability, k_s , is plugged into the t_{Dxe} equation, Eq. 2.9. The second $\frac{1}{2}$ -slope begins when Δp is stabilized in damaged region and acts like skin. Eq. 2.17 can be used to calculate the skin factor in this period.

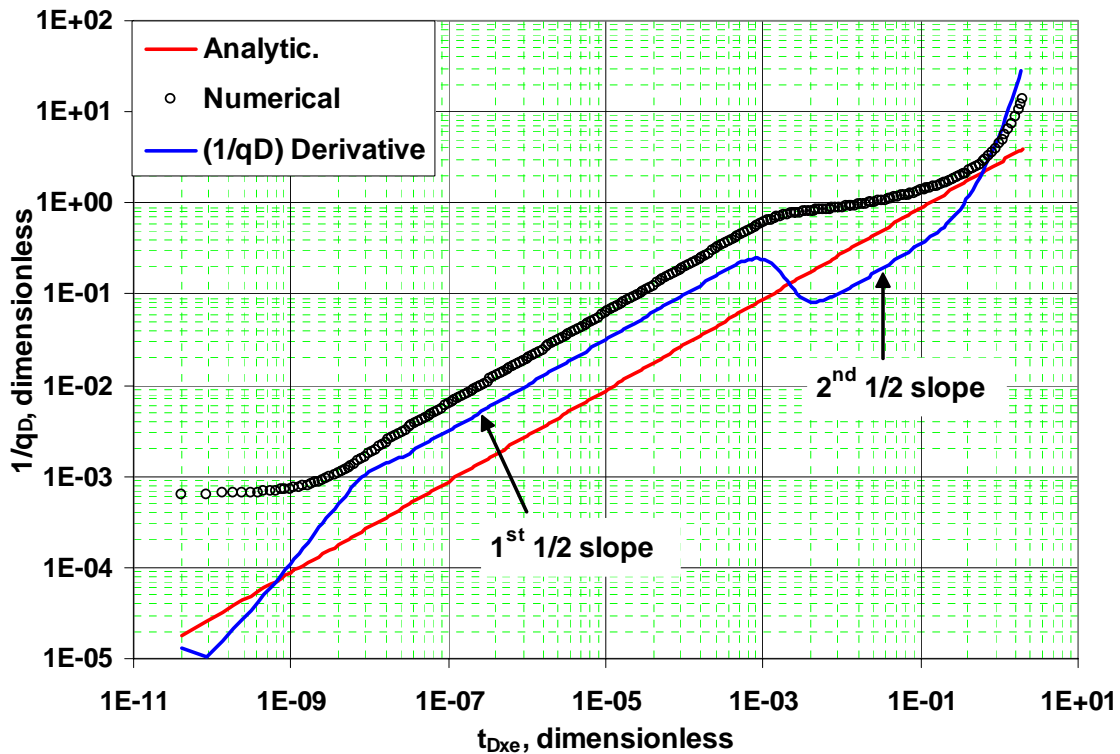


Fig. 2.12 — Type-curve for a single-phase damaged linear reservoir with p_{wf} at 3,600 psi.

Fig. 2.13 shows a different approach for analyzing the simulation results. It is a plot of l/q_D against square root of t_{Dxe} , and it shows two straight lines corresponding to the observed $1/2$ -slopes in **Fig. 2.12**. The extrapolation of the second straight line representing the infinite-acting flow, intercepts the y-axis at 0.69 denoted as the transient skin factor. The skin plot starts decreasing as soon as the infinite-acting flow (second straight line) begins and consequently doesn't give any reasonable value for skin factor. **Fig. 2.14** is a semi-log plot of l/q_D against t_{Dxe} , and it shows that at boundary-dominated flow period, simulation runs have a straight line. The calculated skin factor by using Eq. 2.18 shows a constant value of 0.65 denoted as p_{ss} skin.

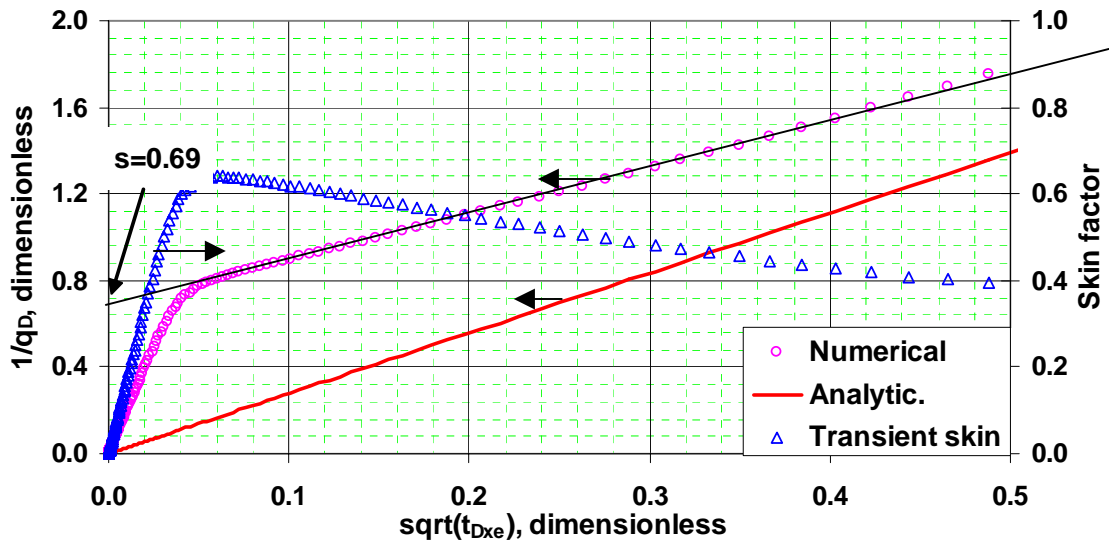


Fig. 2.13 — Transient flow curve for a single-phase damaged linear reservoir with p_{wf} at 3,600 psi.

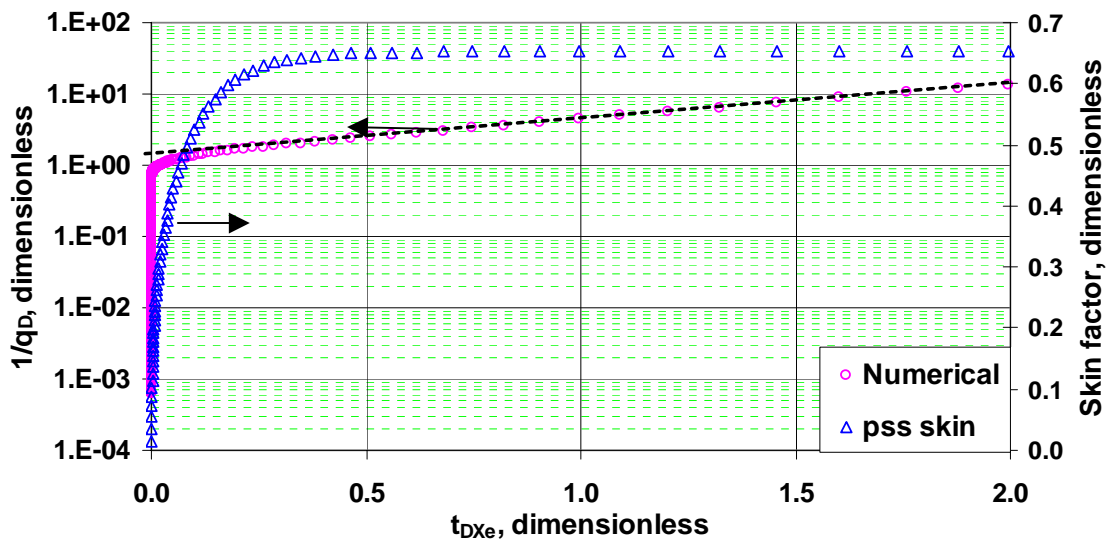


Fig. 2.14 — Boundary-dominated flow curve for single-phase damaged linear reservoir with p_{wf} at 3,600 psi.

Recall the calculated s_{ff} by using Eq. 2.5:

$$s_{ff} = 0.72 \dots\dots\dots (2.11)$$

Although the calculated skin is so small, there is a difference between the obtained skin factors from the simulation results and the value of skin in Eq. 2.11. The same analysis was done for a single phase linear reservoir with damaged zone when the damaged zone permeability, k_s , of 5E-05 md was used. The simulation results for this case have been plotted in **Figs. 2.15–2.17**. The only significant result is that the transient skin plot shows a relatively flat line compared to the skin plot in **Fig. 2.13**. This effect will be more discussed in the next section.

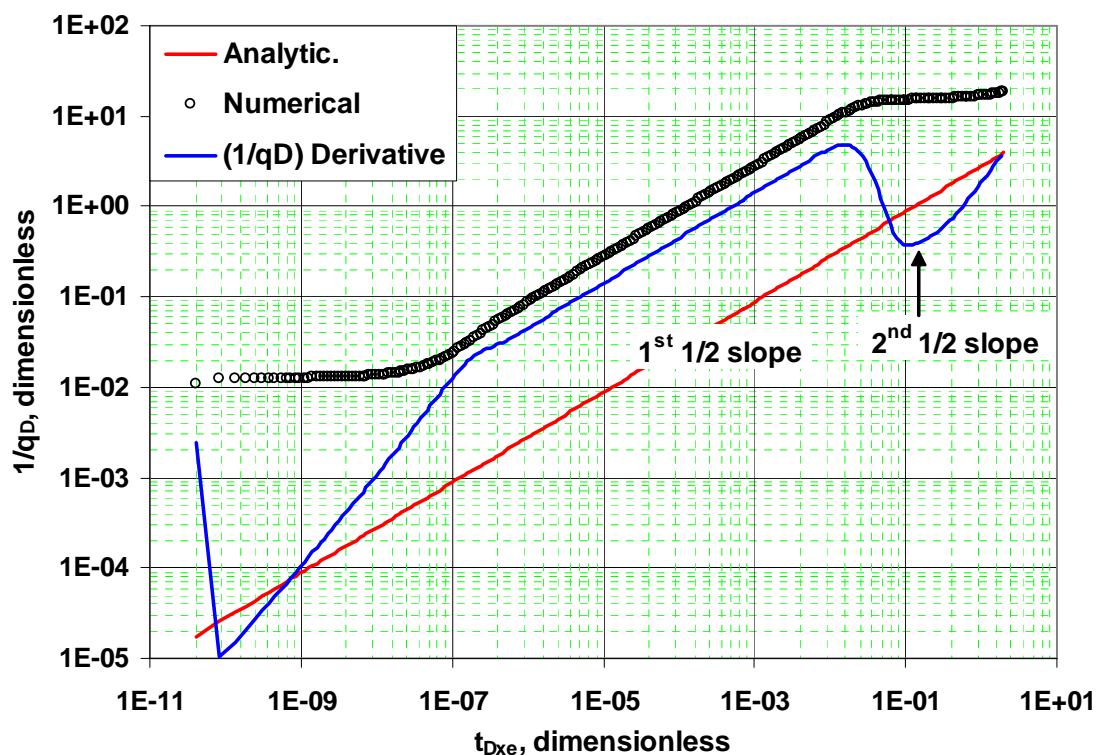


Fig. 2.15 — Type-curve for a single-phase damaged linear reservoir with $k_s=5E-05$ md produced at 3,600 psi.

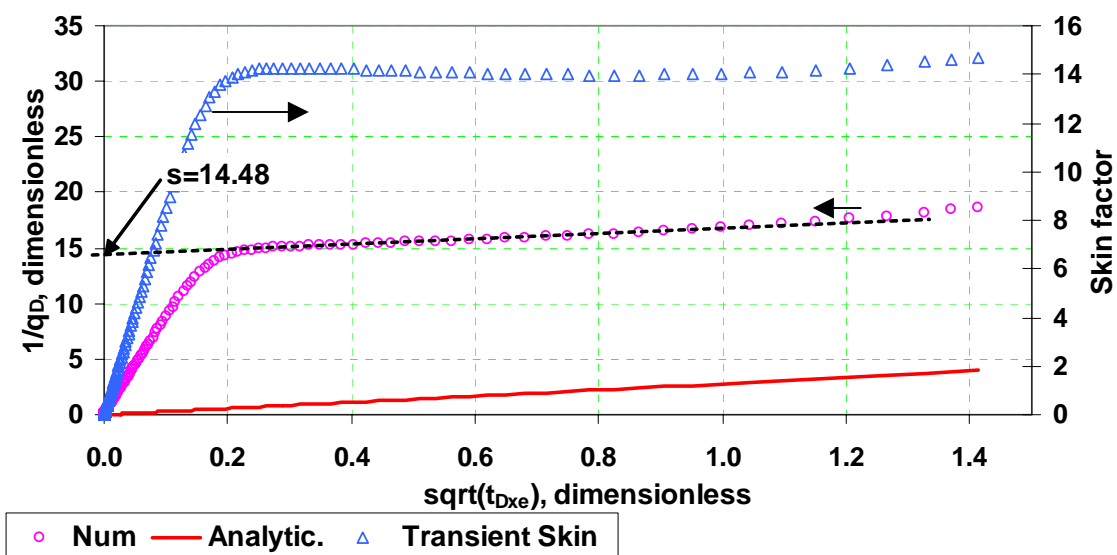


Fig. 2.16 — Transient flow curve for a single-phase linear reservoir with $k_s=5E-05$ md produced at 3,600 psi.

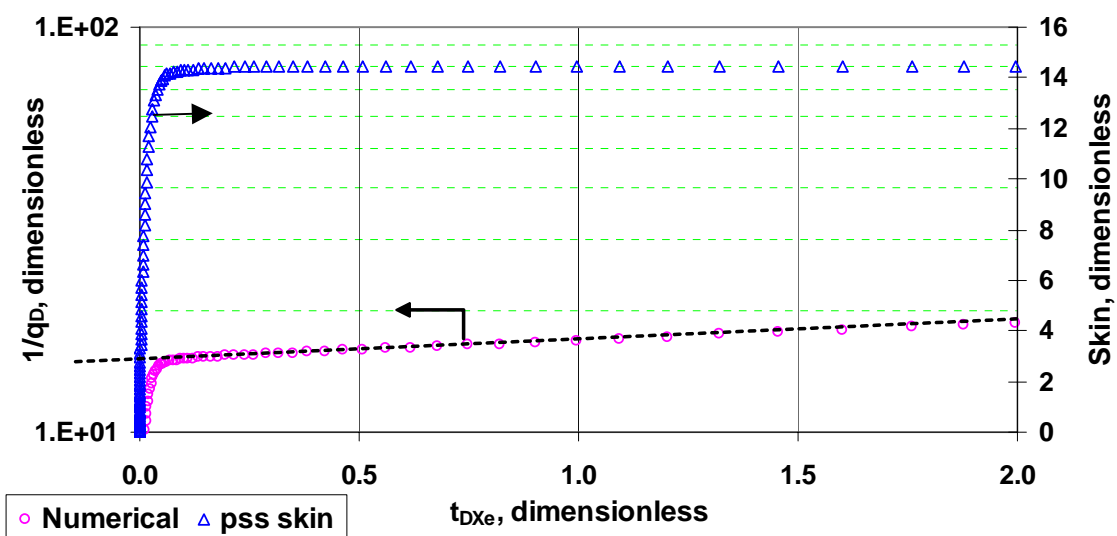


Fig. 2.17 — Boundary-dominated flow curve for single-phase linear reservoir with $k_s=5E-05$ md produced at 3,600 psi.

2.5 Damaged zone permeability effect

A sensitivity analysis was conducted to see how the change in damaged zone permeability affects the production impairment. The linear model used in damage analysis was simulated with different damaged zone permeabilities of 0.0001 md; 0.00005 md; 0.000033 md; and 0.00025 md. For each case, the fracture face skins were calculated by using Eqs. 2.17 and 2.18 at different times and the results have been tabulated in **Table 2.3**. **Table 2.4** depicts the analytical fracture face skins calculated by using Eq. 2.5.

Table 2.3— Transient and p_{ss} fracture face skins for each damaged linear model

Time, Days	$k_s=1E-03$	$k_s=1E-04$	$k_s=5E-05$	$k_s=33E-06$	$k_s=25E-06$
37.57	0.60	6.47	10.24	12.75	14.79
55	0.59	6.89	11.96	15.29	17.85
66.56	0.57	6.98	12.71	16.62	19.56
88.59	0.56	7.04	13.55	18.50	22.21
107.20	0.54	7.05	13.91	19.56	23.93
1055.86	0.65	7.17	14.46	21.78	29.05
2057.57	0.65	7.18	14.47	21.78	29.06
3012.48	0.65	7.18	14.47	21.78	29.07
4009.62	0.65	7.18	14.47	21.78	29.07

Table 2.4— Analytical fracture face skins for each damaged linear model

Different Cases	Analytical s_{ff}
Case 1, $k_s=1E-03$ md	0.72
Case 2, $k_s=1E-04$ md	7.33
Case 3, $k_s=5E-05$ md	14.67
Case 4, $k_s=33E-06$ md	22.04
Case 5, $k_s=25E-06$ md	29.36

Table 2.3 shows that the simulated fracture face skins in p_{ss} period are very close to the analytical skins tabulated in **Table 2.4**, and also shows that as the damaged zone permeability is getting smaller, the p_{ss} skin factors are getting closer to the analytical skins.

2.6 Rate and cumulative production analysis

In the previous sections, it was shown that for a linear reservoir producing at constant rate, fracture face skin is additive to analytical solutions, Eqs. 2.12 and 2.13.

For the constant p_{wf} case, it was assumed that the skin factor was additive to the analytical solutions and based on this assumption, fracture face skin was calculated. The results show that the skin factor changes with time and only in boundary-dominated flow period becomes constant. So, the question was raised about if the constant pressure skin is the real representative of the damage at the fracture face. This question can be more important when we note that only one phase was flowing and for a gas condensate reservoir in which two phases change a lot this method of calculation may not work.

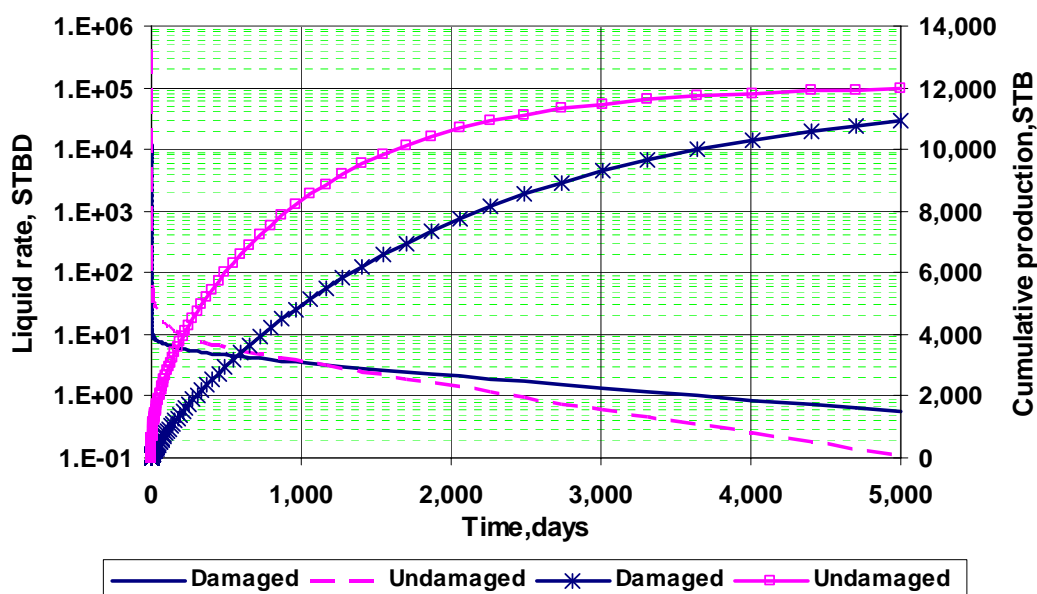


Fig. 2.18 — Comparison between production behavior of undamaged case with that of damaged linear reservoir with $k_s=0.001$ md produced at 3,600 psi.

Recall the damaged linear reservoir with k_s equal to 0.001 md studied in section 2.4. The analytical and numerical skin factors were 0.74 and 0.65 respectively. This degree of fracture face damage seems to be so small compared to the conventional skin analysis. The production rate and cumulative production plots have been shown for this case, **Fig. 2.18**, and were compared to the undamaged plots. **Fig. 2.18** also shows that the difference between the cumulative production rate of the damaged case and that of the undamaged case is considerable, although the calculated skin is very small. Basically, the fracture face skin is the difference between the numerical dimensionless rate and the analytical one and since the pressure drop in a linear reservoir for a particular production rate is much smaller than the pressure drop in radial model, the analytical and numerical dimensionless rate values become small. So, the difference between two small values will result in a small skin, although the numerical dimensionless rate value is half the

analytical one. This effect is more evident for the case of a compositional system which will be discussed in the next chapter.

The results mentioned in this chapter apply to a single-phase fluid system. In the next chapter, similar analysis is done for skin, but instead of a single-phase fluid, the model is a compositional fluid system.

CHAPTER III

GAS CONDENSATE DAMAGE ANALYSIS

In Chapter II, analysis for damage at the face of the fracture was done considering single-phase fluid (liquid or gas). In this chapter, similar analysis is made but with gas condensate fluid. Due to the accumulation of liquid at pressures below the dewpoint, the quantification of damage in this case becomes quite complex. Two case studies are presented with two different fluids utilizing the compositional simulation. Case study 1 investigates condensate damage for a linear reservoir including a relatively lean gas condensate and case study 2 does the same analysis with a rich gas condensate.

3.1 Reservoir description

A linear model was developed to study the condensate damage at the face of the fracture. The linear model is analogous to linear flow toward an infinite conductivity fracture propagating to the entire extent of the rectangular reservoir. **Table 3.1** summarizes the fundamental characteristics of the reservoir.

According to the information presented in **Table 3.1**, the dimensions of the linear model are 933.381 ft in the x and y directions and 50 ft in z direction. These dimensions along with an average porosity of 13% represent the initial gas reservoir volume in the symmetric quarter of an 80 acres drainage area. The model was divided into 40 gridblocks, 40 in the x direction, 1 in the y direction, and 1 in the z direction. The well was located in the first cell (well cell) of the linear model as shown in **Fig. 3.1**. In order to precisely model the linear flow, the Well Cell method (Appendix A) was used by specifying different values of permeability and porosity to the first cell, **Table 3.2**. Also the water saturation was set as 0.16 through the entire model (See Appendix E for data files).

Table 3.1 — Main characteristics of the reservoir model

Reservoir Characteristic	Values
Drainage Area, Acres	~ 80
Reservoir Half Length (x_e), ft	933.381
Reservoir Half Length (y_e), ft	933.381
Thickness (h), ft	50
Absolute permeability (k), md	0.15
Porosity (ϕ), fraction	0.13
Water Saturation (S_w), fraction	0.16
Initial Pressure (p_i), psi	3,900

Table 3.2 — Characteristics of the first gridblock (well cell)

1st grid (well cell) Characteristic	Values
Absolute permeability (k), md	50
Porosity (ϕ), fraction	1E-05

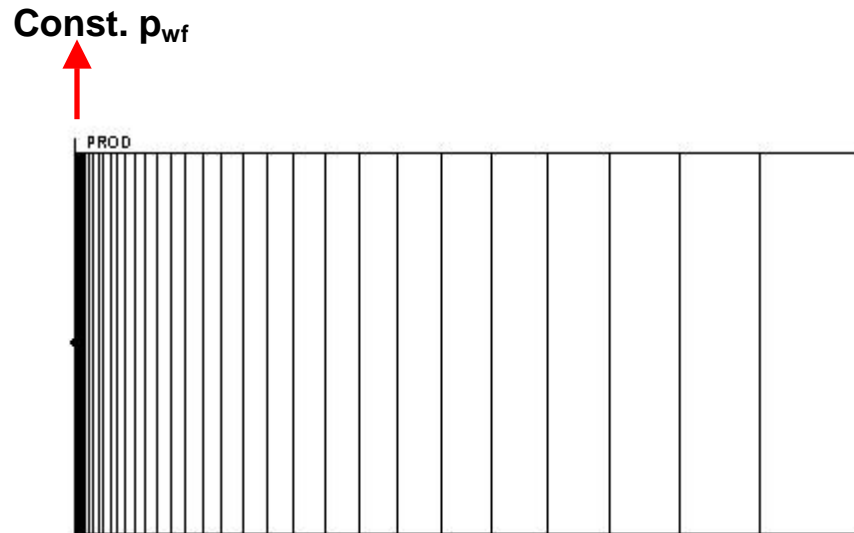


Fig. 3.1 — Schematic of the 1D linear model in CMG.

Once all required information regarding the dimensions of the reservoir model were established, a synthetic simulation model was created using CMG³⁸ version 2002.10. The base saturation-relative permeability tables used were those reported in the data file adopted from CMG sample data related to third SPE Comparative Solution Project³.

Fig. 3.2 shows the relative permeability changes with gas saturation. At pressures above the dewpoint, the reservoir is primarily gas, and the gas relative permeability is at a maximum of 0.74. As the gas is produced, the pressure falls below the dewpoint and condensate starts to accumulate, thereby reducing the relative gas permeability. Once the critical oil saturation of 24% is attained, the oil relative permeability increases and the oil starts to move.

When the reservoir model is completed, a representative gas condensate reservoir fluid for each case study is included into the model. The details of the fluid models are given in the next sections.

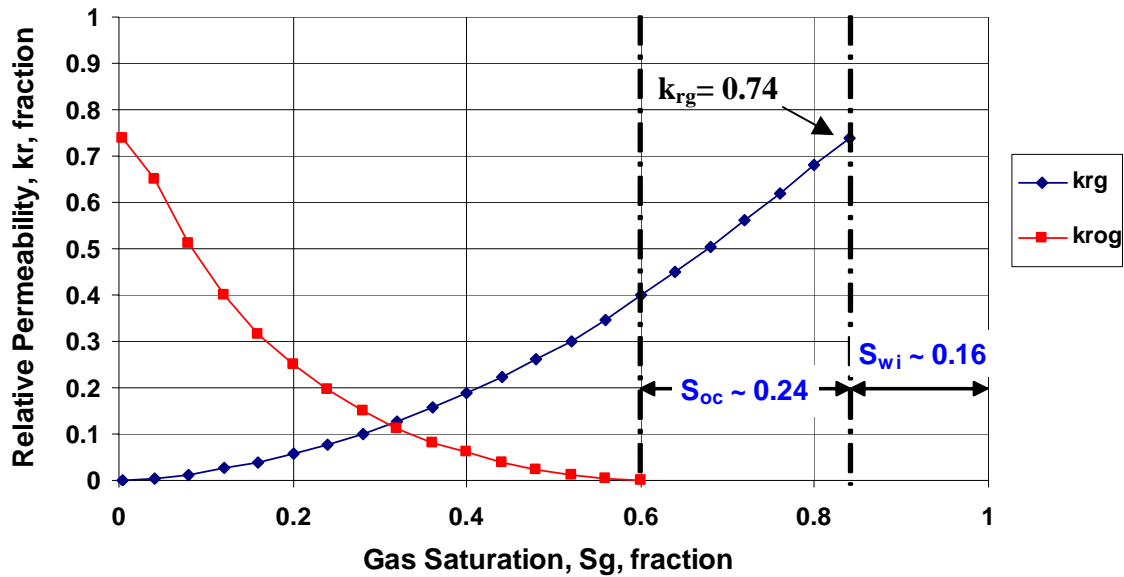


Fig. 3.2 — Gas-liquid relative permeability curves.

3.2 Case study 1: condensate damage analysis for a lean gas condensate reservoir (SPE3)

3.2.1 The SPE3 fluid model

The reservoir fluid selected for case study 1 was that from the third SPE Comparative Solution Project³. The fluid's pseudocomponents and composition are shown in **Table 3.3**. Liquid yield for the three-stage separation is 160 STB/MMscf meaning that the fluid model can be considered to be a lean gas condensate.

In the same SPE comparative project, laboratory tests were done with the compositional fluid, including constant-composition expansion (*CCE*), constant-volume depletion (*CVD*) and swelling test.

Table 3.3 – Case study 1 (SPE3) condensate fluid model

Pseudocomponents	Composition
C ₁	67.93
C ₂	9.90
C ₃	5.91
C ₄	5.17
C ₅	2.69
C ₆	1.81
C ₇ – C ₉	3.99
C ₁₀ – C ₁₁	1.22
C ₁₂ – C ₁₄	0.80
C ₁₅ ⁺	0.58
	100.00

Of relevance to this work is the constant-volume depletion test, and **Fig. 3.3** shows that there is liquid dropout. With laboratory conditions at 200°F, at pressures below the dewpoint of 3,500 psi, there is condensation until about 2,300 psi, beyond which revaporization starts to occur. The revaporization starts at $S_o/(S_o+S_g)$ ratio of about 20%. With the water saturation included, the corresponding oil saturation is approximately

17%. This test gives an idea of what to expect in the simulation results, but does not predict what actually happens in the reservoir.

- SPE 3 Lab data
CVD at 200°F

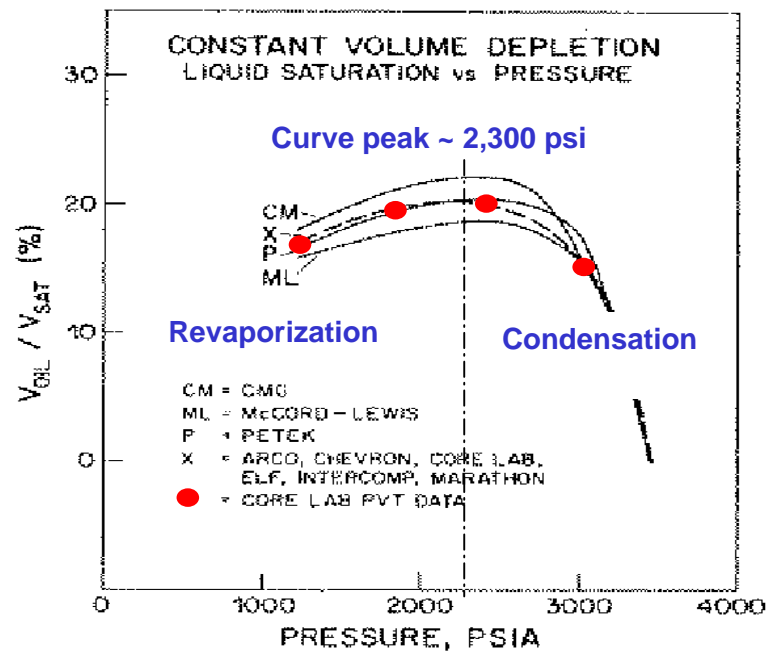


Fig. 3.3 — Constant-volume depletion test after SPE3⁵.

3.2.2 Simulation results

The simulations were done over a 15-year period, with the producer operating at different constant flowing bottomhole pressures (p_{wf}) of 3,500 psi; 3,000 psi; 2,500 psi; 2,000 psi; 1,500 psi; and 1,000 psi. Dewpoint pressure, reservoir temperature and total

compressibility used in simulator are 3,500 psi, 200 °F and 1.0176E-04 psi⁻¹ respectively. Compositional simulation runs were made using CMG, and the results are presented in **Figs. 3.4** and **3.5**.

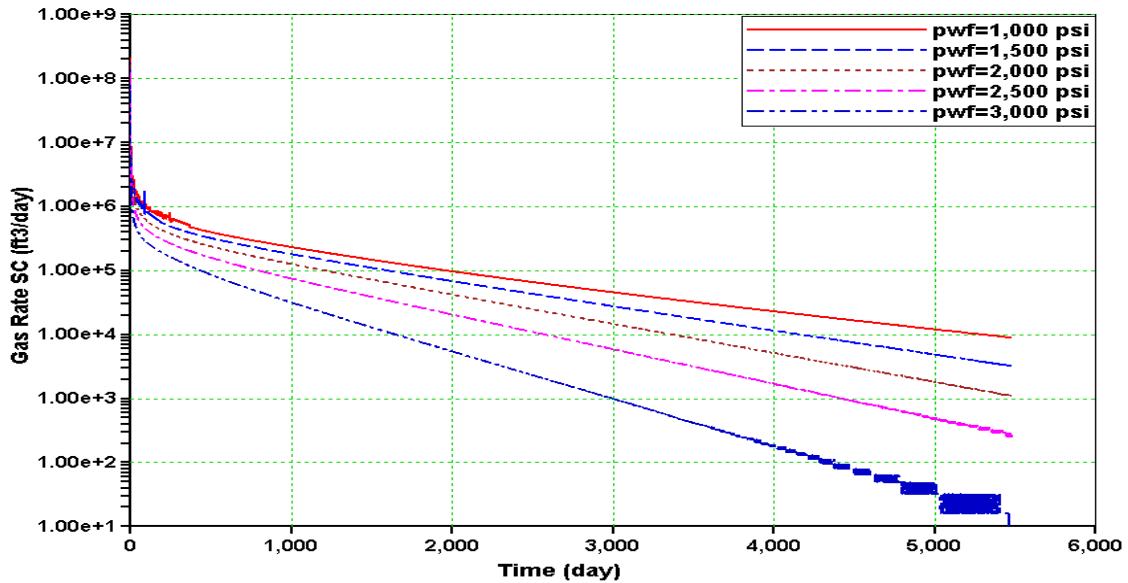


Fig 3.4 — Gas rate plots for case study 1 (SPE3) at different p_{wf} .

The schematic in **Fig. 3.4** shows that the more flowing bottomhole pressure decreases, the higher gas rate is obtained. **Fig. 3.5** also shows that the most cumulative production occurs for p_{wf} of 1,000 psi, and the least is when p_{wf} is at 3,000 psi. What we usually expect to see from a gas condensate reservoir behavior is that at a particular p_{wf} , more reduction in p_{wf} doesn't result in more gas production rate and leads to more liquid dropout, thereby decrease in well productivity. But the simulation results shown in **Figs. 3.4** and **3.5** reveal that condensate damage, if there is, does not have a dramatic effect on productivity.

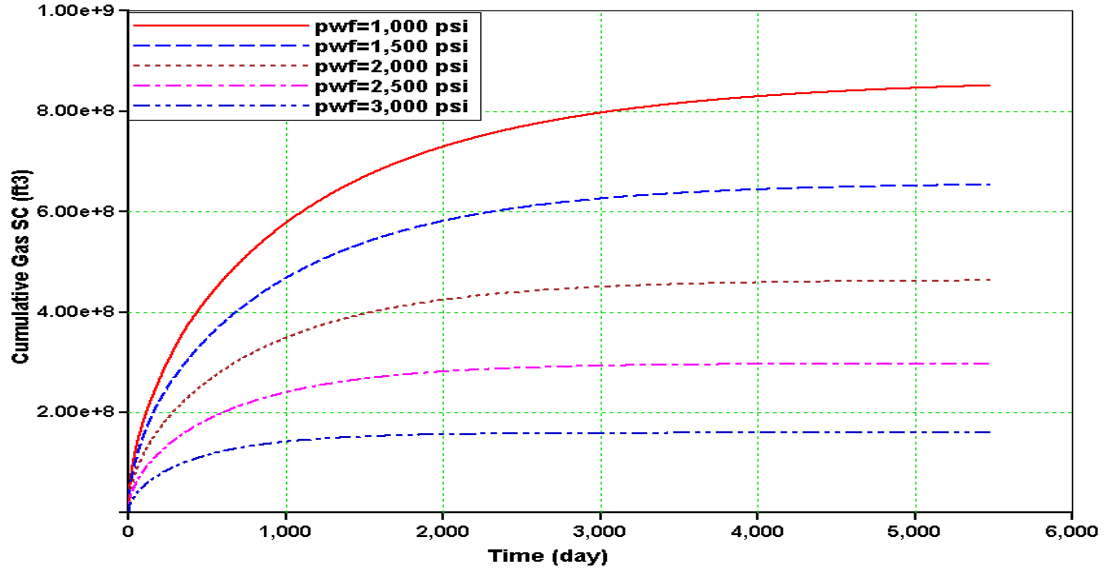


Fig 3.5 — Cumulative gas production plots for case study 1 (SPE3) at different flowing bottomhole pressures.

3.2.3 Damage effects

In the previous section, it was seen that production rate and cumulative production is not affected by the condensate damage. In order to investigate the liquid blocking effect, the gas relative permeability profile and gas and liquid saturation profiles are given in **Figs. 3.6–3.8**. The schematic in **Fig. 3.6** shows that in the near-wellbore region, gas relative permeability has reduced by half. It also shows that when boundary-dominated flow begins, after 699 days; gas relative permeability in the whole reservoir decrease dramatically. Reduction in gas saturation and increase in condensate saturation near the wellbore and at late times in the whole reservoir confirm the existence of the condensate damage in this case study.

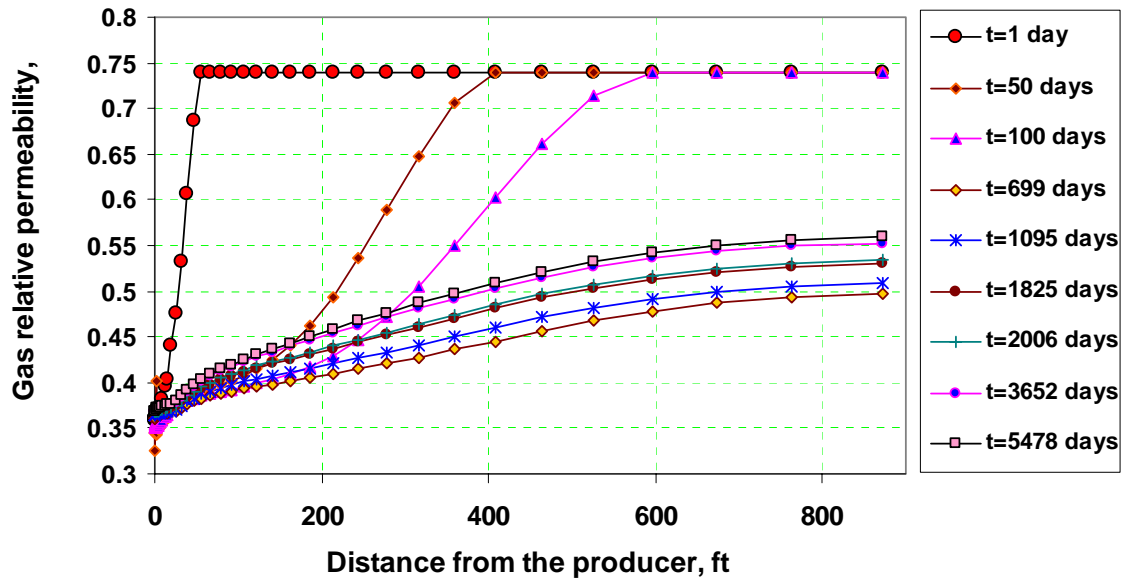


Fig 3.6 — Gas relative permeability profiles for case study 1 (SPE3) with p_{wf} at 1,000 psi.

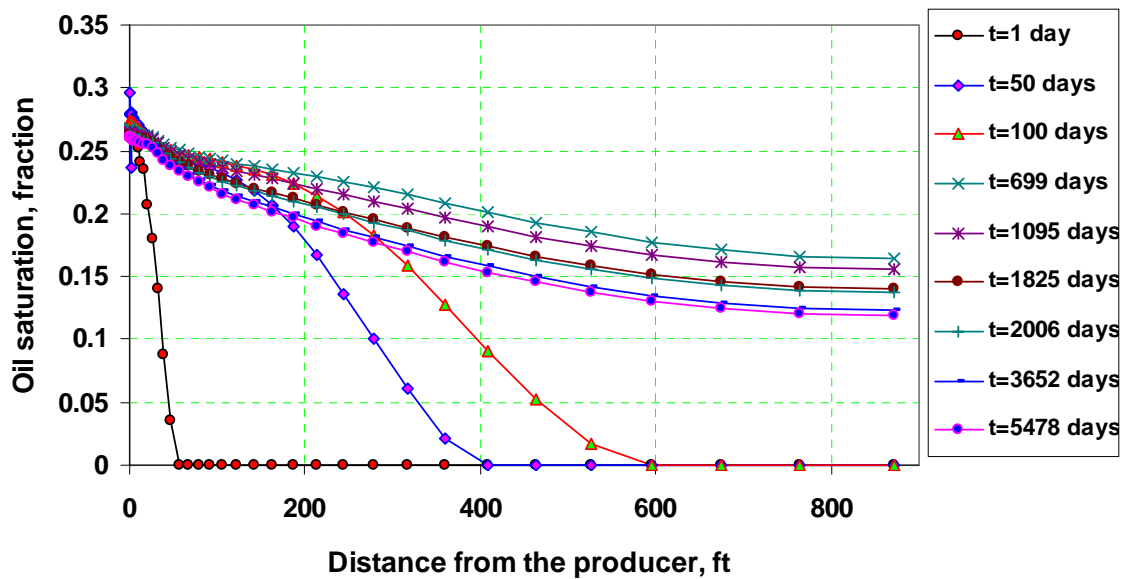


Fig 3.7 — Oil saturation profiles for case study 1 (SPE3) with p_{wf} at 1,000 psi.

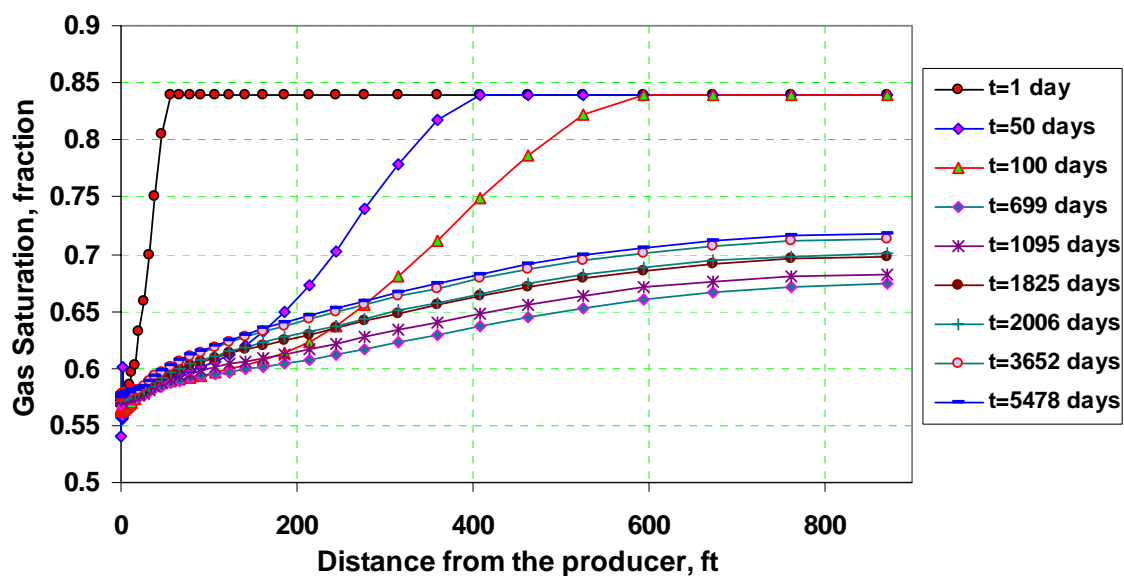


Fig 3.8 — Gas saturation profiles for case study 1 (SPE3) with p_{wf} at 1,000 psi.

In order to better understand the gas condensate damage effect in this case study, the undamaged case was made by changing the gas-liquid relative permeability table. Since the observed gas saturations in this case study range from 0.55 to 0.84, **Fig. 3.8**, only the corresponding gas relative permeability values are changed so that gas flows with initial relative permeability, **Fig. 3.9**. The schematics in **Figs. 3.10** and **3.11** compare the gas rate behavior and cumulative production of the damaged case with those of the undamaged case for SPE3 case study with p_{wf} at 1,000 psi. They also show that at early times the production rate of the undamaged case is much higher than that of the damaged case resulting in more cumulative production. After about 1,000 days, since the undamaged case has produced more, the reservoir pressure is less and the gas rate decreases to a value less than the damaged case gas rate. It is evident from these plots that condensate damage has a considerable effect on production rate and gas recovery.

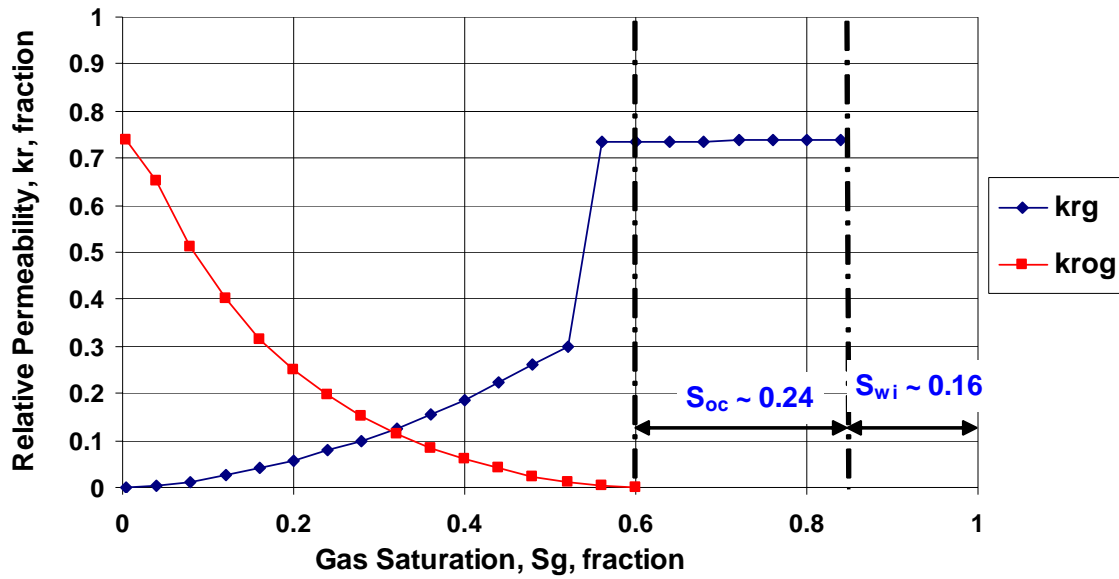


Fig 3.9 — Gas-liquid relative permeability curves for undamaged SPE3 case.

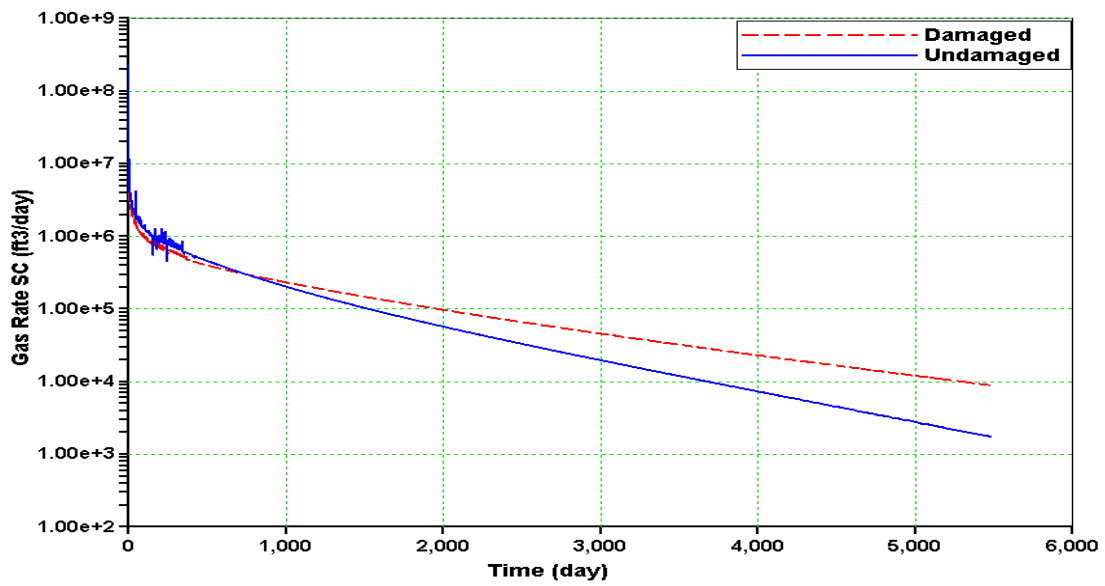


Fig 3.10 — Comparison between the damaged case gas rate and undamaged case one for case study 1 with p_{wf} at 1,000 psi.

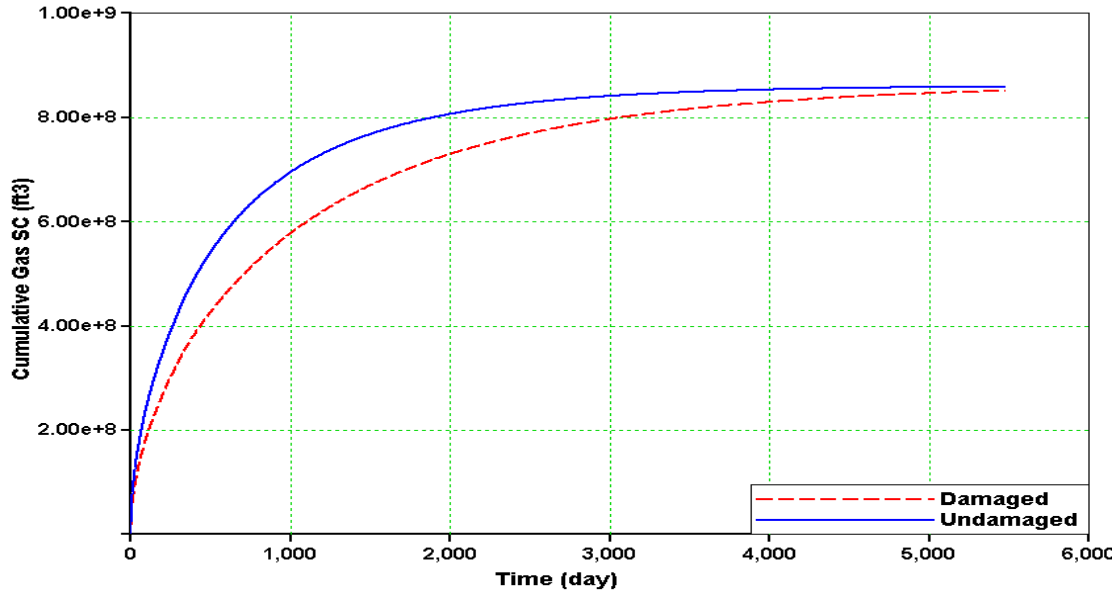


Fig 3.11 — Comparison between the damaged case cumulative production and undamaged case one for case study 1 with p_{wf} at 1,000 psi.

The simulation results of this case study reveal that for a linear lean-gas condensate reservoir producing at constant p_{wf} , although condensate damage has considerable effect on production rate, reduction in p_{wf} results in higher production rate.

3.3 Case study 2: condensate damage analysis for a rich gas condensate reservoir

3.3.1 The fluid model of case study 2

The reservoir fluid selected for case study 2 was that from Ref. 4. The fluid's pseudocomponents and composition are shown in **Table 3.4**. Liquid yield for the three-

stage separation is 347.4 STB/MMscf meaning that the fluid model can be considered to be a very rich gas condensate.

Since for this fluid only constant-composition expansion (*CCE*) test data are available, the *EOS* was tuned by using this data (See Appendix E for data files). **Figs. 3.12–3.14** show the regression summary resulted from *PVT* match by using Winprop, the *PVT* package of CMG ³⁸.

Table 3.4 — Case study 2 condensate fluid model

Pseudocomponents	Composition
N ₂ -C ₁	0.5141
C ₀₂ -C ₂	0.1373
C ₃	0.0759
IC ₄	0.0638
IC ₅	0.0431
FC ₆	0.0592
C ₇ +	0.1066
	1.0000

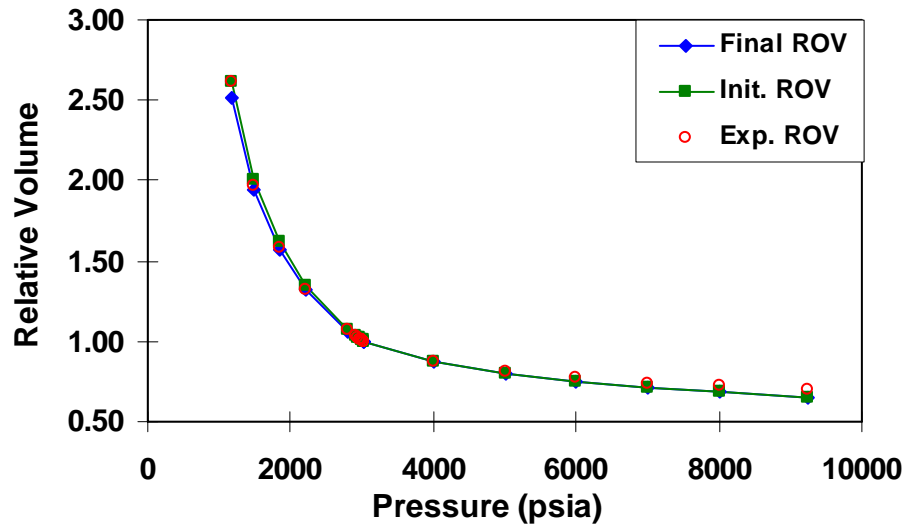


Fig 3.12 — *PVT* match between experimental relative volumes and calculated ones for case study 2.

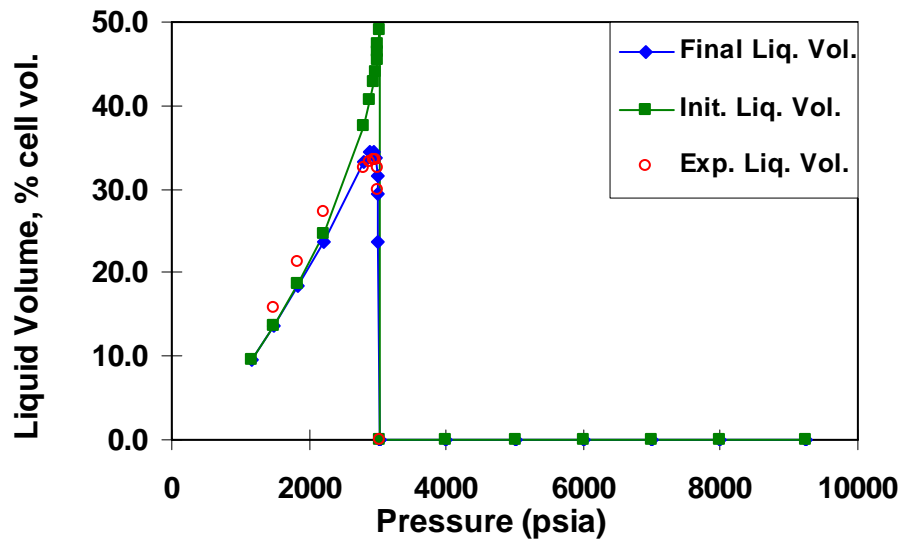


Fig 3.13 — *PVT* match between experimental volume percent liquid and calculated one for case study 2.

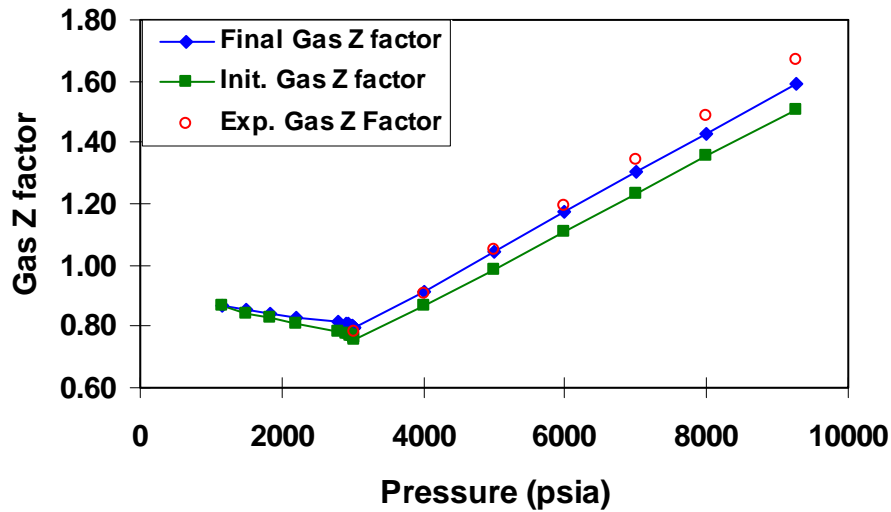


Fig 3.14 — PVT match between experimental Gas Z-factor and calculated one for case study 2.

3.3.2 Simulation results

The simulations were done over a 22-year period, with the producer operating at different constant flowing bottomhole pressures (p_{wf}) of 3,500 psi; 3,000 psi; 2,500 psi; 2,000 psi; 1,500 psi; and 1,000 psi. Dewpoint pressure, reservoir temperature and total compressibility used in simulator are 3,115 psi, 335 °F and $1.07224E-04 \text{ psi}^{-1}$ respectively. Compositional simulation runs were made using CMG, and the results are presented in **Figs. 3.15** and **3.16**.

The schematic in **Fig. 3.15** shows that the more flowing bottomhole pressure decreases, the higher gas rate is obtained. **Fig. 3.16** also shows that the most cumulative production occurs for p_{wf} of 1,000 psi, and the least is when p_{wf} is at 3,000 psi. The simulation results show that even for a linear rich-gas condensate reservoir producing at constant p_{wf} , reduction in p_{wf} will result in more production rate and gas recovery.

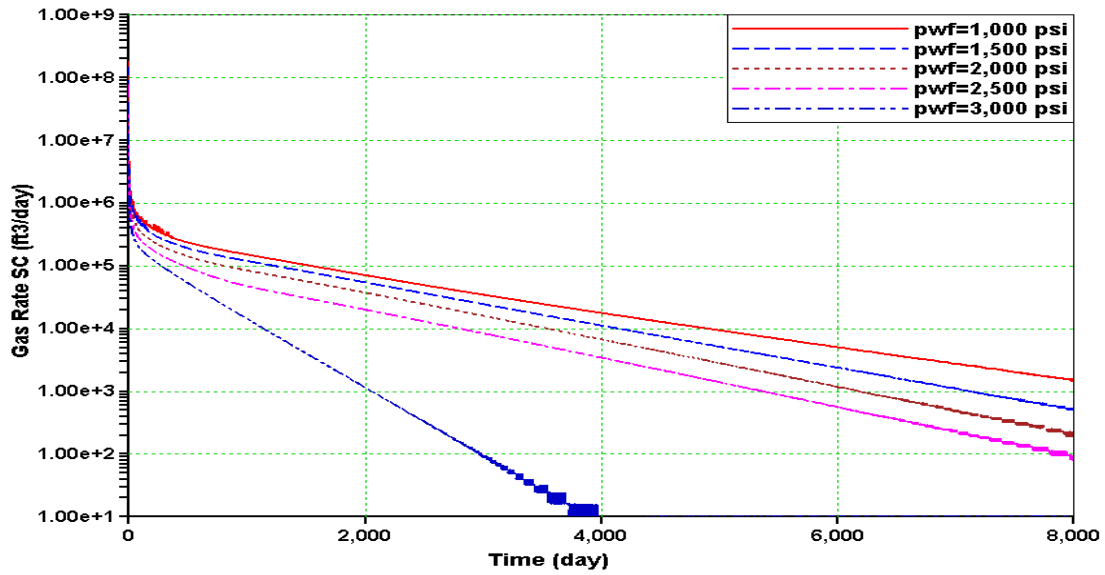


Fig 3.15 — Gas rate plots for case study 2 at different p_{wf} .

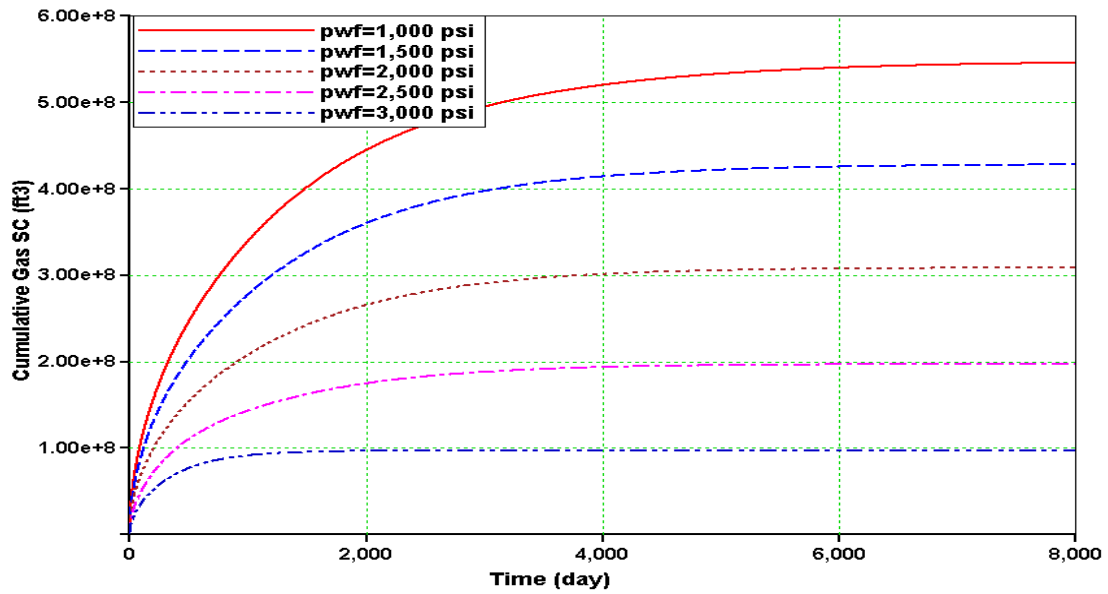


Fig 3.16 — Cumulative gas production plots for case study 2 at different p_{wf} .

3.3.3 Damage effects

In the previous section, it was seen that production rate and cumulative production is not affected by the condensate damage. In order to investigate the liquid blocking effect, the gas relative permeability profile and gas and liquid saturation profiles are given in **Figs. 3.17–3.19**. The schematic in **Fig. 3.17** shows that in the near-wellbore region, gas relative permeability has reduced by half. It also shows that when boundary-dominated flow begins, after 699 days; gas relative permeability in the whole reservoir decrease dramatically. Since the simulation results in transient period are unstable, they are not shown on these plots. Reduction in gas saturation and increase in condensate saturation near the wellbore and at late times in the whole reservoir confirm the existence of the condensate damage in this case study.

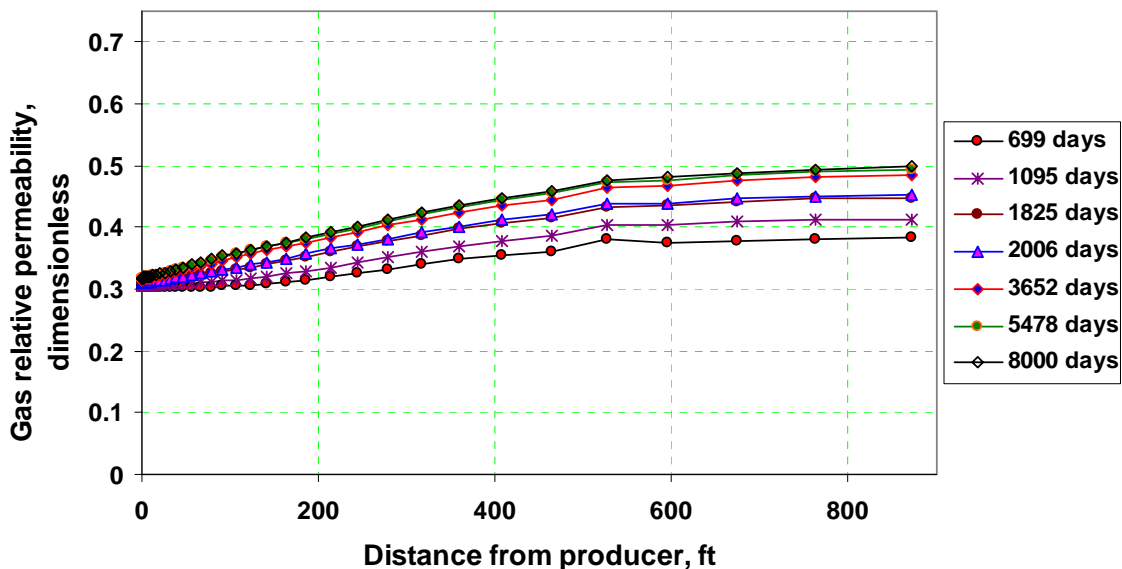


Fig 3.17 — Gas relative permeability profiles for case study 2 with p_{wf} at 1,000 psi.

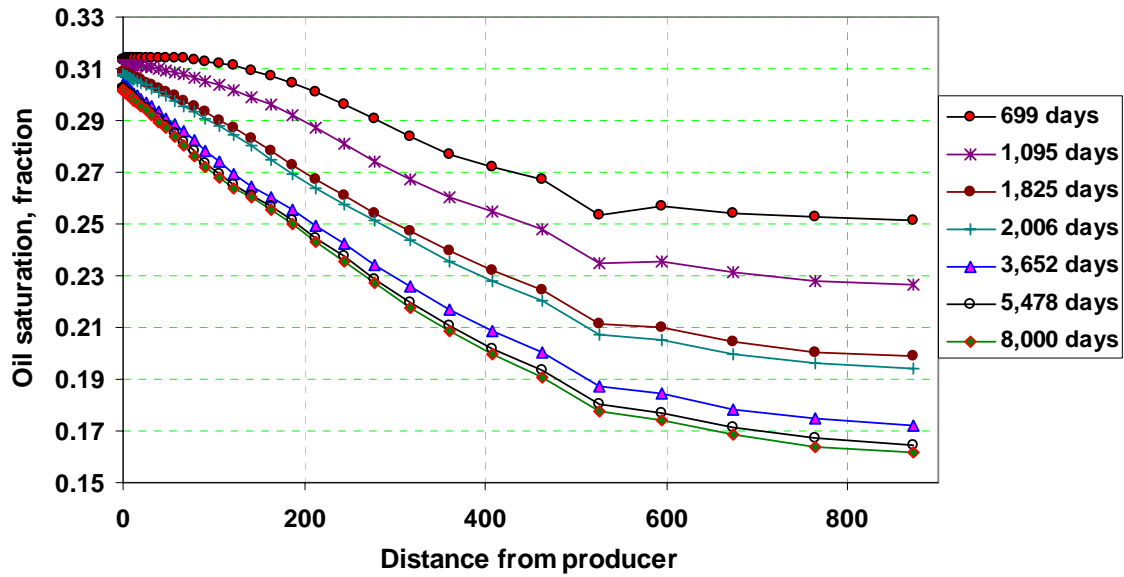


Fig 3.18 — Oil saturation profiles for case study 2 with p_{wf} at 1,000 psi.

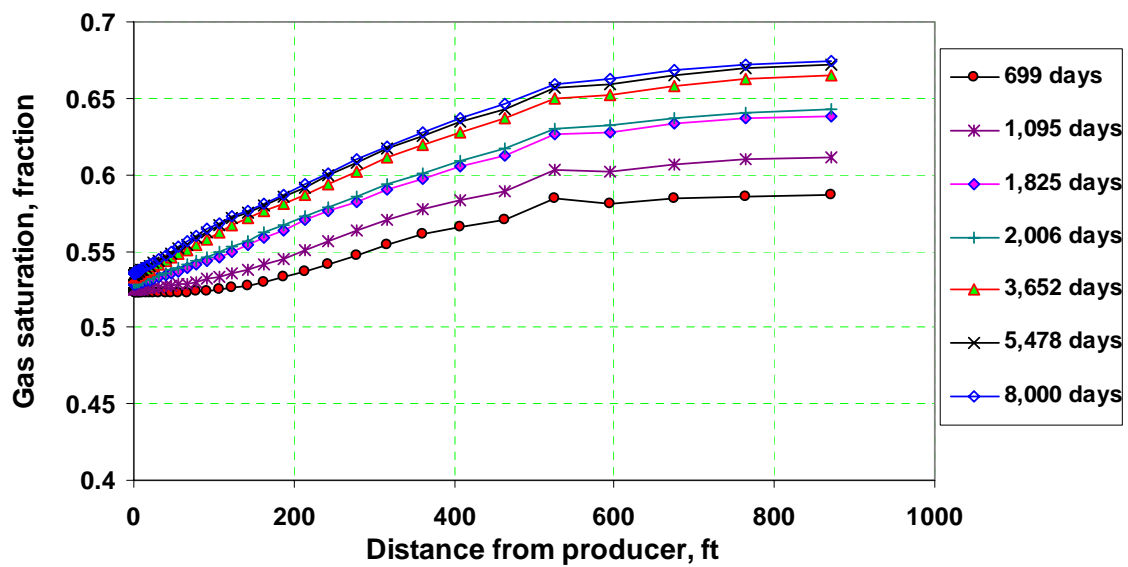


Fig 3.19 — Gas saturation profiles for case study 2 with p_{wf} at 1,000 psi.

The simulation results for a linear gas condensate reservoir producing at constant p_{wf} show that even though, the condensate damage has decreased the gas relative permeability in the near-wellbore region by half, the damage does not stop the cumulative gas production from being the largest. So, the optimum drawdown resulting in most production is when p_{wf} is the lowest.

CHAPTER IV

SIMULATION OF CONDENSATE DAMAGE IN A 2D-MODEL

Tight gas condensate reservoirs including infinite conductivity hydraulic fractures which may extend to the drainage boundary of the well stay in the linear flow regime for a long time. In the previous chapter it was shown that in these reservoirs reduction in p_{wf} results in higher gas production rate, although the condensate damage happens in the whole reservoir and particularly in the near-wellbore region.

This chapter studies the long-term performance of hydraulically fractured gas condensate reservoirs when the hydraulic fracture has infinite conductivity and the reservoir is partially penetrated by the fracture. Three case studies are presented with different aspect ratios (x_e/x_f) of 2, 10 and 100.

4.1 Reservoir description

The reservoir characteristics of third SPE Comparative Solution Project³ were used to develop a 2D-areal model for simulation. **Table 4.1** summarizes the fundamental characteristics of the reservoir. According to the information presented in **Table 4.1**, the dimensions of the linear model are 933 ft in the x and y directions and 50 ft in z direction. These dimensions along with an average porosity of 13% represent the initial gas reservoir volume in the symmetric quarter of an 80 acres drainage area. The model was divided into 220 grid blocks, 20 in the x direction, 11 in the y direction, and 1 in the z direction. In each case study, the number of grids in the x , y and z directions are constant, but the grid sizes are different. **Fig. 4.1** shows the configuration of a 2D model in CMG. In order to get the total gas production rate the reservoir thickness was multiplied by 4. The base saturation-relative permeability tables and selected reservoir fluid used were those reported in the data file adopted from CMG sample data related to third SPE Comparative Solution Project³.

Table 4.1 – Main characteristics of the 2D reservoir model

Reservoir Characteristic	Values
Drainage Area, Acres	~ 80
Reservoir Half Length (x_e), ft	933.381
Reservoir Half Length (y_e), ft	933.381
Thickness (h), ft	50
Absolute permeability (k), md	0.03
Porosity (ϕ), fraction	0.13
Water Saturation (S_w), fraction	0.16
Initial Pressure (p_i), psi	3,900
Dewpoint Pressure (p_d), psi	3,500
Temperature (T), °F	200
Total Compressibility (c_i), psi^{-1}	1.0176E-04

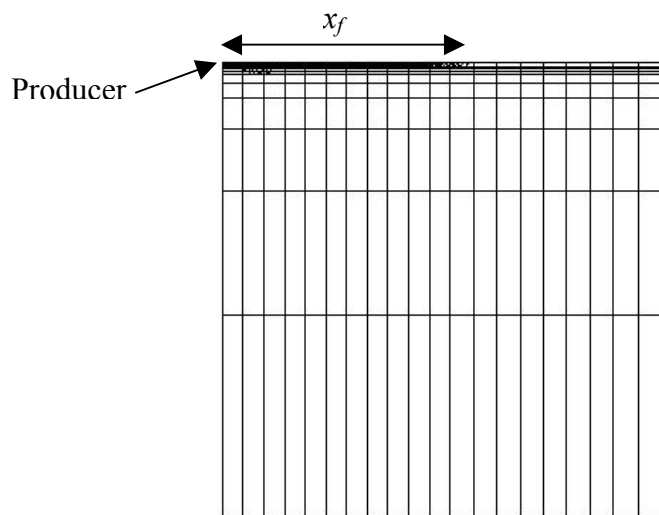


Fig. 4.1 – Schematic of a 2D-areal model with hydraulic fracture.

Since only one quadrant of the drainage area was modeled, the permeability and porosity values of the first row and the first column were modified to keep the total pore volume constant. The summary of data modification has been shown in **Fig. 4.2**.

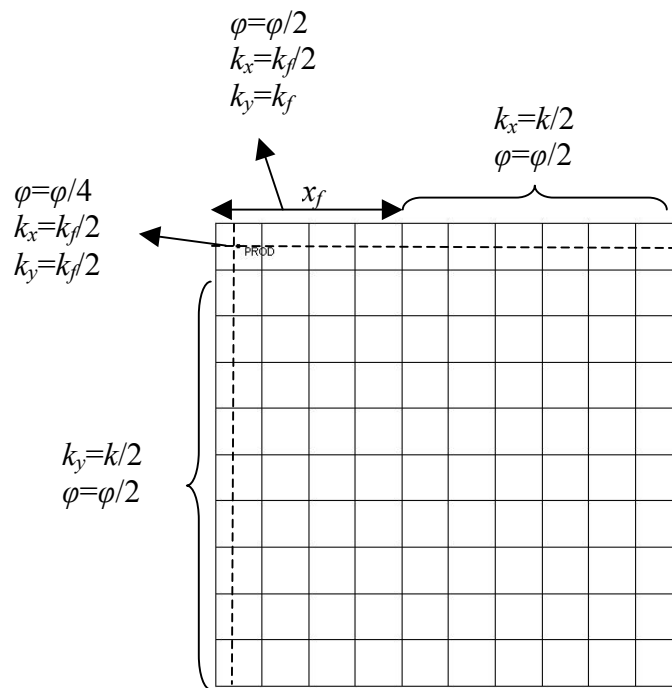


Fig. 4.2 — schematic of a 2D-areal model with data modification.

4.2 Simulation results

The simulations were done over a 15-year period, with the producer operating at different constant flowing bottomhole pressures (p_{wf}) of 3,500 psi; 3,000 psi; 2,500 psi; 2,000 psi; 1,500 psi; and 1,000 psi. Since in each case, fracture half length has different

values, other fracture parameters have been changed so that the dimensionless fracture conductivity, F_{CD} remains constant. **Table 4.2** summarizes the model specifications used in each case. During the study, it was found that the fracture width has to be a relatively large value to make the compositional simulation run possible. **Table 4.2** shows that in all three cases the fracture width of 10 ft was used (See Appendix E for data files). To compensate the effect of large fracture width, other fracture parameters were selected so that the fracture has infinite conductivity ($F_{CD} > 50$). Compositional simulation runs were made using CMG, and the results are presented in **Figs. 4.3–4.8**. These figures show that even for aspect ratios greater than one, any decrease in flowing bottomhole pressure will result in more gas production rate and more cumulative production. They also show that the shorter hydraulic fracture is, the less cumulative production was observed, **Figs. 4.9** and **4.10**. This is probably because in models with shorter fractures, the flow area is smaller.

Table 4.2 — Main fracture parameters used in each case for 2D model

Model Properties	$x_e/x_f=2$	$x_e/x_f=10$	$x_e/x_f=100$
Fracture Width (w), ft	10	10	10
Fracture Half Length (x_f), ft	466.6905	93.3381	9.33381
Fracture Permeability (k_f), md	100	20	2
Reservoir Permeability (k), md	0.03	0.03	0.03
No. of Gridblocks in X-Direction	20	20	20
No. of Gridblocks in Y-Direction	11	11	11
Fracture Conductivity (F_{CD})	71.42	71.42	71.42

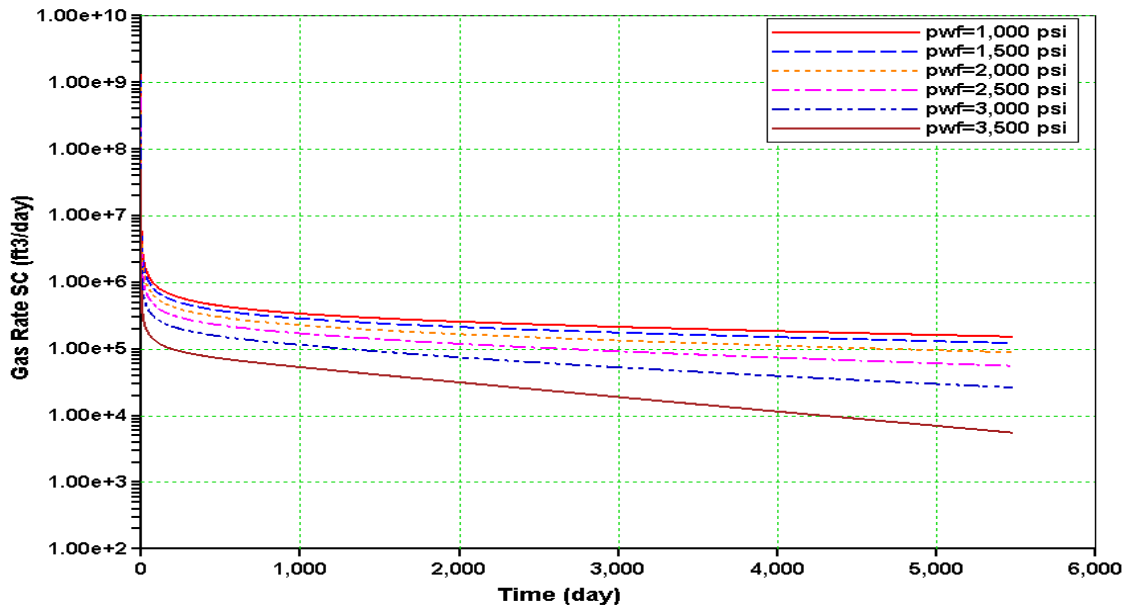


Fig. 4.3 — Gas production rates for a 2D-model with $x_e/x_f=2$ at different p_{wf} .

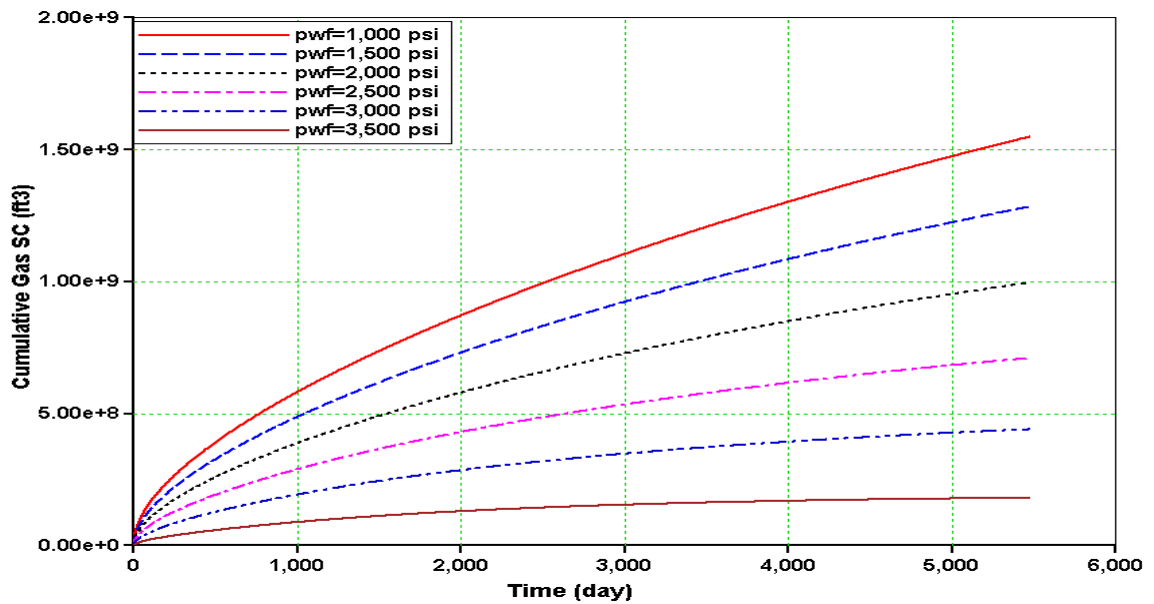


Fig. 4.4 — Cumulative gas productions for a 2D-model with $x_e/x_f=2$ at different p_{wf} .

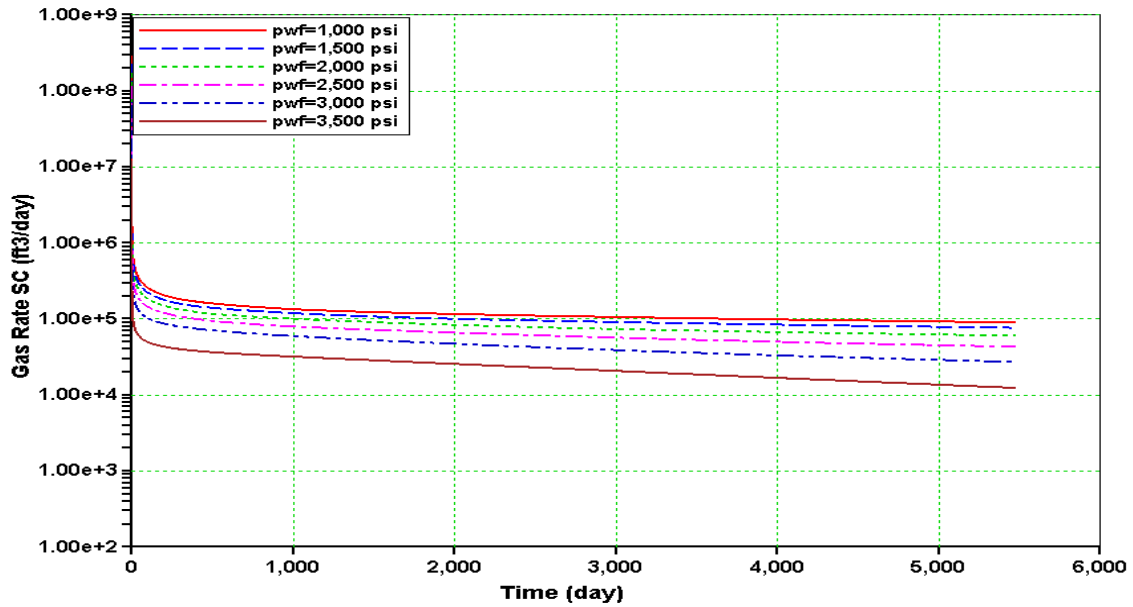


Fig. 4.5 — Gas production rates for a 2D-model with $x_e/x_f=10$ at different p_{wf} .

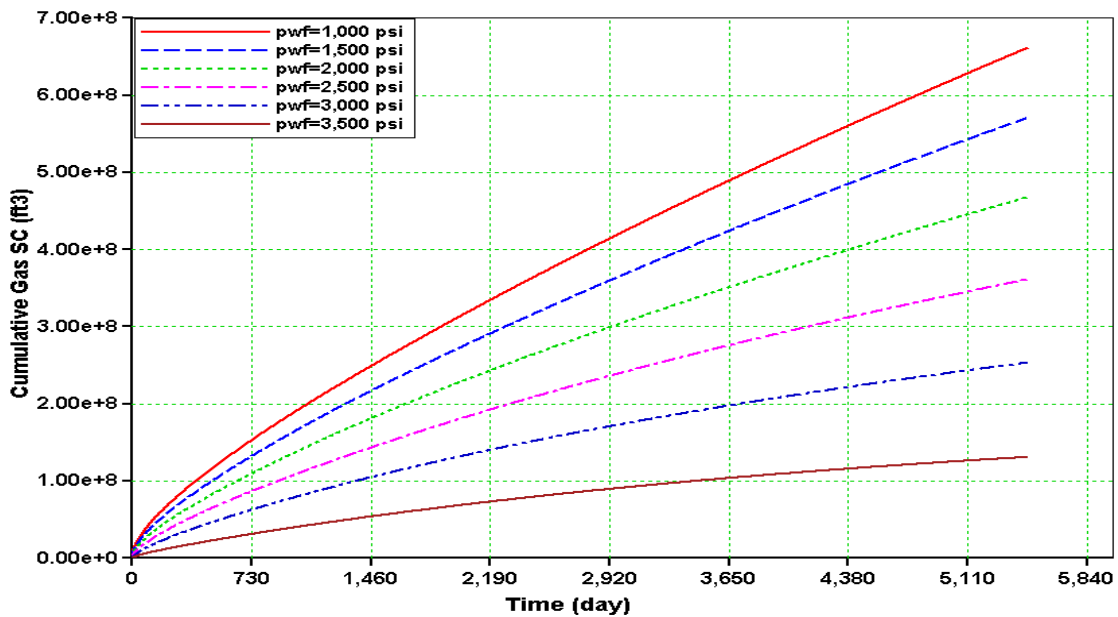


Fig. 4.6 — Cumulative gas productions for a 2D-model with $x_e/x_f=10$ at different p_{wf} .

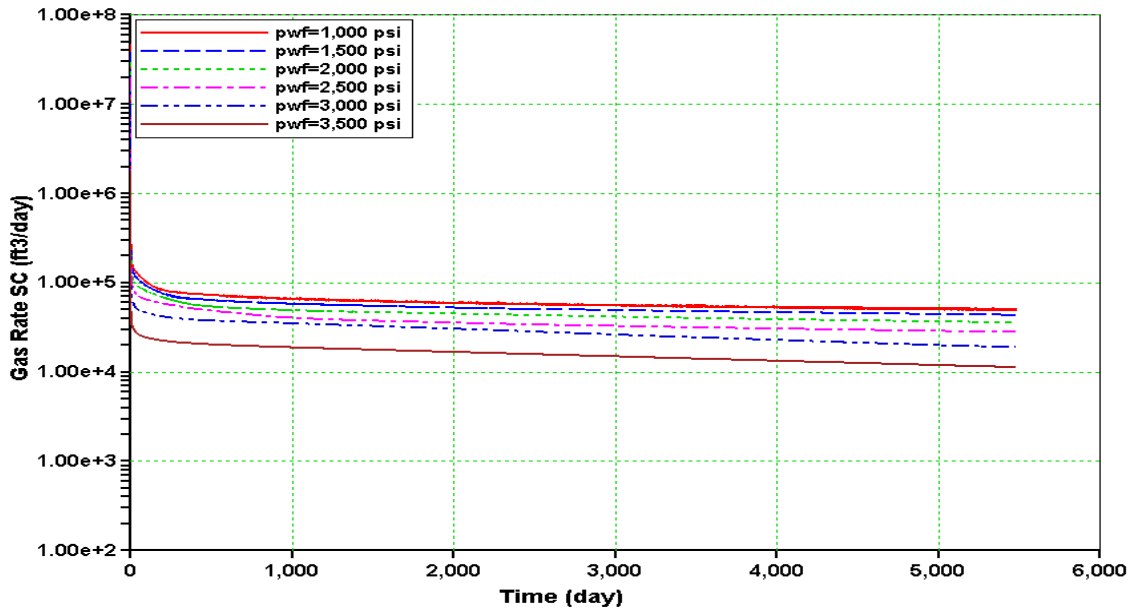


Fig. 4.7 — Gas production rates for a 2D-model with $x_e/x_f=100$ at different p_{wf} .

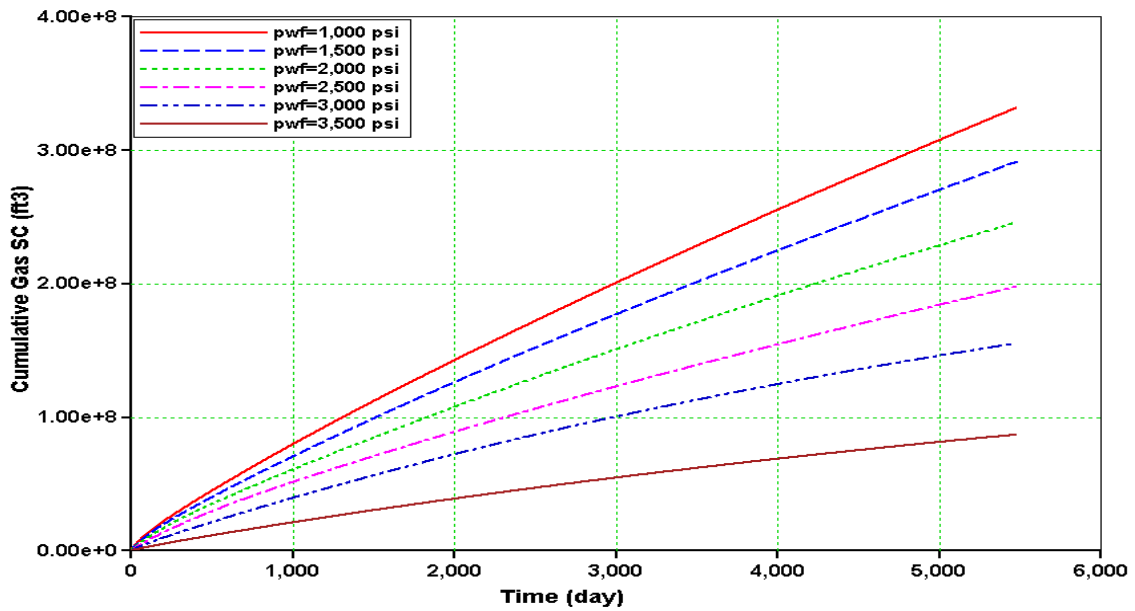


Fig. 4.8 — Cumulative gas productions for a 2D-model with $x_e/x_f=100$ at different p_{wf} .

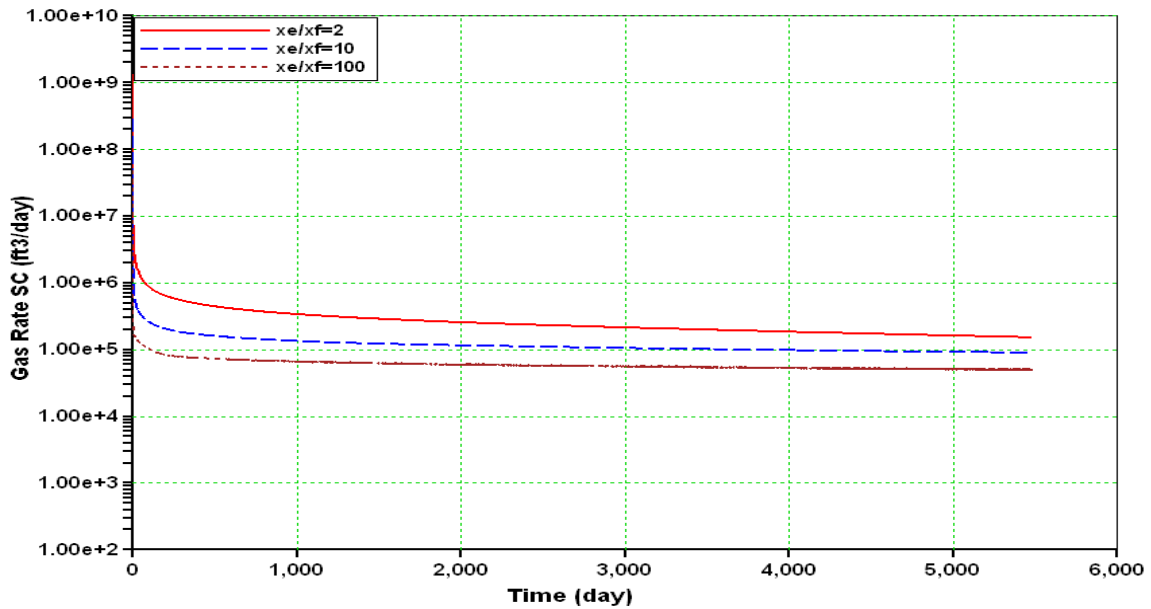


Fig. 4.9 — Comparison of gas production rates for a 2D-model with p_{wf} at 1,000 psi and with different fracture lengths.

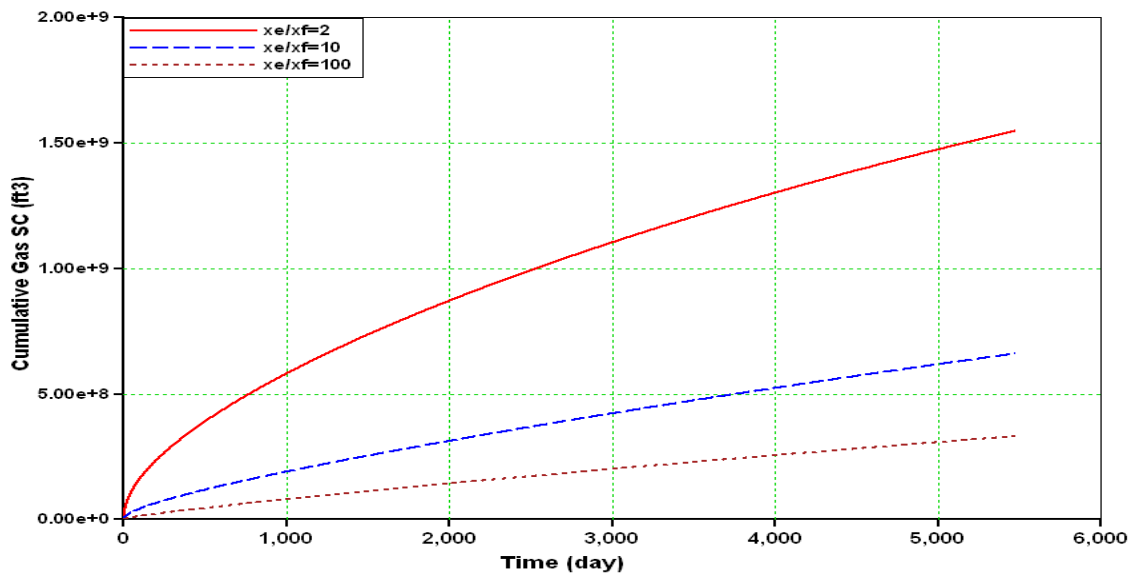


Fig. 4.10 — Comparison of cumulative gas productions for a 2D-model with p_{wf} at 1,000 psi and with different fracture lengths.

The study conducted in this chapter shows that in a 2D gas condensate reservoir with hydraulic fracture shorter than the reservoir extension, the optimum drawdown resulting in most production is when p_{wf} is the lowest. The summary and conclusions are made in the next chapter.

CHAPTER V

DISCUSSION AND CONCLUSIONS

5.1 Discussion

This work is a result of a problem encountered in producing Smith #1, a hydraulically fractured well owned by El Paso Production Company. The well was producing a tight gas condensate reservoir and the flowing bottomhole pressure, p_{wf} , was above the dewpoint pressure. They were concerned about what would happen if p_{wf} dropped below the dewpoint pressure. It was observed in the field that the more p_{wf} was lowered below the dewpoint pressure, the higher gas rate was obtained.

The study in this work used a linear model representing the linear flow of gas condensate from the formation into the hydraulic fracture. Since the actual field data was not available, the reservoir and fluid properties were taken from Refs. 3 and 4. The relative permeability data used in this study were taken from Ref. 3. Relative permeability data were based on the simplistic assumption that the relative permeability of any phase depends only on its own saturation. It has been shown by many authors that relative permeability to gas data is the most sensitive parameter for predicting gas condensate well productivity. Hinchman and Barree¹⁹ showed that the conventional drainage relative permeability data results in a more pessimistic production decline prediction. The actual liquid condensation in the reservoir is better represented by imbibition relative permeability resulting in lower productivity loss predictions. It also have been shown that the productivity index of a gas condensate well is affected by changes in relative permeability due to *IFT*, gravity and flow rate (modeled based on capillary number). Narayanaswamy *et al.*³⁹ showed that when capillary number effects are considered, high capillary numbers seen in the near wellbore region can significantly reduce condensate saturation and increase gas relative permeability resulting in productivity greater than when capillary number effects are not considered. They also

showed that accurate measurement of the critical condensate saturation and endpoint relative permeabilities at various capillary numbers is very important for accurate prediction of the productivity index.

Although the data used in this study are not the actual field data, the simulation results verify what was observed in the field. It has been seen the same kind of problem in other places when reduction in p_{wf} below the dewpoint pressure does not lead to increase in production rate. For instance, there have been three hydraulically fractured wells in a gas condensate reservoir in Saudi Arabia in which condensate damage along the hydraulic fracture resulted from decrease in p_{wf} below dewpoint pressure ruined the wells completely and they are not producing any more. So, in this case, having a model with actual field data which takes into account a proper relative permeability data including the variation of IFT , gravity and flow rate expressed as capillary number is essential.

5.2 Conclusions

The following main conclusions can be drawn from this work:

1. Single-phase damage analysis shows that for a linear reservoir producing at constant rate conditions, s_{ff} is additive to the analytical solutions. It also shows that s_{ff} calculated in transient and p_{ss} periods are identical to that calculated by using Cinco and Samaniego equation.
2. The same analysis for the constant p_{wf} case assuming that the s_{ff} is additive to the analytical solutions shows that the calculated skin in transient period changes with time. It also shows that the skin calculated in p_{ss} period agrees with the one calculated by using Cinco and Samaniego equation. The calculated skin values are small, because the reciprocal of dimensionless rates have small values, and the difference between two small values will result in a small skin, although the numerical dimensionless rate value is half the analytical one.
3. The gas condensate damage analysis shows that assuming the infinite conductivity hydraulic fracture which extends to the entire drainage boundary of

the well, the linear flow is impaired by condensate blocking and the flow impairment is worse in near-wellbore region.

4. The main conclusion of this work from gas condensate damage analysis is that the optimum drawdown corresponds to the lowest p_{wf} giving the largest cumulative gas production at any time. The condensate damage does not prevent the lowest drawdown, $p_{wf} = 1,000$ psi, from producing the highest cumulative gas.
5. The analysis on various fluids shows that even for the case of a very rich gas condensate, the optimum drawdown corresponds to the lowest p_{wf} .
6. For a gas condensate reservoir with infinite conductivity fracture which partially penetrates the reservoir, any decrease in flowing bottomhole pressure will result in more gas production rate and more cumulative production.
7. Gas condensate reservoirs with longer fractures will result in higher rates and cumulative production compared to those with shorter fractures.

5.3 Recommendations for future work

In field operations, optimum drawdown depends on the economics of the project and the environmental conditions surrounding the project. This work done in this project uses idealized field data in its study, and therefore it will be helpful to do the same work with actual field data, to see if similar conclusions can be reached. Future work should consider cases where capillary numbers are considered and capillary number dependent relative permeabilities and/or imbibition relative permeability data are used.

NOMENCLATURE

A	Drainage area, $L^2\text{-ft}^2$
A_C	Cross sectional area, L^2 , ft^2
B	FVF, dimensionless, rb/STB
B_o	Oil formation volume factor, rb/STB
C	Specific capacity, $Q/M/\nu$ (Carslaw and Jaeger)
c_g	Gas compressibility, L^2/m , psia^{-1}
c_t	total compressibility, L^2/m , psia^{-1}
f	Rate of heat flow per unit time per unit area, $Q/A/T$ (Carslaw and Jaeger)
F_o	Heat flow rate, $Q/A/T$ (Carslaw and Jaeger)
F_{cD}	Dimensionless fracture conductivity
h	Net formation thickness, L , ft
J	productivity index, $L^3/\text{t/m/Lt}^2$, STB/D-psia
J_{model}	Well index, md-ft
K	Heat conductivity, $Q/L/T/\nu$ (Carslaw and Jaeger)
κ	Diffusivity of the substance, L^2 / T , ft^2/hr (Carslaw and Jaeger)
k	permeability, L^2 , md
k_g	Effective gas permeability, L^2 , md
k_{rog}	Oil relative permeability, fraction
k_{rg}	Gas relative permeability, fraction
k_s	Damaged zone permeability, L^2 , md
k_x	Reservoir permeability in x direction, L^2 , md
k_y	Reservoir permeability in y direction, L^2 , md
k_f	Fracture permeability, L^2 , md
λ	Reservoir length in Y direction, L , ft
N_p	Cumulative production, L^3 , STB
P	Absolute pressure, m/Lt^2 , psia
\bar{p}	Average reservoir pressure, m/Lt^2 , psia

p_D	dimensionless pressure, $\frac{k h (p_i - p)}{141.2 q B \mu}$
p_{wD}	dimensionless pressure, $\frac{k h (p_i - p_{wf})}{141.2 q B \mu}$
p_{wf}	bottom-hole flowing pressure, m/Lt ² , psia
p_i	Initial reservoir pressure, m/Lt ² , psia
p_{cell}	Cell pressure, m/Lt ² , psia
p_e	Reservoir pressure at the boundary, m/Lt ² , psia
Δp	Pressure difference, m/Lt ² , psia
Q	Heat, cal (Carslaw and Jaeger)
q	Flow rate, RB/D
q_D	Dimensionless flow rate
q_o	Oil production rate, STB/D
r_w	Wellbore radius, L ,ft
r_s	Damaged zone radius, L , ft
s	Skin factor, dimensionless
s_{ff}	Fracture face skin, dimensionless
S_{cc}	Critical condensate saturation, fraction
S_{oc}	Critical oil saturation, fraction
T	Temperature, °F
t	Producing time, t , days
t_D	Dimensionless time, dimensionless
t_{Dxe}	Dimensionless time based on x_e
T	Dimensionless time (Carslaw and Jaeger)
ν	Temperature, °C (Carslaw and Jaeger)
V	Temperature, °C (Carslaw and Jaeger)
V_p	Pore volume, L ³ , ft ³
w_s	Width (extent) of damage on the fracture, L, ft
x_f	Fracture half-length, L ,ft

REFERENCES

1. Indriati, S., Wang, X., and Economides, M.J.: "Adjustment of Hydraulic Fracture Design in Gas-Condensate Wells," paper SPE 73751 presented at the 2002 SPE Annual Technical Conference and Exhibition, Lafayette, LA, 20-21 February.
2. Wattenbarger, R.A., El-Banbi, A.H., Villegas, M.E., and Maggard, J.B.: "Production Analysis of Linear Flow into Fractured Tight Gas Wells," paper SPE 39931 presented at the 1998 Rocky Mountain Regional/Low-Permeability Reservoirs Symposium and Exhibition, Denver, 5-8 April.
3. Kenyon, D.E. and Behie, G.A.: "Third SPE Comparative Solution Project: Gas Cycling of Retrograde Condensate Reservoirs," *JPT* (August 1987) 981.
4. Coats, K.H.: "Simulation of Gas Condensate Reservoir Performance," *JPT* (October 1985) 1870.
5. McCain, W.D.: *Properties of Petroleum Fluids*, PennWell Publishing, Tulsa (1989).
6. Peng, D.Y. and Robinson, D.B.: "A New Two-Constant Equation of State," *Ind. Eng. Chem. Fundamentals* (1976) **15**, 15-59.
7. Soave, G.: "Equilibrium Constants From a Modified Redlich Kwong of State," *Chem. Eng. Sci.* (1972) **27**, 1197-1203.
8. Katz, D.L. and Firoozabadi, A.: "Predicting Phase Behavior of Condensate/Crude-Oil Systems Using Methane Intersection Coefficients," *JPT* (November 1978) 1649-55; *Trans., AIME*, **265**, 343-356.
9. Firoozabadi, A., Hekim, Y., and Katz, D.L.: "Reservoir Depletion Calculations for Gas Condensate Using Extended Analyses in the Peng-Robinson Equation of State," *Cdn. J. Chem. Eng.* (1978) **56**, 610-15.
10. Yarborough, L.: "Application of a Generalized Equation of State to Petroleum Reservoir Fluids," *Equation of State in Engineering*, Advances in Chemistry Series, K.C. Caho and R.L. Robinson (eds.), American Chemical Society, Washington, DC (1979) **182**, 385-435.

11. Baker, L.E. and Luks, K.D.: "Critical Point and Saturation Pressure Calculations for Multicomponent Systems," *JPT* (February 1980) 15-24.
12. Vogel, J.L. and Yarborough, L.: "The Effect of Nitrogen on the Phase Behavior and Physical Properties of Reservoir Fluids," paper SPE 8815 presented at the 1980 SPE/DOE Enhanced Oil Recovery Symposium, Tulsa, OK, 20-23 April.
13. Whitson, C.H.: "Characterizing Hydrocarbon Plus Fractions," *JPT* (August 1983) 683-94.
14. Whitson, C.H. and Torp, S.B.: "Evaluating Constant-Volume Depletion Data," *JPT* (March 1983) 683-94.
15. Peneloux, A., Jain, C., and Behar, E.: "Application of the Developed Redlich-Kowang Equation of State to Predict the Thermodynamics Properties of Condensate Gases," paper SPE 8287 presented at the 1979 SPE Annual Technical Conference and Exhibition, Las Vegas, NV, 23-26 September.
16. Williams, C.A., Zana, E.N., and Humphrys, G.E.: "Use of the Peng-Robinson Equation of State to Predict Hydrocarbon Phase Behavior and Miscibility for Fluid Displacement," paper SPE 8817 presented at the 1980 SPE/DOE Enhanced Oil Recovery Symposium, Tulsa, OK, 20-23 April.
17. Coats, K.H. and Smart, G.T.: "Application of a Regression Based EOS PVT Program to Laboratory Data," SPE 11197, *SPEREE* (May 1986) 277-299.
18. Fevang, O., Kameshwar, S., and Whitson, C.H.: "Guidelines for Choosing Compositional and Black-oil Models for Volatile Oil and Gas Condensate Reservoirs," paper SPE 63087 presented at the 2000 SPE Annual Technical Conference and Exhibition, Dallas, 1-4 October.
19. Hinchman, S. B. and Barree, R. D., "Productivity Loss in Gas Condensate Reservoirs," paper SPE 14203 presented at the 1985 SPE Annual Technical Conference and Exhibition, Las Vegas, NV, 22-25 September.
20. Barnum, R.S., Brinkman, F.P., Richardson, T.W., and Spillette, A.G.: "Gas Condensate Reservoir Behavior: Productivity and Recovery Reduction Due to

- Condensation,” paper SPE 30767 presented at the 1995 SPE Annual Technical Conference and Exhibition, Dallas, 22 – 25 October.
21. Whitson, C.H., Fevang, O., and Saevareid, A.: “Gas Condensate Relative Permeability for Well Calculations,” paper SPE 56476 presented at the 1999 SPE Annual Technical Conference and Exhibition, Houston, 3-6 October.
 22. Gringarten, A.C., Al-Lamki, A.: “Well Test Analysis in Gas-Condensate Reservoirs,” paper SPE 62920 presented at the 2000 SPE Annual Technical Conference and Exhibition, Dallas, 1-4 October.
 23. Fussel, D.D.: “Single-Well Performance Predictions for Gas Condensate Reservoirs,” *JPT* (July 1973) 860-870.
 24. Clark, T.J.: “The Application of a 2-D Compositional, Radial Model to Predict Single-Well Performance in a Rich Gas Condensate Reservoir,” paper SPE 14413 presented at the 1985 Annual Technical Conference and Exhibition, Las Vegas, NV, 22-25 September.
 25. McCain, W.D., Jr. and Alexander, R.A.: “Sampling Gas-Condensate Wells,” *SPEREE* (August 1992) 358-362.
 26. Novosad, Z.: “Composition and Phase Changes in Testing and Producing Retrograde Gas Wells,” *SPEREE* (November 1996) 231-235.
 27. Ahmed, T., Evans, J., Kwan, R., and Vivian, T.: “Wellbore Liquid Blockage in Gas-Condensate Reservoirs,” paper SPE 51050 presented at the 1998 SPE Eastern Regional Meeting, Pittsburg, PA, 9-11 November.
 28. El-Banbi, A.H., McCain, W.D. and Semmelbeck, M.E.: “Investigation of Well Productivity in Gas-Condensate Reservoirs,” paper SPE 59773 presented at the 2000 SPE/CERI Gas Technology Symposium, Calgary, 3 – 5 April.
 29. Cannan, W.L., Jennings, A.R., Huseini, S., Bordelon, T.P., Sardjono, S.: “Increasing Arun Well Deliverability Through Effective Acid Fracturing,” prepared for presentation at the 1992 SPE International Meeting on Petroleum Engineering, Beijing, 24-27 March.

30. Settari, A., Bachman, R.C., Hovem K., and Paulsen, S.G.: "Productivity of Fractured Gas Condensate Wells-A Case Study of the Smorbukk Field," paper SPE 35604 presented at the 1996 SPE Gas Technology Conference, Calgary, April 28-May 1.
31. Sognesand, S.: "Long-Term Testing of Vertically Fractured Gas Condensate Wells," paper SPE 21704 presented at the 1991 SPE Production Operations Symposium, Oklahoma City, OK, 7-9 April.
32. Hsu, H.H., Ponting, D.K., and Wood, L.: "Field-Wide Compositional Simulation for HPHT Gas Condensate Reservoirs Using an Adaptive Implicit Method," paper SPE 29948 presented at the 1995 SPE International Meeting on Petroleum Engineering, Beijing, 14-17 November.
33. Carlson, M.R., and Myer, J.W.G.: "The Effects of Retrograde Liquid Condensation on Single Well Productivity Determined via Direct (Compositional) Modeling of a Hydraulic Fracture in a Low-Permeability Reservoir," paper SPE 29561 presented at the 1995 SPE Rocky Mountain Regional/Low-Permeability Reservoirs Symposium, Denver, 20-22 March.
34. Afdick, D., Kaczorowski, N.J., and Bette, S.: "Production Performance of a Retrograde Gas Reservoir: A Case Study of the Arun Field," paper SPE 28749 presented at the 1994 SPE Asia Pacific Oil and Gas Conference, Melbourne, 7-10 November.
35. Al-Hashim, H.S., and Hashmi, S.S.: "Long-Term Performance of Hydraulically Fractured Layered Rich Gas Condensate Reservoir," paper SPE 64774 presented at the 2000 SPE International Oil and Gas Conference and Exhibition, Beijing, 7 – 10 November.
36. Cinco-Ley, H., and Samaniego, V.F.: "Effect of Wellbore Storage and Damage on the Transient Pressure Behavior of Vertically Fractured Wells," paper SPE 6752 presented at the 1977 SPE-AIME Annual Fall Technical Conference and Exhibition, Denver, 9-12 October.

37. Carslaw, H.S., and Jaeger, J.C.: *Conduction of Heat in Solids*, second edition, Oxford University Press, London (1959).
38. CMG GEM, *Version 2001 User's Guide*, Computer Modeling Group Ltd., Calgary, Alberta (2001).
39. Narayanaswamy, G., Pope, G.A., Sharma, M.M., Hwang, M.K., and Vaidya, R.N.: "Predicting Gas Condensate Well Productivity Using Capillary Number and Non-Darcy Effects," paper SPE 51910 presented at the 1999 Reservoir Simulation Symposium, Houston, 14-17 February.
40. Peaceman, D.W.: "Interpretation of Well-Block Pressures in Numerical Reservoir Simulation," paper SPE 6893 presented at the 1977 SPE-AIME Annual Fall Technical Conference and Exhibition, Denver, 9-12 October.
41. El-Ahmady, M.H.: "Coarse Scale Simulation of Tight Gas Reservoirs," Ph.D. dissertation, Texas A&M University, College Station, Texas (2003).
42. Archer, R.A, and Yildiz, T.T.: "Transient Well Index for Numerical Well Test Analysis," paper SPE 71572 presented at the 2001 SPE Annual Fall Technical Conference and Exhibition, Houston, 30 September- 3 October.

APPENDIX A

LINEAR FLOW MODELING

A.1 Well cell method

Fig. A.1 shows the schematic graph of a 1D linear model and the corresponding plot of cell pressures. Since the model is symmetrical, we can work only on one-half of the actual model. The wellbore modeling in the one-half model can be done by using *Well Cell method*.

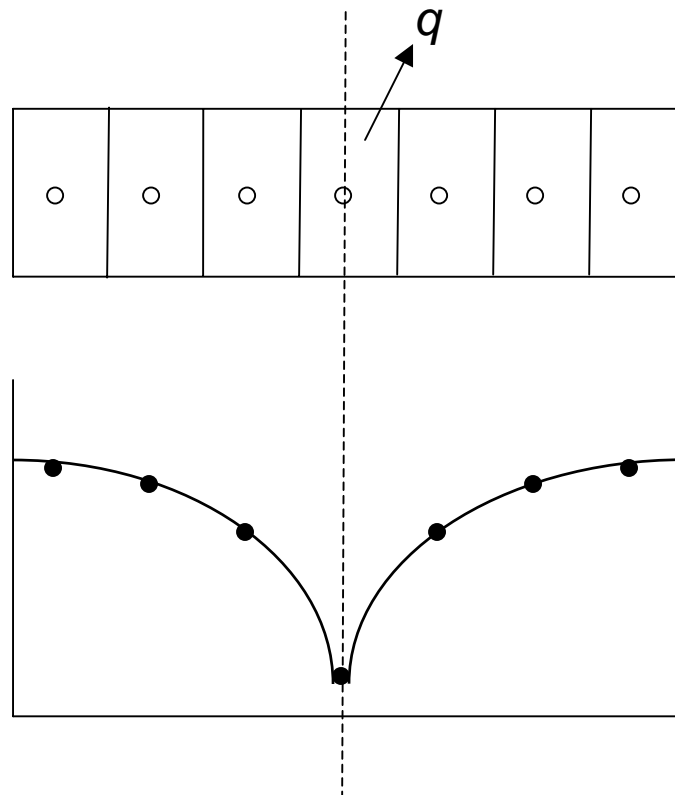


Fig. A.1 — Schematic of a 1D linear model and the corresponding cell pressure profile.

Gridblocks containing wells are usually too coarse to model wells directly. Therefore the calculated pressures in gridblocks containing wells, p_{cell} , must be corrected to formation face pressure, p_{wf} . This correction is done using what is known as Peaceman's⁴⁰ equation:

$$p_{wf} = p_{cell} - \frac{q\mu B}{J_{model}} \dots\dots\dots(A.1)$$

Where:

$$J_{model} = \frac{0.00708 kh}{\ln(0.208\Delta x) / r_w} \dots\dots\dots(A.2)$$

These equations are programmed into any conventional reservoir simulator for the case of radial flow. So, special care must be taken when we are modeling the 1D linear flow. The *Well Cell method* has the advantage of making the well cell pressure, p_{cell} , equal to the flowing bottomhole pressure p_{wf} . **Fig. A.2** illustrates the application of the *Well Cell method* in a one-half linear reservoir. Theoretically, an additional gridblock is added to the model so that the actual reservoir begins at the right boundary of the first gridblock. In order to keep the total pore volume constant, a very small porosity is assigned to the first grid. Since the first gridblock permeability is very high, the well index, J_{model} , will have a high value (See Eq. A.2), making p_{cell} equal to p_{wf} (See Eq. A.1). Another advantage of having high permeability in the first gridblock is that pressure gradient along the first cell will be zero meaning that well will be located at the right boundary of the first gridblock. In summary, the first gridblock which was added to the actual model has no pore volume and just acts like a well. So, applying the *Well Cell* method to a linear reservoir producing at constant p_{wf} results in correct values of q and p_{cell} which can be used in flow analysis.

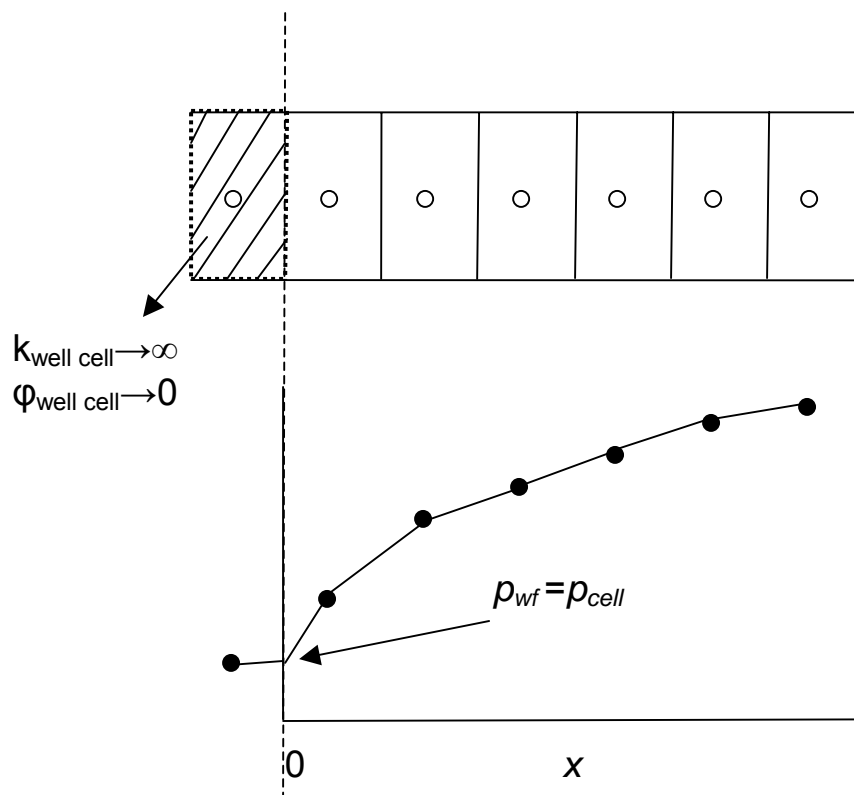


Fig. A.2 — Schematic of application of *Well Cell* method in the one-half of a 1D linear model and the corresponding cell pressure profile.

A.2 Simulation verification for a linear reservoir producing at constant rate

In order to verify applicability of *Well Cell method* in a linear reservoir producing at constant rate, simulation runs were done on GASSIM, a 2D single-phase simulator. The reservoir and fluid properties are tabulated in **Table A.1**.

Table A.1 – Reservoir and fluid properties for constant rate case

Reservoir Characteristic	Values
Thickness (h), ft	50
Absolute Permeability (k_x), md	0.05
Absolute Permeability (k_y), md	0.05
Porosity (ϕ), fraction	0.13
Initial Pressure (p_i), psi	3,900
Reservoir Half Length (x_e), ft	933.381
Reservoir Half Length (y_e), ft	933.381
Viscosity (μ_o), cp	0.7
Total Compressibility (c_t), 1/psi	0.00001
Production Rate (q_o), STBD	1
Formation Volume Factor (B_o), RB/STB	1

The analytical solution in transient period for constant rate case is calculated by using the following equation:

$$p_{wD} = \sqrt{\pi t_{Dxe}} \dots\dots\dots (A.3)$$

The dimensionless variables, p_{wD} and t_{Dxe} are calculated by using the following equations:

$$p_{wD} = \frac{k h (p_i - p_{wf})}{141.2 q_o B_o \mu_o} \dots\dots\dots (A.4)$$

$$t_{Dxe} = \frac{0.00633 kt}{\phi\mu c_t x_e^2} \dots\dots\dots(A.5)$$

Fig. A.3 shows the simulation results for a linear reservoir modeled by using the *Well Cell method*. The values of 12,000 md and 0.00001 were used for permeability and porosity of the first gridblock respectively. As we expected, the simulation results of a linear reservoir modeled by using the *Well Cell method* are completely in agreement with the analytical solution.

A.3 Simulation verification for a linear reservoir producing at constant p_{wf}

In order to verify applicability of *Well Cell method* in a linear reservoir producing at constant p_{wf} , simulation runs were done on GASSIM, a 2D single-phase simulator. The reservoir and fluid properties are tabulated in **Table A.2**.

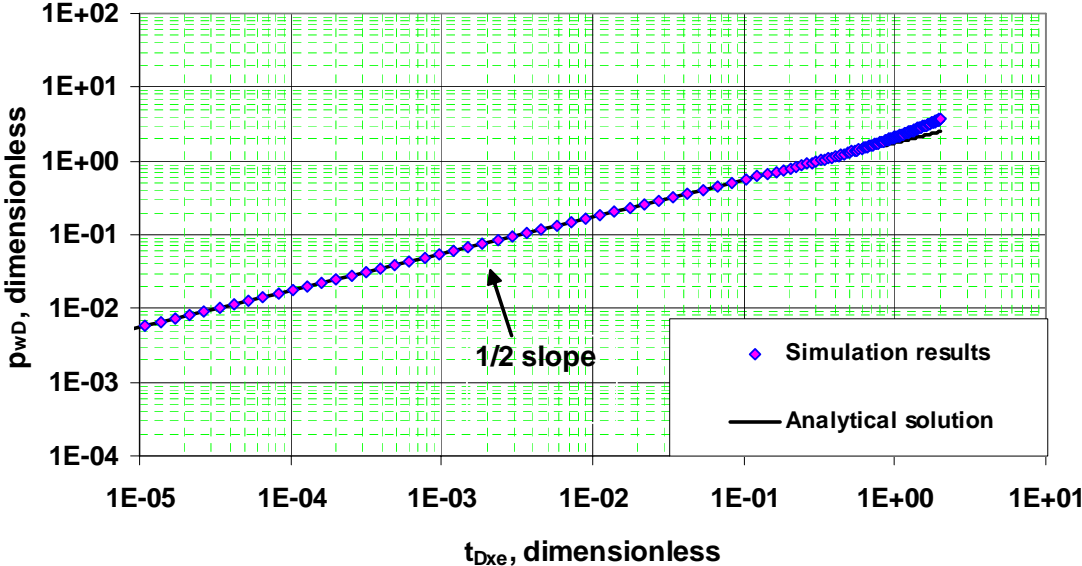


Fig. A.3 — Type-curve plot using p_{cell} data for a linear reservoir producing at constant rate and modeled by using *Well Cell method*.

Table A.2 – Reservoir and fluid properties for constant p_{wf} case

Reservoir Characteristic	Values
Thickness (h), ft	50
Absolute Permeability (k_x), md	0.05
Absolute Permeability (k_y), md	0.05
Porosity (ϕ), fraction	0.13
Initial Pressure (p_i), psi	3,900
Reservoir Half Length (x_e), ft	933.381
Reservoir Half Length (y_e), ft	933.381
Viscosity (μ_o), cp	0.7
Total Compressibility (c_t), 1/psi	0.00001
Constant bottomhole pressure (p_{wf}), psi	3,600
Formation Volume Factor (B_o), RB/STB	1

The following equations show the analytical solution and dimensionless variables used for the analysis of the constant p_{wf} case:

$$\frac{1}{q_D} = \frac{\pi}{2} \sqrt{\pi t_{Dx_e}} \dots\dots\dots (A.6)$$

$$t_{Dx_e} = \frac{0.00633 kt}{\phi \mu c_t x_e^2} \dots\dots\dots (A.7)$$

$$\frac{1}{q_D} = \frac{k h (p_i - p_{wf})}{141.2 q_o B_o \mu_o} \dots\dots\dots (A.8)$$

The schematic in **Fig. A.4** shows use of the *Well Cell method* in a linear reservoir producing at constant p_{wf} when the p_{wf} data were used. Since this method makes p_{wf} equal to p_{cell} , it wouldn't make any difference if we used p_{cell} instead.

In summary, for a linear reservoir producing at constant p_{wf} the *Well Cell method* is the proper way to model.

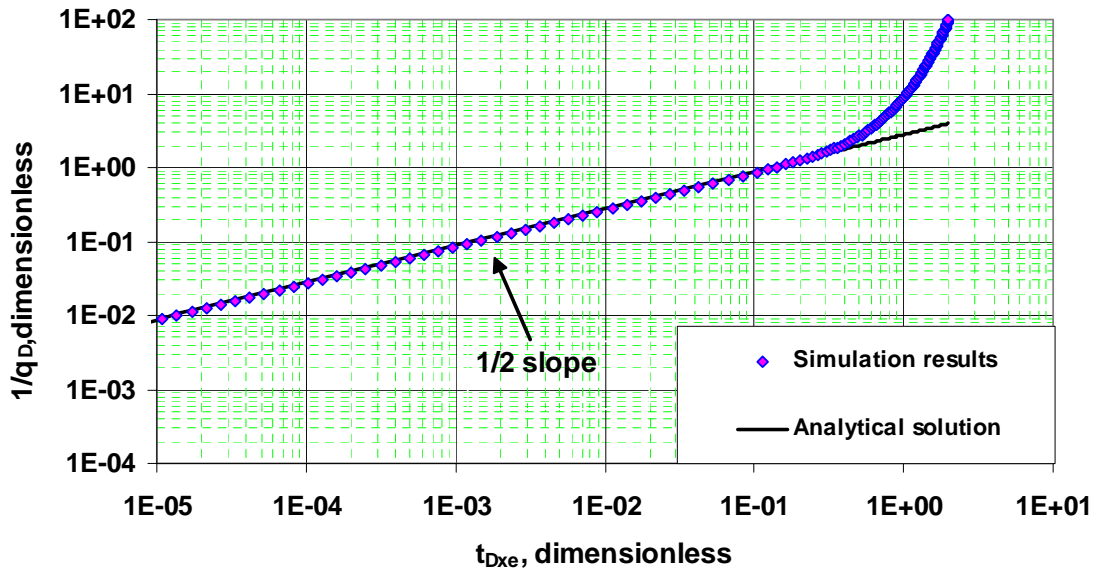


Fig. A.4 — Type-curve plot using p_{wf} data for a linear reservoir producing at constant bottomhole pressure and modeled by using *Well Cell method*.


```

10 10 10 10 10 10 10 10 10 10
10 10 10 10 10 10 10 15 20 35 53.8481624
DELY 933.381
KX 0.05
KY 0.05
H 50
WIND 1 1 1 1
PHI 0.00001
KX 50000
KY 50000
WIND 2 15 1 1
KX 0.001
KY 0.001
END
CMNT Schedule Data
CMNT Well No. i - location j - location skin
WELL 1
PMAP 2
PLOT 2
NAME 1 1 1 0
CMNT Well No. scf/D
QG 1 5.615
ALPH 1.25
DTMN 0.000001
DTMX 50
DELT 0.0001
TIME 5000
END

```

B.2 GASSIM data file for constant pressure s_{ff} analysis (Damaged case)

```

CMNT
CMNT This is a simple test case for a 1D liquid problem.
CMNT For the liquid case, compressibility and viscosity are constant.
CMNT
CMNT
CMNT
CMNT
CMNT Single Value Input Data
IMAX 100
JMAX 1
CMNT [specifies liquid case]
CNST 1 0.7
CROC 0.00001
PREF 3900
CMNT [the following five data are for gas case- not used for liquid]
GRAV 0.6
TSC 520
PSC 14.7
T 735
BETA 0

```

```

CMNT
NEWT 1 [SHOULD USE NEWT=2 or 3 for gas]
CMNT [the next two are output control]
TABL 0 [table of fluid properties]
IMAP 1 [array maps of the initial data]
END
CMNT
CMNT Grid Input Data
CMNT
PHI 0.13
POI 3900
DELX -1
  0.01 0.015 0.0225 0.03375 0.050625 0.0759375 0.11390625 0.170859375 0.2562890625
0.38443359375
  0.576650390625 0.8649755859375 1.29746337890625 1.94619506835938 2.91929260253906
4.37893890380859 6.56840835571289 9.85261253356934 10 10
  10 10 10 10 10 10 10 10 10 10
  10 10 10 10 10 10 10 10 10 10
  10 10 10 10 10 10 10 10 10 10
  10 10 10 10 10 10 10 10 10 10
  10 10 10 10 10 10 10 10 10 10
  10 10 10 10 10 10 10 10 10 10
  10 10 10 10 10 10 15 20 35 53.8531624
DELY 933.381
KX 0.05
KY 0.05
H 50
WIND 1 1 1 1
PHI 0.00001
KX 50000
KY 50000
WIND 2 15 1 1
KX 0.001
KY 0.001
END
CMNT Schedule Data
CMNT Well No. i - location j - location skin
WELL 1
PMAP 2
PLOT 2
NAME 1 1 1 0
CMNT Well No. scf/D
PWF 1 3600
ALPH 1.1
DTMN 0.00000001
DTMX 1000000000
DELT 0.0000001
TIME 5000
END

```

APPENDIX C

ANALYTICAL SOLUTIONS TO CLOSED, LINEAR RESERVOIRS

In Appendix C the required solutions to closed, linear reservoir produced at constant pressure and constant rate have been provided. In order to derive a proper equation for each case, the following assumptions have been made:

- 1-Homogeneous, isotropic formation
- 2-The viscosity of the fluid is constant
- 3-The reservoir is horizontal
- 4-The system is assumed to be under isothermal conditions and the fluid and formation are compressible.

Combining the analogy between the conduction of heat in solids and fluid flow in porous media, we can come up with the equations describing the linear flow of fluids from the formation into the hydraulic fracture. For each case, we start with the heat equation taken from *Conduction of Heat in Solids* by Carslaw and Jaeger³⁷. Then, we replace the heat conduction terms by the equivalent fluid flow terms and finalize the equation. The heat conduction terms and their equivalent in fluid flow porous media are listed as follow:

$$\begin{array}{ll}
 K \equiv \frac{0.00633 k}{\mu} & \kappa = \frac{K}{\rho c} \equiv \frac{0.00633 k}{\phi \mu c_f} \\
 f \equiv \frac{q}{A_C} & v \equiv \Delta p \\
 \frac{\kappa t}{\lambda^2} \equiv t_D & \frac{vK}{Q\lambda} \equiv p_D \\
 f = -K \frac{\partial v}{\partial x} & \frac{q}{A_C} = -\frac{k}{\mu} \frac{\partial p}{\partial x}
 \end{array}$$

C.1 Solutions to closed, linear reservoir produced at constant rate

C.1.1 Early-time solution to closed, linear reservoir produced at constant rate

(Infinite-acting)

The semi-infinite solid. The flux of heat at $x=0$ a prescribed function of the time. Zero initial temperature (from Ref. 37, page 75, Eq. 7)

$$v = \frac{2F_o}{K} \left\{ \left(\frac{\kappa t}{\pi} \right)^{1/2} e^{-x^2/4\kappa t} - \frac{x}{2} \operatorname{erfc} \frac{x}{2\sqrt{\kappa t}} \right\} \dots\dots\dots (C.1.1)$$

Knowing that $v = \Delta p$, $F_o = \frac{q}{A_c}$, $K = \frac{0.00633 k}{\mu}$ and $\kappa = \frac{0.00633 k}{\phi \mu c_t}$ we get:

$$\frac{\Delta p}{q / 0.00633 A_c \frac{\mu}{k}} = \frac{0.00633 A_c k \Delta p}{q \mu B} = 2 \left\{ \left(\frac{0.00633 \kappa t}{\phi \mu c_t \pi} \right)^{1/2} \exp\left(-\frac{x^2}{4 * \frac{0.00633 \kappa t}{\phi \mu c_t}}\right) - \frac{x}{2} \operatorname{erfc} \frac{x}{2 \sqrt{\frac{0.00633 \kappa t}{\phi \mu c_t}}} \right\} \dots\dots\dots (C.1.2)$$

Then, multiplying through by 2π , dividing q by 5.615 and regrouping terms we get:

$$2\pi * \frac{1.127 * 10^{-3} * 5.615 * 4x_f h * k \Delta p}{q \mu B} = 4\pi \left\{ \left(\frac{0.00633 \kappa t}{\phi \mu c_t x_e^2} \frac{1}{\pi} \right)^{1/2} x_e * \exp\left[-\frac{x^2}{4 * \left(\frac{0.00633 \kappa t}{\phi \mu c_t x_e^2} \right) * \frac{1}{x_e^2}}\right] - \frac{x}{2} \operatorname{erfc} \frac{x}{2x_e \sqrt{\frac{0.00633 \kappa t}{\phi \mu c_t x_e^2}}} \right\} \dots\dots\dots (C.1.3)$$

The term $\frac{0.00633kt}{\phi\mu c_t x_e^2}$ is defined as dimensionless time, then:

$$\frac{kh \Delta p}{141.2 qB\mu} = \frac{\pi}{x_f} \left\{ x_e \sqrt{\frac{t_{Dxe}}{\pi}} e^{-x^2/4x_e^2 t_{Dxe}} - \frac{x}{2} \operatorname{erfc}\left(\frac{x}{2x_e \sqrt{t_{Dxe}}}\right) \right\} \dots\dots\dots (C.1.4)$$

The left-hand side is the definition of dimensionless pressure. If $x_f=x_e$ then:

$$p_D = \frac{\pi}{x_e} \left\{ x_e \sqrt{\frac{t_{Dxe}}{\pi}} e^{-x^2/4x_e^2 t_{Dxe}} - \frac{x}{2} \operatorname{erfc}\left(\frac{x}{2x_e \sqrt{t_{Dxe}}}\right) \right\} \dots\dots\dots (C.1.5)$$

Where:

$$p_D = \frac{kh(p_i - p)}{141.2 qB\mu} \dots\dots\dots (C.1.6)$$

Eq. C.1.5 gives the pressure profile at infinite-acting period for a linear reservoir produced at constant rate. Considering $x=0$ results in the early-time solution at the wellbore:

$$p_{wD} = \frac{\pi}{x_e} * x_e \sqrt{\frac{t_{Dxe}}{\pi}} = \sqrt{\pi t_{Dxe}} \dots\dots\dots (C.1.7)$$

Where:

$$p_{wD} = \frac{kh(p_i - p_{wf})}{141.2 qB\mu} \dots\dots\dots (C.1.8)$$

Finally,

$$p_{wD} = \sqrt{\pi t_{Dxe}} \dots\dots\dots (C.1.9)$$

C.1.2 Pressure profile for a closed, linear reservoir produced at constant rate

The slab with prescribed flux at its surface. The region $0 < x < \lambda$. Zero initial temperature. Constant flux F_0 into the solid at $x=\lambda$. No flow of heat over $x=0$. (from Ref. 37, page 112, Eq. 3)

$$\frac{v}{F_o} = \frac{t}{\rho c \lambda} + \frac{\lambda}{K} \left\{ \frac{3x^2 - \lambda^2}{6\lambda^2} - \frac{2}{\pi^2} \sum_{n=1}^{\infty} \frac{(-1)^n}{n^2} e^{-\frac{\kappa n^2 \pi^2 t}{\lambda^2}} \cos \frac{n\pi x}{\lambda} \right\} \dots\dots\dots (C.1.10)$$

Multiplying through by K we have:

$$\frac{Kv}{F_o} = \frac{K}{\rho c} \frac{t}{\lambda} + \lambda \left\{ \frac{3x^2 - \lambda^2}{6\lambda^2} - \frac{2}{\pi^2} \sum_{n=1}^{\infty} \frac{(-1)^n}{n^2} e^{-\frac{\kappa n^2 \pi^2 t}{\lambda^2}} \cos \frac{n\pi x}{\lambda} \right\} \dots\dots\dots (C.1.11)$$

Knowing that $\kappa = \frac{K}{\rho c} \equiv \frac{0.00633k}{\phi\mu c_t}$, $K \equiv \frac{0.00633k}{\mu}$, $v \equiv \Delta p$ and $F_o \equiv \frac{q}{A_C}$ we will get:

$$\begin{aligned} \frac{0.00633k A_C \Delta p}{q\mu B} &= \frac{0.00633kt}{\phi\mu c_t x_e^2} \frac{x_e^2}{\lambda} + \\ &+ \lambda \left\{ \frac{3x^2 - \lambda^2}{6\lambda^2} - \frac{2}{\pi^2} \sum_{n=1}^{\infty} \frac{(-1)^n}{n^2} e^{-\left[\frac{0.00633kt}{\phi\mu c_t x_e^2} \frac{n^2 \pi^2 x_e^2}{\lambda^2} \right]} \cos \frac{n\pi x}{\lambda} \right\} \dots\dots\dots (C.1.12) \end{aligned}$$

Replacing A_C (cross sectional area) by $4x_f h$, multiplying through by 2π , we will have:

$$\begin{aligned} \frac{2\pi * 1.127 * 10^{-3} kh \Delta p}{5.615} * 4X_f &= 2\pi t_{Dx_e} \frac{x_e^2}{\lambda} + \\ &+ 2\pi * \lambda \left\{ \frac{3x^2 - \lambda^2}{6\lambda^2} - \frac{2}{\pi^2} \sum_{n=1}^{\infty} \frac{(-1)^n}{n^2} e^{-\left[t_{Dx_e} \frac{n^2 \pi^2 x_e^2}{\lambda^2} \right]} \cos \frac{n\pi x}{\lambda} \right\} \dots\dots\dots (C.1.13) \end{aligned}$$

Rearranging Eq. C.1.13 results in:

$$\frac{kh \Delta p}{141.2 q B \mu} = \frac{\pi}{2} t_{Dx_e} \frac{x_e^2}{\lambda x_f} + \frac{\pi \lambda}{2 x_f}$$

$$+ \left\{ \frac{3x^2 - \lambda^2}{6\lambda^2} - \frac{2}{\pi^2} \sum_{n=1}^{\infty} \frac{(-1)^n}{n^2} e^{-[t_{Dx_e} \frac{n^2 \pi^2 x_e^2}{\lambda^2}]} \cos \frac{n\pi x}{\lambda} \right\} \dots\dots\dots (C.1.14)$$

Finally, making $x_f = x_e, \lambda = y_e$ and moving well to $x=0$, will give us the pressure profile equation at any time and at any distance from the producer, in transient and p_{ss} periods, for linear flow at constant rate conditions:

$$p_D = \frac{\pi}{2} t_{Dx_e} \left(\frac{x_e}{y_e} \right) + \frac{\pi}{2} \left(\frac{y_e}{x_e} \right) * \left\{ \frac{3(y_e - x)^2 - y_e^2}{6y_e^2} - \frac{2}{\pi^2} \sum_{n=1}^{\infty} \frac{(-1)^n}{n^2} e^{-[t_{Dx_e} \frac{n^2 \pi^2 x_e^2}{y_e^2}]} \cos \frac{n\pi(y_e - x)}{y_e} \right\} \dots\dots\dots (C.1.15)$$

Where:

$$p_D = \frac{kh(p_i - p)}{141.2 qB\mu} \dots\dots\dots (C.1.6)$$

C.1.3 Complete solution to a closed, linear reservoir at the wellbore produced at constant rate

Recalling Eq. C.1.15 at the wellbore we have:

$$p_{wD} = \frac{\pi}{2} \left[\frac{1}{3} \left(\frac{y_e}{x_e} \right) + \left(\frac{x_e}{y_e} \right) t_{Dx_e} \right] - \frac{1}{\pi} \left(\frac{y_e}{x_e} \right) \sum_{n=1}^{\infty} \frac{(-1)^n}{n^2} e^{-[t_{Dx_e} \frac{n^2 \pi^2 x_e^2}{y_e^2}]} \cos n\pi \dots\dots\dots (C.1.16)$$

$\cos n\pi$ cancels out $(-1)^n$, so:

$$p_{wD} = \frac{\pi}{2} \left[\frac{1}{3} \left(\frac{y_e}{x_e} \right) + \left(\frac{x_e}{y_e} \right) t_{Dx_e} \right] - \frac{1}{\pi} \left(\frac{y_e}{x_e} \right) \sum_{n=1}^{\infty} \frac{1}{n^2} \exp[-n^2 \pi^2 \left(\frac{x_e}{y_e} \right)^2 t_{Dx_e}] \dots\dots\dots (C.1.17)$$

Where:

$$p_{wD} = \frac{kh(p_i - p_{wf})}{141.2 qB\mu} \dots\dots\dots (C.1.8)$$

Eq. C.1.17 is the complete solution to a closed, linear reservoir at the wellbore and at any time after production begins produced at constant rate.

C.1.4 Long-term solution to a closed, linear reservoir at the wellbore produced at constant rate

When the reservoir boundaries are seen at the wellbore, the boundary-dominated equations govern the fluid flow in the linear reservoir. At this time, t_{Dx_e} has a large value and makes the third term in Eq. C.1.17 negligible. Thus:

$$p_{wD} = \frac{\pi}{2} \left(\frac{x_e}{y_e} \right) * t_{Dx_e} + \frac{\pi}{6} \left(\frac{y_e}{x_e} \right) \dots\dots\dots (C.1.18)$$

C.1.5 Stabilized equation for a closed, linear reservoir produced at constant rate

Substituting Eq. C.1.8 into Eq. C.1.18 we have:

$$\frac{kh(p_i - p_{wf})}{141.2 qB\mu} = \frac{\pi}{2} \left(\frac{x_e}{y_e} \right) \frac{0.00633 kt}{\phi\mu c_t x_e^2} + \frac{\pi}{6} \left(\frac{y_e}{x_e} \right) \dots\dots\dots (C.1.19)$$

Rearranging Eq. C.1.19 results in:

$$q = \frac{kh(p_i - p_{wf})}{141.2 B \mu \left[\frac{\pi}{2} \left(\frac{x_e}{y_e} \right) \frac{0.00633 kt}{\phi\mu c_t x_e^2} + \frac{\pi}{6} \left(\frac{y_e}{x_e} \right) \right]} \dots\dots\dots (C.1.20)$$

Rewriting Eq. C.1.20 in terms of average reservoir pressure, \bar{p} , we have:

$$q = \frac{kh[(\bar{p} - p_{wf}) - (\bar{p} - p_i)]}{141.2 B \mu \left[\frac{\pi}{2} \left(\frac{x_e}{y_e} \right) \frac{0.00633 kt}{\phi\mu c_t x_e^2} + \frac{\pi}{6} \left(\frac{y_e}{x_e} \right) \right]} \dots\dots\dots (C.1.21)$$

From material balance equation we know:

$$\bar{p} = p_i - \frac{BN_p}{V_p c_t} \dots\dots\dots (C.1.22)$$

Where:

$$N_p = q * t * 5.615 \text{ STB} \dots\dots\dots (C.1.23)$$

Substituting Eqs. C.1.22 and C.1.23 into Eq. C.1.21 gives:

$$q = \frac{kh[(\bar{p} - p_{wf}) - \frac{B}{V_p c_t} 5.615 qt]}{141.2 B\mu[\frac{\pi}{2}(\frac{x_e}{y_e}) \frac{0.00633 kt}{\phi\mu c_t x_e^2} + \frac{\pi}{6}(\frac{y_e}{x_e})]} \dots\dots\dots (C.1.24)$$

Regrouping the terms including q , we have:

$$q = \frac{kh(\bar{p} - p_{wf})}{141.2 B\mu[\frac{\pi}{2}(\frac{x_e}{y_e}) \frac{0.00633 kt}{\phi\mu c_t x_e^2} + \frac{\pi}{6}(\frac{y_e}{x_e}) - \frac{5.615 kh B t}{141.2 B\mu * 4x_f h y_e \phi c_t}]} \dots\dots\dots (C.1.25)$$

Simplifying Eq. C.1.25, the first and third terms in the denominator cancel out. So:

$$q = \frac{kh(\bar{p} - p_{wf})}{141.2 B\mu[\frac{\pi}{6}(\frac{y_e}{x_e})]} \dots\dots\dots (C.1.26)$$

Eq. C.1.26 is the stabilized equation for a well producing a closed, linear reservoir at constant rate conditions.

C.1.6 Simulation verification

Fig. C.1.1 shows the geometry of a hydraulic fractured well whose fracture continues to the lateral boundaries². The well is in the center of a rectangular drainage area. From the center of the rectangle, the fracture half-length is x_f and continue to the boundary in the x- direction, x_e , this means that $x_f = x_e$. The distance to the outer boundary in the direction perpendicular to the fracture is y_e . The drainage area of the well is $4x_e y_e$. For a square drainage shape with 80-acre spacing, $x_f = x_e = y_e = 933.38$ ft. Since the reservoir is symmetrical, only one quadrant of the reservoir has been modeled. In order to get the right values of pressures using the analytical solutions, the constant rate should be multiplied by 4.

The linear model includes 40 grid blocks and uses liquid as the reservoir fluid. The reservoir and fluid properties have been tabulated in **Table C.1.1**.

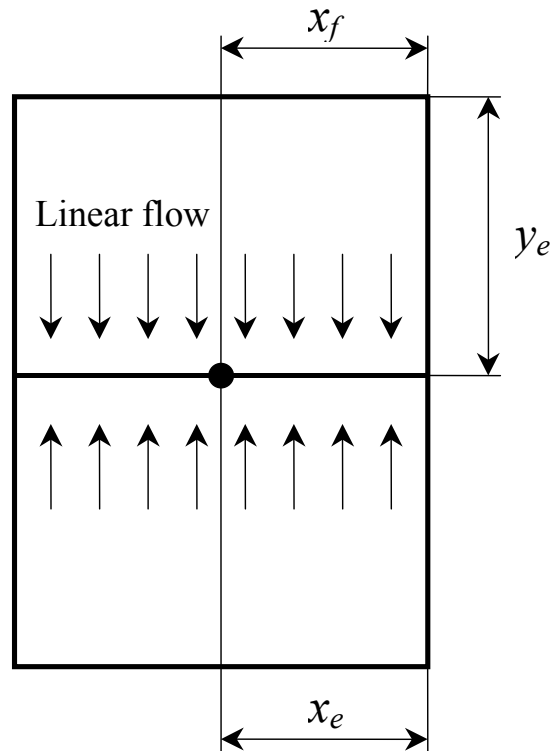


Fig. C.1.1 — Top view of a rectangular reservoir and a hydraulically fractured well which has only linear flow into the fracture ($x_f = x_e$).

Table C.1.1 — Reservoir and fluid properties

Reservoir Characteristic	Values
Reservoir Half Length (x_e), ft	933.381
Reservoir Half Length (y_e), ft	933.381
Absolute Permeability (k_x), md	0.05
Absolute Permeability (k_y), md	0.05

Table C.1.1 – Continued

Reservoir Characteristic	Values
Thickness (h), ft	50
Porosity (ϕ), fraction	0.13
Initial Pressure (p_i), psi	3,900
Viscosity (μ), cp	0.7
Total compressibility, 1/psi	0.00001
Constant Flow rate (q_o), STBD	10
Formation Volume Factor (B_o), RB/STB	1

The model was run on Gassim, a 2D single-phase reservoir simulator, and the simulation results were plotted against analytical results at seven different times after production begins. **Fig. C.1.2** illustrates the pressure profile for a closed, linear reservoir produced at constant rate. The blue lines are the results of simulation run when the red circles represent the pressures calculated using Eq. C.1.5. **Fig. C.1.2** shows that the pressure profile equation in infinite-acting period can perfectly match the pressures obtained using reservoir simulation. Since at $t=308.8$ days the infinite-acting period has elapsed, the analytical solution is unable to correctly predict the reservoir pressure.

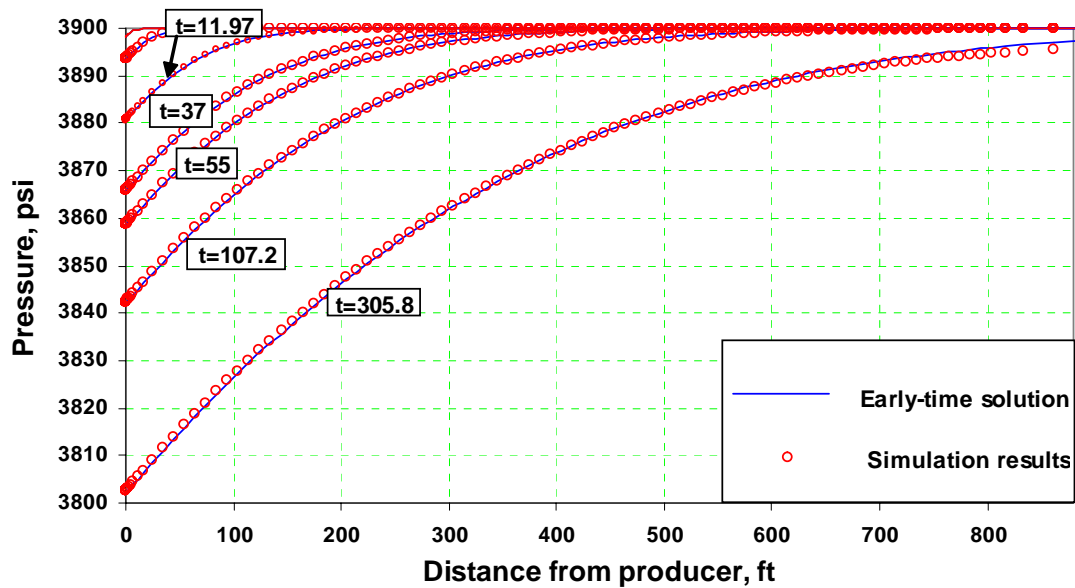


Fig. C.1.2 — Comparison between analytical pressure profile and numerically calculated pressures at early times using a closed, linear reservoir produced at constant rate.

Fig. C.1.3 was made to give us the capability of comparing the complete pressure profile equation against the simulation results. Again, the blue solid lines are the simulated pressures for a closed, linear reservoir produced at constant rate where the red circles represent the calculated pressures by using Eq. C.1.15. **Fig. C.1.3** also shows that, the analytical solution can reasonably predict the reservoir pressure at any distance from the producer and at any time after production begins.

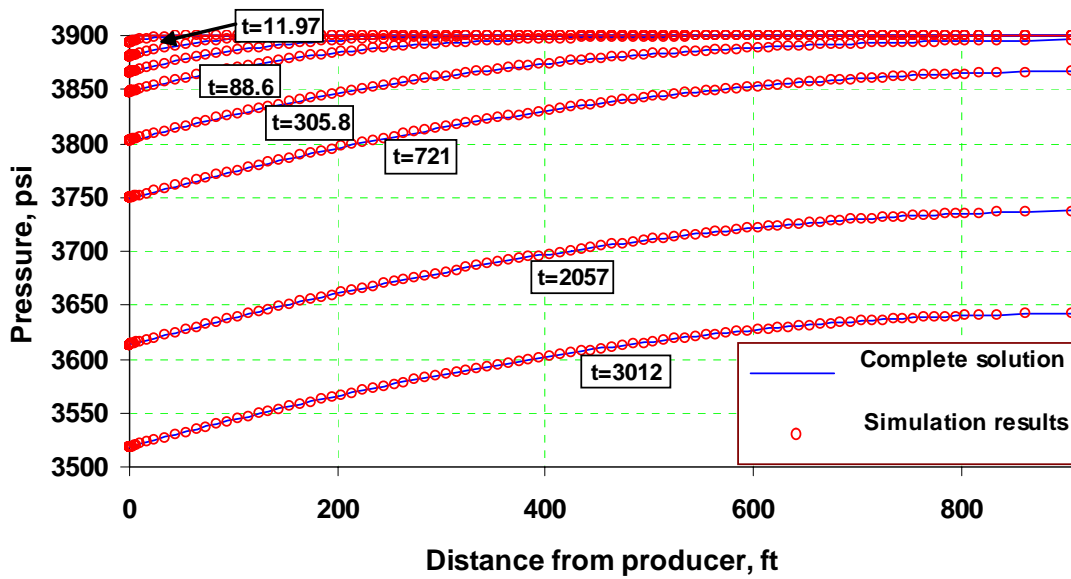


Fig. C.1.3 — Comparison between analytical pressure profile and numerically calculated pressures at any times using a closed, linear reservoir produced at constant rate.

C.2 Solutions to closed, linear reservoir produced at constant wellbore pressure

C.2.1 Pressure profile at early times for a closed, linear reservoir produced at constant wellbore pressure

The semi-infinite solid. The boundary $x=0$ is kept at constant V and the initial temperature is zero. (from Ref. 37, page 60, Eq. 10)

$$v = V \operatorname{erfc} \frac{x}{2\sqrt{\kappa t}} \dots\dots\dots (C.2.1)$$

Replacing v and V by the equivalent terms in porous media, we have:

$$(p_i - p) = (p_i - p_{wf}) \left(1 - \operatorname{erf} \frac{x}{2\sqrt{\kappa t}}\right) \dots\dots\dots (C.2.2)$$

Simplifying Eq. C.2.2 results in:

$$p = p_i \operatorname{erf}\left(\frac{x}{2\sqrt{\kappa t}}\right) + p_{wf} \operatorname{erfc}\left(\frac{x}{2\sqrt{\kappa t}}\right) \dots\dots\dots (C.2.3)$$

Then, substituting the equivalent value of $\kappa \equiv \frac{0.00633 k}{\phi \mu c_i}$, we have:

$$p = p_i \operatorname{erf}\left(\frac{x}{2x_e \sqrt{\frac{kt}{\phi \mu c_i x_e^2}}}\right) + p_{wf} \operatorname{erfc}\left(\frac{x}{2x_e \sqrt{\frac{kt}{\phi \mu c_i x_e^2}}}\right) \dots\dots\dots (C.2.4)$$

Finally, rearranging Eq. C.2.4, we get the early-time solution to a closed, linear reservoir at constant pressure conditions:

$$p = p_i \operatorname{erf}\left(\frac{x}{2x_e \sqrt{t_{Dxe}}}\right) + p_{wf} \operatorname{erfc}\left(\frac{x}{2x_e \sqrt{t_{Dxe}}}\right) \dots\dots\dots (C.2.5)$$

Using Eq. C.2.5 we can come up with a plot of pressure versus the distance from the producer (pressure profile) at early times in the life of the reservoir.

C.2.2 Complete pressure profile equation for a closed, linear reservoir produced at constant wellbore pressure

The region $-\lambda < x < \lambda$ with zero initial temperature and with the surfaces $x = \lambda, -\lambda$ kept at constant temperature V for $t > 0$. (from Ref. 37, page 100, Eq. 4)

$$\frac{v}{V} = 1 - \frac{4}{\pi} \sum_{n=0}^{\infty} \frac{(-1)^n}{2n+1} e^{-(2n+1)^2 \pi^2 T / 4} \cos \frac{(2n+1)\pi \xi}{2} \dots\dots\dots (C.2.6)$$

Where:

$$\xi = \frac{x}{\lambda} \dots\dots\dots (C.2.7)$$

$$T = \frac{\kappa t}{\lambda^2} \dots\dots\dots (C.2.8)$$

Applying the equivalent terms, we will have:

$$T = \frac{\kappa t}{\lambda^2} = \frac{0.00633 \kappa t}{\phi \mu c_i y_e^2} = \frac{0.00633 \kappa t}{\phi \mu c_i x_e^2} \left(\frac{x_e}{y_e}\right)^2 \dots\dots\dots (C.2.9)$$

$$\frac{v}{V} = \frac{(p_i - p)}{(p_i - p_{wf})} \dots\dots\dots(C.2.10)$$

Therefore:

$$\begin{aligned} \frac{(p_i - p)}{(p_i - p_{wf})} = 1 - \frac{4}{\pi} \sum_{n=0}^{\infty} \frac{(-1)^n}{2n+1} \exp\left[-\frac{(2n+1)^2 \pi^2}{4} t_{Dx_e} \left(\frac{x_e}{y_e}\right)^2\right] \\ * \cos\left[\frac{(2n+1)\pi}{2} \frac{x}{y_e}\right] \dots\dots\dots(C.2.11) \end{aligned}$$

In Eq. C.2.11, the well is located at $x=\lambda$. So, we rearrange the equation so that the well will be located at $x=0$:

$$\begin{aligned} p = p_{wf} + \frac{4}{\pi} (p_i - p_{wf}) \sum_{n=0}^{\infty} \frac{(-1)^n}{2n+1} \exp\left[-\frac{(2n+1)^2 \pi^2}{4} t_{Dx_e} \left(\frac{x_e}{y_e}\right)^2\right] \\ * \cos\left[\frac{(2n+1)\pi}{2} \frac{(y_e - x)}{y_e}\right] \dots\dots\dots(C.2.12) \end{aligned}$$

In Eq. C.2.12, we can replace $\cos\left[\frac{(2n+1)\pi}{2} \frac{(y_e - x)}{y_e}\right]$ by $\sin\left[\frac{2n+1}{2} \frac{\pi x}{y_e}\right] * (-1)^n$, so:

$$\begin{aligned} p = p_{wf} + \frac{4}{\pi} (p_i - p_{wf}) \sum_{n=0}^{\infty} \frac{(-1)^n}{2n+1} \exp\left[-\frac{(2n+1)^2 \pi^2}{4} t_{Dx_e} \left(\frac{x_e}{y_e}\right)^2\right] * \\ * \sin\left[\frac{2n+1}{2} \frac{\pi x}{y_e}\right] * (-1)^n \dots\dots\dots(C.2.13) \end{aligned}$$

Simplifying Eq. C.2.13, we will have:

$$p = p_{wf} + \frac{4}{\pi} (p_i - p_{wf}) \sum_{n=odd}^{\infty} \frac{1}{n} \exp\left[-\frac{n^2 \pi^2}{4} t_{Dx_e} \left(\frac{x_e}{y_e}\right)^2\right] * \sin\left[\frac{n}{2} \frac{\pi x}{y_e}\right] \dots\dots\dots(C.2.14)$$

Eq. C.2.14 is used to get the pressure profile at any time after production begins.

C.2.3 Complete solution to a closed, linear reservoir produced at constant wellbore pressure (flow equation at the wellbore)

Recalling Eq. C.2.6, we get:

$$\frac{v}{V} = 1 - \frac{4}{\pi} \sum_{n=0}^{\infty} \frac{(-1)^n}{2n+1} e^{-(2n+1)^2 \pi^2 T/4} * \cos \frac{(2n+1)\pi \xi}{2} \dots\dots\dots(C.2.6)$$

Differentiating Eq. C.2.6, we have:

$$\frac{1}{V} \frac{\partial v}{\partial (\frac{x}{\lambda})} = -\frac{4}{\pi} \sum_{n=0}^{\infty} \frac{(-1)^n}{2n+1} e^{-(2n+1)^2 \pi^2 T/4} [-\sin \frac{(2n+1)\pi \xi}{2}] \frac{(2n+1)\pi}{2} \dots\dots\dots(C.2.15)$$

Evaluating $\frac{\partial v}{\partial (\frac{x}{\lambda})}$ at $x = \lambda$ (since well originally is located at $x = \lambda$), we will get:

$$\frac{1}{V} \left(\frac{\partial v}{\partial (\frac{x}{\lambda})} \right)_{\lambda} = \frac{4}{\pi} \sum_{n=0}^{\infty} \frac{(-1)^n}{2n+1} e^{-(2n+1)^2 \pi^2 T/4} \sin \left(\frac{(2n+1)\pi}{2} \right) \frac{(2n+1)\pi}{2} \dots\dots\dots(C.2.16)$$

Knowing that $\sin(\frac{(2n+1)\pi}{2})$ cancels out $(-1)^n$, we have:

$$\frac{1}{V} \left(\frac{\partial v}{\partial (\frac{x}{\lambda})} \right)_{\lambda} = 2 \sum_{n=odd}^{\infty} e^{-n^2 \pi^2 T/4} \dots\dots\dots(C.2.17)$$

If we invert the two sides of Eq. C.2.17, we will get:

$$\frac{V}{\lambda \frac{\partial v}{\partial x}} = \frac{1}{2} \frac{1}{\sum_{n=odd}^{\infty} e^{-n^2 \pi^2 T/4}} \dots\dots\dots(C.2.18)$$

The heat and flow equations are as follow:

$$f = -K \frac{\partial v}{\partial x} \dots\dots\dots(C.2.19)$$

$$\frac{q}{A_c} = -0.00633 \frac{k}{\mu} \frac{\partial p}{\partial x} \dots\dots\dots(C.2.20)$$

Then, substituting the equivalent terms using Eqs. C.2.9, C.2.19 and C.2.20, results in:

$$\frac{0.00633k * 4x_f h \Delta p}{q \mu \lambda} = \frac{1}{2} \frac{1}{\sum_{n=odd}^{\infty} \exp[\frac{-n^2 \pi^2}{4} t_{Dx_e} (\frac{x_e}{y_e})^2]} \dots\dots\dots(C.2.21)$$

Multiplying through by 2π and rearranging Eq. C.2.21, we have:

$$\frac{kh\Delta p}{141.2 q \mu B} * \frac{4x_e}{y_e} = \frac{\pi}{\sum_{n=odd}^{\infty} \exp\left[-\frac{n^2 \pi^2}{4} t_{Dx_e} \left(\frac{x_e}{y_e}\right)^2\right]} \dots\dots\dots (C.2.22)$$

Finally, knowing that dimensionless rate is defined as $\frac{1}{q_D} = \frac{kh\Delta p}{141.2 q \mu B}$, we will get:

$$\frac{1}{q_D} = \frac{\pi}{4} \left(\frac{y_e}{x_e}\right) * \frac{1}{\sum_{n=odd}^{\infty} \exp\left[-\frac{n^2 \pi^2}{4} \left(\frac{x_e}{y_e}\right)^2 t_{Dx_e}\right]} \dots\dots\dots (C.2.23)$$

Eq. C.2.23 is used to calculate flow rate at the wellbore at any time after production begins.

C.2.4 Early-time solution to closed, linear reservoir produced at constant wellbore pressure. (Infinite-acting)

Recall Eq. C.2.1:

$$v = V \operatorname{erfc} \frac{x}{2\sqrt{\kappa t}} \dots\dots\dots (C.2.1)$$

Differentiating Eq. C.2.1 results in:

$$\frac{1}{V} \left(\frac{\partial v}{\partial(x)} \right) = -\frac{1}{2\sqrt{\kappa t}} * \frac{2}{\sqrt{\pi}} e^{\frac{-x^2}{4\kappa t}} \dots\dots\dots (C.2.24)$$

Inverting Eq. C.2.24, we have:

$$\frac{V}{\left(\frac{\partial v}{\partial x}\right)} = -\sqrt{\pi \kappa t} * \exp\left[\frac{x^2}{4\kappa t}\right] \dots\dots\dots (C.2.25)$$

Evaluating Eq. C.2.25 at the wellbore $x=0$, we get:

$$\frac{V}{\left(\frac{\partial v}{\partial x}\right)} = -\sqrt{\pi \kappa t} \dots\dots\dots (C.2.26)$$

Substituting the equivalent terms using Eqs. C.2.19 and C.2.20, we will have:

$$\frac{-0.00633k * 4x_f h \Delta p}{q\mu B} = -x_e \sqrt{\frac{0.00633kt}{\phi\mu c_i x_e^2}} \pi \dots\dots\dots (C.2.27)$$

Multiplying through by 2π and rearranging the equation, we will have:

$$\frac{1}{q_D} = \frac{\pi}{2} \sqrt{\pi t_{Dx_e}} * \frac{x_e}{x_f} \dots\dots\dots (C.2.28)$$

Where:

$$\frac{1}{q_D} = \frac{kh(p_i - p_{wf})}{141.2 q\mu B} \dots\dots\dots (C.2.29)$$

Finally, if fracture continues to the drainage boundaries of the well, $x_e = x_f$. So:

$$\frac{1}{q_D} = \frac{\pi}{2} \sqrt{\pi t_{Dx_e}} \dots\dots\dots (C.2.30)$$

Eq. C.2.30 is used to calculate the flow rate at the wellbore at early times after production begins.

C.2.5 Stabilized equation for a closed, linear reservoir at constant wellbore pressure

Recall Eq. C.2.23:

$$\frac{1}{q_D} = \frac{\pi}{4} \left(\frac{y_e}{x_e}\right) * \frac{1}{\sum_{n=odd}^{\infty} \exp\left[\frac{-n^2 \pi^2}{4} \left(\frac{x_e}{y_e}\right)^2 t_{Dx_e}\right]} \dots\dots\dots (C.2.23)$$

Rearranging Eq. C.2.23, we have:

$$q = \frac{kh(p_i - p_{wf}) \sum_{n=odd}^{\infty} \exp\left[\frac{-n^2 \pi^2}{4} \left(\frac{x_e}{y_e}\right)^2 t_{Dx_e}\right]}{141.2 B\mu * \frac{\pi}{4} \left(\frac{y_e}{x_e}\right)} \dots\dots\dots (C.2.31)$$

Average reservoir pressure is calculated as a volumetric average pressure. Since here the reservoir porosity is homogeneous and the reservoir cross section is constant we calculate average reservoir as:

$$\bar{p}(t) = \frac{1}{Y_e} \int_0^{Y_e} p(x, t) dx \dots\dots\dots (C.2.33)$$

Substituting Eq. C.2.14 into Eq. C.2.32 gives us:

$$\begin{aligned} \bar{p}(x, t) = p_{wf} + \frac{4(p_i - p_{wf})}{\pi y_e} \sum_{n=odd}^{\infty} \frac{1}{n} \exp\left[-\frac{n^2 \pi^2}{4} * t_{Dx_e} \left(\frac{x_e}{y_e}\right)^2\right] \\ * \int_0^{Y_e} \sin\left[\frac{n \pi x}{2 Y_e}\right] dx \dots\dots\dots (C.2.33) \end{aligned}$$

Then:

$$\begin{aligned} \bar{p}(x, t) = p_{wf} - \frac{8}{\pi^2} (p_i - p_{wf}) \sum_{n=odd}^{\infty} \frac{1}{n^2} \exp\left[-\frac{n^2 \pi^2}{4} * t_{Dx_e} \left(\frac{x_e}{y_e}\right)^2\right] \\ * \cos\left[\frac{n \pi x}{2 y_e}\right]_0^{y_e} \dots\dots\dots (C.2.34) \end{aligned}$$

Finally:

$$\bar{p}(x, t) = p_{wf} + \frac{8}{\pi^2} (p_i - p_{wf}) \sum_{n=odd}^{\infty} \frac{1}{n^2} \exp\left[-\frac{n^2 \pi^2}{4} * t_{Dx_e} \left(\frac{x_e}{y_e}\right)^2\right] \dots\dots\dots (C.2.35)$$

The productivity index is defined as the ratio of rate to difference between average and flowing pressure. Therefore:

$$J = \frac{q}{(\bar{p} - p_{wf})} \dots\dots\dots (C.2.36)$$

Substituting Eqs. C.2.31 and C.2.35, we have:

$$\begin{aligned} J = \frac{kh(p_i - p_{wf}) \sum_{n=odd}^{\infty} \exp\left[-\frac{n^2 \pi^2}{4} * t_{Dx_e} \left(\frac{x_e}{y_e}\right)^2\right]}{141.2 B \mu * \frac{\pi}{4} \left(\frac{y_e}{x_e}\right)} \dots\dots\dots (C.2.37) \\ \frac{8}{\pi^2} (p_i - p_{wf}) \sum_{n=odd}^{\infty} \frac{1}{n^2} \exp\left[-\frac{n^2 \pi^2}{4} * t_{Dx_e} \left(\frac{x_e}{y_e}\right)^2\right] \end{aligned}$$

$$\begin{aligned} J = \frac{kh}{141.2 B \mu \left[\frac{2}{\pi} \left(\frac{y_e}{x_e}\right)\right]} * \frac{\sum_{n=odd}^{\infty} \exp\left[-\frac{n^2 \pi^2}{4} * t_{Dx_e} \left(\frac{x_e}{y_e}\right)^2\right]}{\sum_{n=odd}^{\infty} \frac{1}{n^2} \exp\left[-\frac{n^2 \pi^2}{4} * t_{Dx_e} \left(\frac{x_e}{y_e}\right)^2\right]} \dots\dots\dots (C.2.38) \end{aligned}$$

If we use the long-term solution, which is valid only for $t_{Dx_e} > 0.7$ then:

$$J = \frac{kh}{141.2 B \mu \left[\frac{2}{\pi} \left(\frac{y_e}{x_e} \right) \right]} \dots\dots\dots (C.2.39)$$

Finally:

$$q = \frac{kh(\bar{p} - p_{wf})}{141.2 B \mu \left[\frac{2}{\pi} \left(\frac{y_e}{x_e} \right) \right]} \dots\dots\dots (C.2.40)$$

Eq. C.2.40 is the stabilized equation for a well producing a closed, linear reservoir at constant flowing bottomhole pressure.

C.2.6 Simulation verification

In order to verify the analytical pressure profile equations, the linear model explained in Section C.1, was used which includes $p_{wf}=1000$ psi as the well constraint. The reservoir and fluid properties are tabulated in **Table C.2.1**.

The model was run on Gassim, a 2D single-phase reservoir simulator, and the simulation results were plotted against analytical results at seven different times after production begins. **Fig. C.2.1** illustrates the pressure profile for a closed, linear reservoir produced at constant wellbore pressure. The blue lines are the results of simulation run when the red circles represent the pressures calculated using Eq. C.2.5. **Fig. C.2.1** shows that the pressure profile equation in infinite-acting period can perfectly match the pressures obtained using reservoir simulation. Since at $t=308.8$ days the infinite-acting period has elapsed, the analytical solution is unable to correctly predict the reservoir pressure.

Table C.2.1 – Reservoir and fluid properties

Reservoir Characteristic	Values
Thickness (h), ft	50
Absolute Permeability (k_x), md	0.05
Absolute Permeability (k_y), md	0.05
Porosity (ϕ), fraction	0.13
Initial Pressure (p_i), psi	3,900
Reservoir Half Length (x_e), ft	933.381
Reservoir Half Length (y_e), ft	933.381
Viscosity (μ), cp	0.7
Total Compressibility (c_t), 1/psi	0.00001
Constant Flowing Pressure (p_{wf}), psi	1,000
Formation Volume Factor (B_o), RB/STB	1

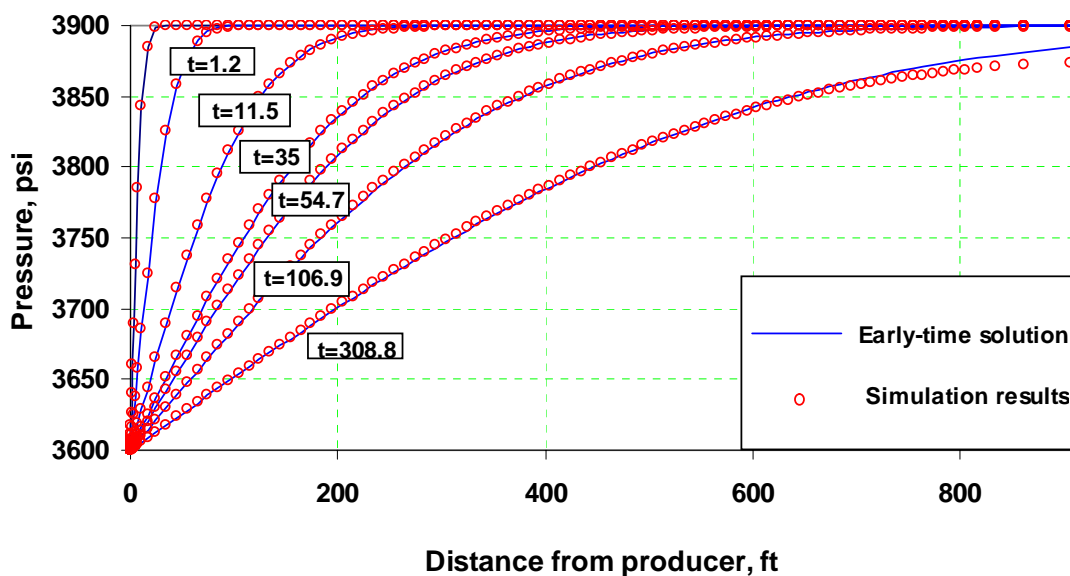


Fig. C.2.1 — Comparison between analytical pressure profile and numerically calculated pressures at early times using a closed, linear reservoir produced at constant wellbore pressure.

Fig. C.2.2 was made to give us the capability of comparing the complete pressure profile equation against the simulation results. Again, the blue solid lines are the simulated pressures for a closed, linear reservoir produced at constant p_{wf} where the red circles represent the calculated pressures by using Eq. C.2.14. **Fig. C.2.2** also shows that, the analytical solution can reasonably predict the reservoir pressure at any distance from the producer and at any time after production begins.

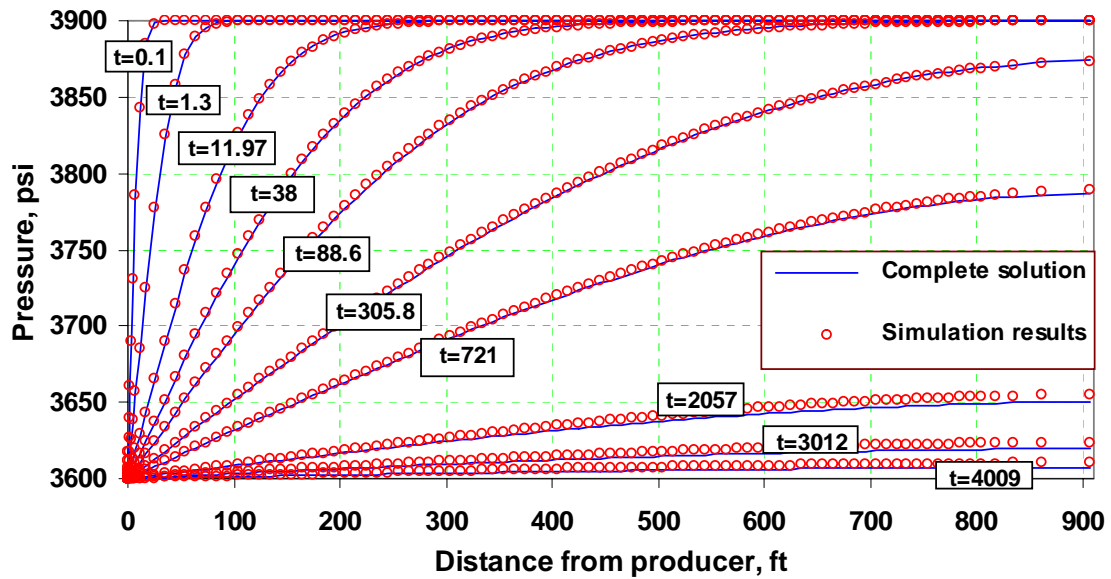


Fig. C.2.2 — Comparison between analytical pressure profile and numerically calculated pressures at any times using a closed, linear reservoir produced at constant wellbore pressure.

APPENDIX D

ARTIFACT WELLBORE STORAGE

The schematic in **Fig. D.1** shows the analytical and numerical type-curves for a 1D-linear reservoir. It also shows that at very early times, the simulation results depart from the analytical solution ($1/2$ -slope). This early-time numerical error is common in tight gas reservoirs that are modeled with wellbore gridblocks that are coarse.

This combination of a coarse well gridblock and a tight gas reservoir causes to have what may be described as a long transient period within the well gridblock while the adjacent gridblocks remain at initial pressure⁴¹.

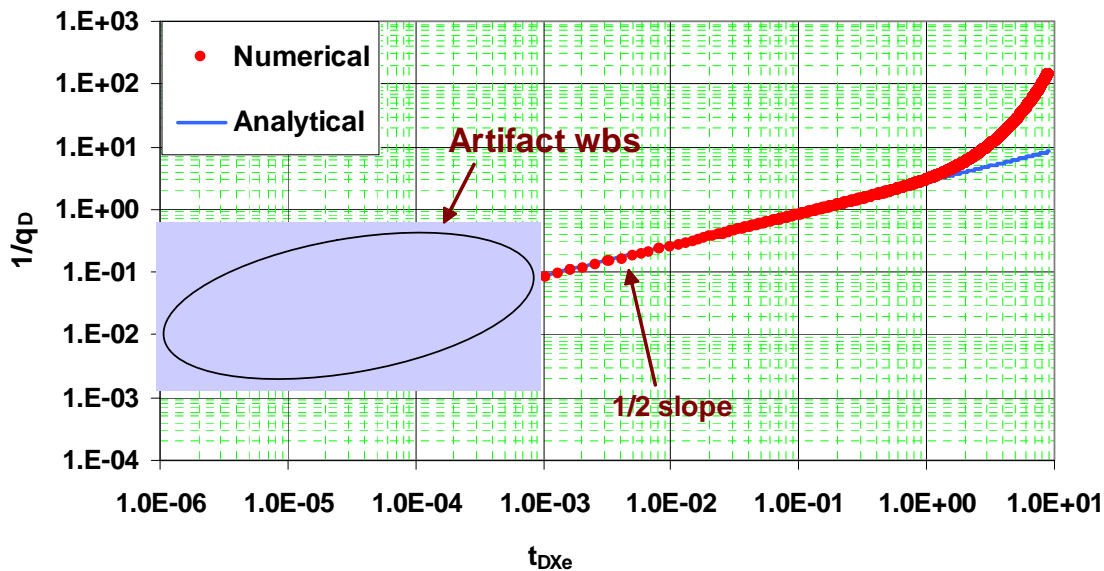


Fig. D.1 — The early-time numerical error in linear flow on a type-curve plot.

Archer and Yildiz⁴² mentioned that this so called *artifact wellbore storage* (early-time unit slope on the pressure derivative only) occurs in low permeability reservoirs and in cases with large grid cells. This numerical error can be removed by using refined grids around wells and making very careful choices of timestep sizes. They presented a new well index formulation that allows well test to be simulated accurately in finite-difference simulators using uniform, relatively coarse grids, without the problem of artifact wellbore storage. They also introduced an equation which gives the time and corresponding radius of investigation at which the artifact wellbore storage was completed.

D.1 Artifact wellbore storage in linear flow at constant rate

In this section reservoir simulation is employed to investigate the effect of artifact wellbore storage for the case of linear flow at constant rate conditions. A linear model was constructed including liquid as the reservoir fluid and by using the *Well Cell method* (See Appendix A) and was run on GASSIM, a 2D one-phase simulator. The linear reservoir is a square with 1,000 ft dimension and was modeled with equally spaced grids 1x11, 1x26, 1x51 and 1x101. Since in each case the first gridblock was used for applying the *Well Cell method*, the effective grids used in the model are 1x10, 1x25, 1x50 and 1x100. The reservoir and fluid properties have been tabulated in **Table D.1**. (See Appendix B for data files). The schematic in **Fig. D.2** compares the analytical and numerical pressure solutions for different grid size for linear flow case. At very early times pressure solutions obtained from the numerical model do not match the analytical solutions represented by $\frac{1}{2}$ -slope. The simulation results approach the analytical solution at later times which depend on the grid size. A model with smaller grids matches the analytical solutions earlier than the one with bigger grids.

Table D.1— Reservoir and liquid properties of the model used in GASSIM

Reservoir Characteristic	Values
Reservoir Half Length (x_e), ft	1,000
Reservoir Half Length (y_e), ft	1,000
Thickness (h), ft	50
Absolute permeability (k_x), md	0.05
Absolute permeability (k_y), md	0.05
Porosity (ϕ), fraction	0.13
Initial Pressure (p_i), psi	3,900
Formation Volume Factor (B_o), RB/STB	1
Viscosity (μ), cp	0.7
Total Compressibility (c_i), psi ⁻¹	0.00001
Production Rate (q_o), STBD	1

Based on the simulation results we developed a relation to estimate t_{min} for linear flow at constant rate at which the *Artifact Wellbore Storage* ends and the pressure solutions are accurate

$$t_{min} = 136.1 \frac{\phi \mu c_i (\Delta x)^2}{k} \dots\dots\dots(D.1)$$

Fig. D.3 shows the simulation results for the case of 1x100 grids. It also shows that the early-time numerical error is represented by the unit slope on derivative plot.

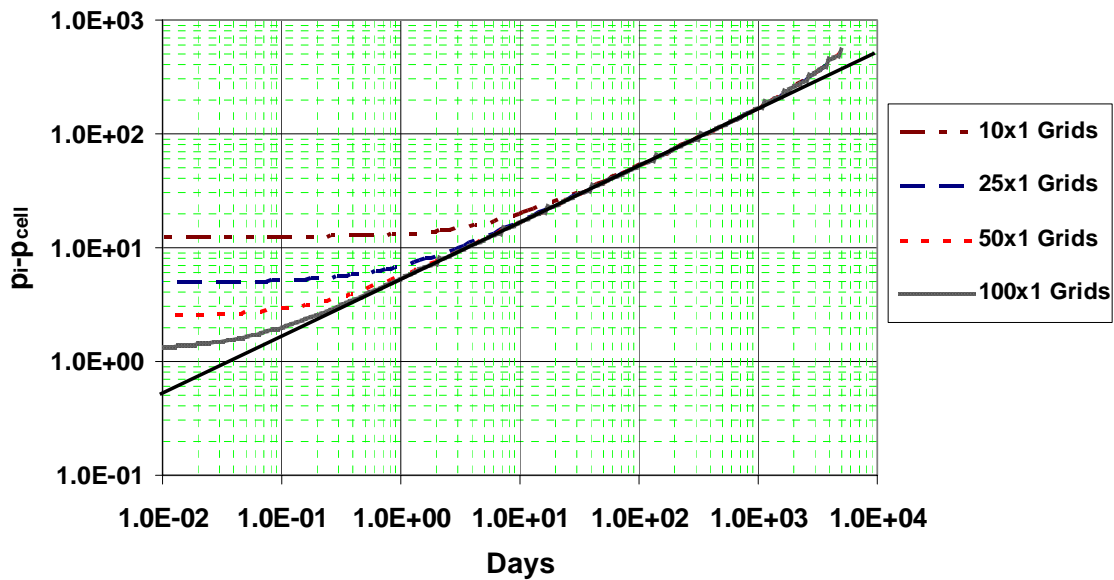


Fig D.2 — Effect of different grid sizes on accuracy of the simulation results for linear flow at constant rate.

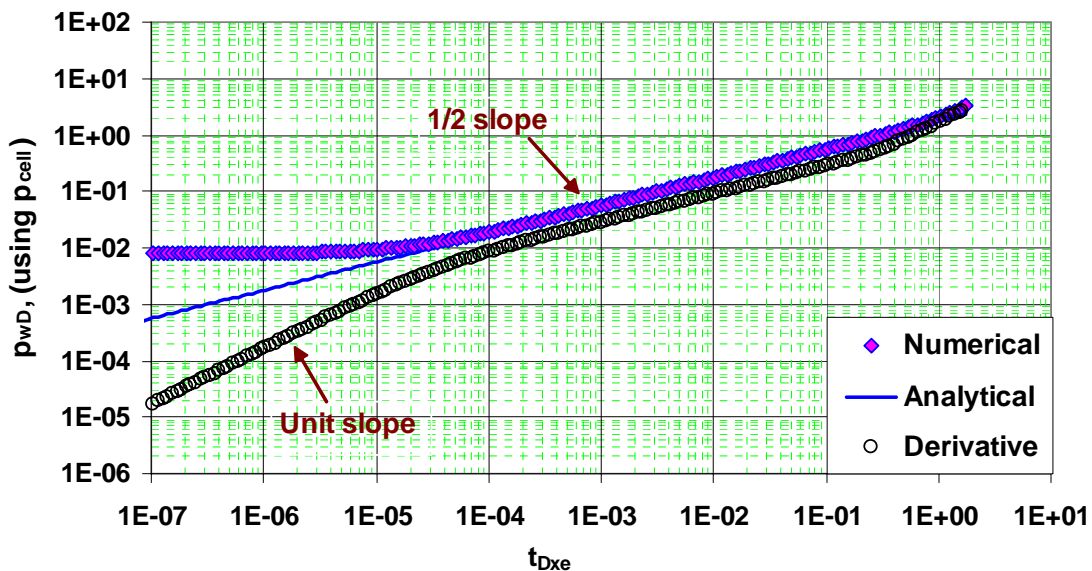


Fig. D.3 — Early-time numerical error for a linear reservoir with 1x100 grids at constant rate.

D.2 Artifact wellbore storage in linear flow at constant wellbore pressure

This section uses the reservoir simulation to investigate the early-time numerical error for linear flow at constant flowing bottomhole pressure. The reservoir and fluid properties are the same as those tabulated in **Table D.1** except that p_{wf} of 3,600 psi was used for the well constraint. In order to see how the grid size affects the accuracy of the simulation results, four different grids of 100x1, 50x1, 25x1 and 10x1 were used.

The schematic in **Fig. D.4** compares the analytical and numerical solution for the case of 1x100 grids. At very early times, solutions obtained from the numerical model do not match the analytical solutions represented by $\frac{1}{2}$ -slope. At point **A**, the numerical solution approaches the analytical solution and at later times again departs from the analytical solutions. So, point **B** is the real time at which the *Artifact Wellbore Storage* ends.

Fig. D.4 also shows that the early-time numerical error has a unit slope on derivative plot.

The schematic in **Fig. D.5** shows that the accuracy of the simulation results depends on the grid size of the model. The model with smaller grids leads us to better accuracy and shorter period of *Artifact Wellbore Storage*.

Based on the simulation results we developed a relation to estimate t_{min} for linear flow at constant p_{wf} at which the *Artifact Wellbore Storage* ends and the pressure solutions are accurate

$$t_{min} = 340.66 \frac{\phi \mu c_t (\Delta x)^2}{k} \dots\dots\dots(D.2)$$

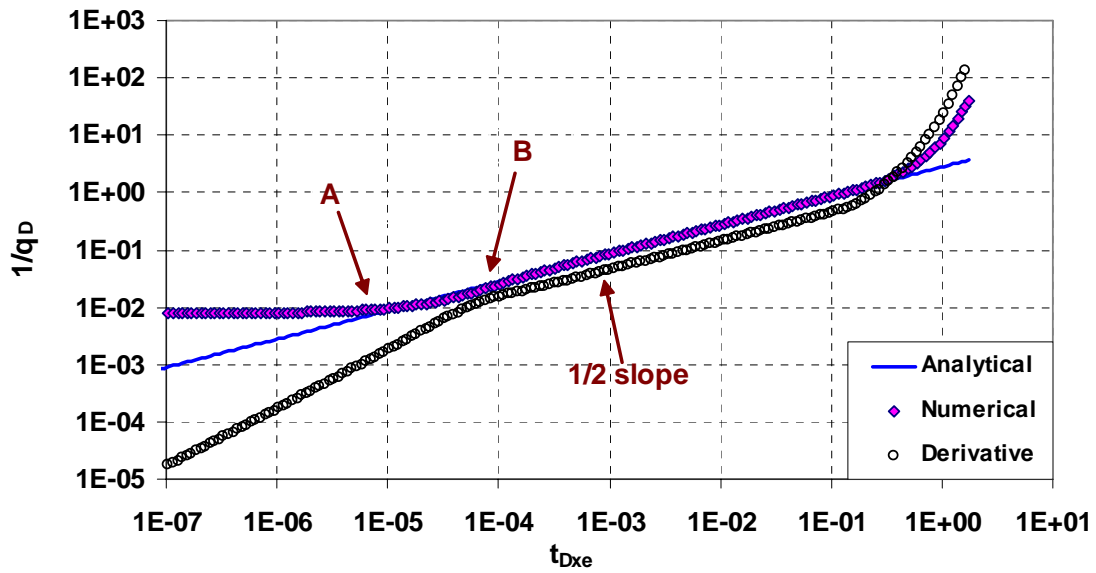


Fig. D.4 — Early-time numerical error for a linear reservoir with 1x100 grids at constant p_{wf} .

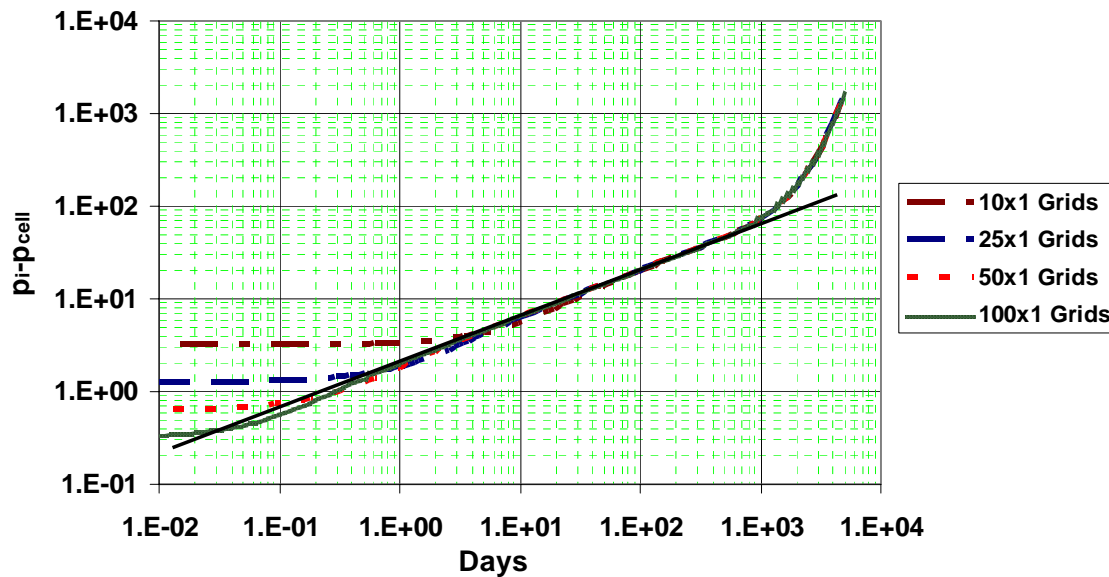


Fig. D.5 — Effect of different grid sizes on accuracy of the simulation results for linear flow at constant p_{wf} .

APPENDIX E

CMG DATA FILES

E.1 CMG data file for SPE3 case study

RESULTS SIMULATOR GEM
RESULTS SECTION INOUT

*TITLE1 'SPE3 modified to specify drawdown'
*INUNIT *FIELD

*INTERRUPT *INTERACTIVE
*RANGECHECK *ON
*XDR *ON
*MAXERROR 20
*WRST *TIME
*WPRN *WELL *TIME
*WPRN *GRID *TIME
*WPRN *ITER *BRIEF
*WSRF *WELL 1
*WSRF *GRID 10
*DIARY *CHANGES
*OUTPRN *WELL *ALL
*OUTPRN *GRID ADS 'C1' SG SO PRES SW

*OUTPRN *RES *ALL
*OUTSRF *WELL *SO 1 1 1
 *SG 1 1 1
 *KRG 1 1 1
 *SO 40 1 1
 *SG 40 1 1
 *KRG 40 1 1

*OUTSRF *GRID PRES SO SG SW RHO0 RHO0 SIG VISO

*OUTSRF *RES *ALL
*DIM *MDDD 3000 **\$ ModelBuilder passed through this Keyword

RESULTS XOFFSET 0.
RESULTS YOFFSET 0.
RESULTS ROTATION 0

GRID VARI 40 1 1
KDIR DOWN
DI IVAR

0.2 0.25 0.3125 0.39063 0.48828 0.61035 0.76294 0.95367 1.19209 1.49012
1.86265 2.32831 2.91038 3.63798 5.336 6.013 6.777 7.639 8.609 9.703 10.935

12.325 13.89 15.655 17.644 19.886 22.412 25.26 28.469 32.086 36.162 40.756
 45.934 51.77 58.347 65.76 74.114 83.53 94.142 123.037

DJ CON 933.381

DK CON 50.
 PAYDEPTH ALL
 40*5025.

**\$ RESULTS PROP NULL Units: Dimensionless
 **\$ RESULTS PROP Minimum Value: 1 Maximum Value: 1
 **\$ 0 = NULL block, 1 = Active block
 NULL CON 1.

**\$ RESULTS PROP PINCHOUTARRAY Units: Dimensionless
 **\$ RESULTS PROP Minimum Value: 1 Maximum Value: 1
 **\$ 0 = PINCHED block, 1 = Active block
 PINCHOUTARRAY CON 1.
 RESULTS SECTION GRID

RESULTS SPEC 'Grid Top'
 RESULTS SPEC SPECNOTCALCVAL 0
 RESULTS SPEC REGION 'All Layers (Whole Grid)'
 RESULTS SPEC REGIONTYPE 0
 RESULTS SPEC LAYERNUMB 0
 RESULTS SPEC PORTYPE 1
 RESULTS SPEC CON 5000
 RESULTS SPEC STOP

RESULTS SPEC 'Grid Thickness'
 RESULTS SPEC SPECNOTCALCVAL 0
 RESULTS SPEC REGION 'Layer 1 - Whole layer'
 RESULTS SPEC REGIONTYPE 1
 RESULTS SPEC LAYERNUMB 1
 RESULTS SPEC PORTYPE 1
 RESULTS SPEC CON 50
 RESULTS SPEC STOP
 RESULTS PINCHOUT-VAL 0.0002 'ft'
 RESULTS SECTION NETPAY
 RESULTS SECTION NETGROSS
 RESULTS SECTION POR

RESULTS SPEC 'Porosity'
 RESULTS SPEC SPECNOTCALCVAL 0
 RESULTS SPEC REGION 'Layer 1 - Whole layer'
 RESULTS SPEC REGIONTYPE 1
 RESULTS SPEC LAYERNUMB 1
 RESULTS SPEC PORTYPE 1
 RESULTS SPEC CON 0.13
 RESULTS SPEC STOP

**\$ RESULTS PROP POR Units: Dimensionless
 **\$ RESULTS PROP Minimum Value: 1E-005 Maximum Value: 0.13
 POR IVAR

1.E-05 39*0.13

RESULTS SECTION PERMS

**\$ RESULTS PROP PERMI Units: md

**\$ RESULTS PROP Minimum Value: 0.15 Maximum Value: 50
PERMI IVAR

50. 39*0.15

**\$ RESULTS PROP PERMJ Units: md

**\$ RESULTS PROP Minimum Value: 0.15 Maximum Value: 50
PERMJ EQUALSI

**\$ RESULTS PROP PERMK Units: md

**\$ RESULTS PROP Minimum Value: 0.015 Maximum Value: 5
PERMK EQUALSI * 0.1

RESULTS SECTION TRANS

RESULTS SECTION FRACS

RESULTS SECTION GRIDNONARRAYS

CPOR MATRIX 4.E-06

PRPOR MATRIX 3900.

RESULTS SECTION VOLMOD

RESULTS SECTION SECTORLEASE

RESULTS SECTION ROCKCOMPACTION

RESULTS SECTION GRIDOTHER

RESULTS SECTION MODEL

*MODEL *PR

*NC 10 10

*COMPNAME 'C1' 'C2' 'C3' 'C4' 'C5'
'C6' 'C7-9' 'C10-11' 'C12-14' 'C15+'

*HCFLAG 0 0 0 0 0
0 0 0 0 0

*TRES 200.

*PCRIT 40.000000 48.200000 42.010000 37.470000 33.310000
29.920000 26.253000 23.184000 19.987000 12.554400

*TCRIT 194.44600 305.43000 369.90000 425.20000 469.60000
507.90000 573.45000 637.79000 685.75000 748.33100

*AC 0.013000 0.098600 0.152400 0.201000 0.253900
0.300700 0.361300 0.450100 0.533900 0.724400

*VCRIT 0.099000 0.148000 0.200000 0.255000 0.311000
0.368000 0.465700 0.569400 0.690100 0.964800

*MW 16.04300 30.07000 44.09700 58.12400 72.15100
86.17800 114.43000 144.83000 177.78000 253.63000

*VSHIFT -0.217010 0.000000 0.000000 0.000000 0.000000
0.000000 0.258450 0.205220 0.164540 0.094711

*BIN

0.0

0.0 0.0

0.0 0.0 0.0

0.0 0.0 0.0 0.0

0.0 0.0 0.0 0.0 0.0

0.0	0.0	0.0	0.0	0.0	0.0
0.0	0.0	0.0	0.0	0.0	0.0
0.0					
0.0	0.0	0.0	0.0	0.0	0.0
0.0	0.0				
0.2466	0.0	0.0	0.0	0.0	0.0
0.0	0.0	0.0			

*PHASEID *GAS
 *PSAT 3500.
 *RHOW 1587.757
 *CW 3.6E-06
 *REFPW 3900.
 *VISW 0.3049

RESULTS SECTION MODELARRAYS

RESULTS SECTION ROCKFLUID

**-----ROCK FLUID-----

*ROCKFLUID

*RPT 1 *DRAINAGE

*SWT

0.160000	0.000000	0.740000	50.000000
0.200000	0.002000	0.680000	32.000000
0.240000	0.010000	0.620000	21.000000
0.280000	0.020000	0.562000	15.500000
0.320000	0.033000	0.505000	12.000000
0.360000	0.049000	0.450000	9.200000
0.400000	0.066000	0.400000	7.000000
0.440000	0.090000	0.348000	5.300000
0.480000	0.119000	0.300000	4.200000
0.520000	0.150000	0.260000	3.400000
0.560000	0.186000	0.222000	2.700000
0.600000	0.227000	0.187000	2.100000
0.640000	0.277000	0.156000	1.700000
0.680000	0.330000	0.126000	1.300000
0.720000	0.390000	0.100000	1.000000
0.760000	0.462000	0.078000	0.700000
0.800000	0.540000	0.058000	0.500000
0.840000	0.620000	0.040000	0.400000
0.880000	0.710000	0.026000	0.300000
0.920000	0.800000	0.013000	0.200000
0.960000	0.900000	0.005000	0.100000
0.995000	1.000000	0.000000	0.000000

*SGT

0.005000	0.000000	0.740000	0.000000
0.040000	0.005000	0.650000	0.000000
0.080000	0.013000	0.513000	0.000000
0.120000	0.026000	0.400000	0.000000
0.160000	0.040000	0.315000	0.000000

0.200000 0.058000 0.250000 0.000000
 0.240000 0.078000 0.196000 0.000000
 0.280000 0.100000 0.150000 0.000000
 0.320000 0.126000 0.112000 0.000000
 0.360000 0.156000 0.082000 0.000000
 0.400000 0.187000 0.060000 0.000000
 0.440000 0.222000 0.040000 0.000000
 0.480000 0.260000 0.024000 0.000000
 0.520000 0.300000 0.012000 0.000000
 0.560000 0.348000 0.005000 0.000000
 0.600000 0.400000 0.000000 0.000000
 0.640000 0.450000 0.000000 0.000000
 0.680000 0.505000 0.000000 0.000000
 0.720000 0.562000 0.000000 0.000000
 0.760000 0.620000 0.000000 0.000000
 0.800000 0.680000 0.000000 0.000000
 0.840000 0.740000 0.000000 0.000000

*KROIL *STONE2 *SWSG

RESULTS SECTION ROCKARRAYS

**\$ RESULTS PROP ADGMAXC 'C1' Units: gmole/lb

**\$ RESULTS PROP Minimum Value: 0.084843 Maximum Value: 0.084843

ADGMAXC 'C1' CON 0.084843

**\$ RESULTS PROP ADGCSTC 'C1' Units: 1/psi

**\$ RESULTS PROP Minimum Value: 0.0008882 Maximum Value: 0.0008882

ADGCSTC 'C1' CON 0.0008882

RESULTS SECTION INIT

**-----INITIAL CONDITION---

*INITIAL

*VERTICAL *BLOCK_CENTER *COMP

*NREGIONS 1

*REFDEPTH 5000.

*REFPRES 3900.

*DWOC 7500.

*ZDEPTH

7500. 0.6793 0.099 0.0591 0.0517 0.0269 0.0181 0.0399 0.0122 0.008 0.0058

*SEPARATOR

815 80

65 80

14.7 60

RESULTS SECTION INITARRAYS

RESULTS SECTION NUMERICAL

**-----NUMERICAL-----

*NUMERICAL

*DTMAX 365.

*DTMIN 1.E-05

*ITERMAX 100

*NORM *PRESS 145.04
 *NORM *GMOLAR 0.15
 *NORM *SATUR 0.15
 *CONVERGE *PRESS 0.514884

RESULTS SECTION NUMARRAYS
 RESULTS SECTION GBKEYWORDS
 RUN

DATE 1986 01 01

DTWELL 5.

AIMWELL WELLNN

*DTMAX 1.

*DTMIN 1.E-05

**\$ RESULTS PROP AIMSET Units: Dimensionless
 **\$ RESULTS PROP Minimum Value: 1 Maximum Value: 1
 AIMSET CON 1.

WELL 1 'PROD'
 CYCLPROD 'PROD'
 OPERATE MIN BHP 1000. CONT

GEOMETRY K 0.25 0.37 1. 1.39
 PERF GEO 'PROD'
 1 1 1. OPEN FLOW-TO 'SURFACE'

DATE 1986 01 02

DATE 1986 01 03

DATE 1986 01 04

.
 .
 .

TIME 3652

TIME 5478

STOP

***** TERMINATE SIMULATION *****

RESULTS SECTION WELLDATA
 RESULTS SECTION PERFS

E.2 CMG data file for Coats case study

RESULTS SIMULATOR GEM
RESULTS SECTION INOUT

*TITLE1 'Linear model with the coats fluid'
*INUNIT *FIELD

*INTERRUPT *INTERACTIVE
*RANGECHECK *ON
*XDR *ON
*MAXERROR 20
*WRST *TIME
*WPRN *WELL *TIME
*WPRN *GRID *TIME
*WPRN *ITER *BRIEF
*WSRF *WELL 1
*WSRF *GRID 10
*DIARY *CHANGES
*OUTPRN *WELL *ALL
*OUTPRN *GRID SG SO PRES SW

*OUTPRN *RES *ALL
*OUTSRF *WELL *SO 1 1 1
 *SG 1 1 1
 *KRO 1 1 1
 *KRG 1 1 1
 *SO 40 1 1
 *SG 40 1 1
 *KRO 40 1 1
 *KRG 40 1 1
 *PAVG

*OUTSRF *GRID PRES SO SG SW RHOO RHOG SIG VISO

*OUTSRF *RES *ALL
*DIM *MDDD 5780 **\$ ModelBuilder passed through this Keyword

*DIM *MDV 180 **\$ ModelBuilder passed through this Keyword
RESULTS XOFFSET 0.
RESULTS YOFFSET 0.
RESULTS ROTATION 0

GRID VARI 40 1 1
KDIR DOWN
DI IVAR

0.2 0.25 0.3125 0.39063 0.48828 0.61035 0.76294 0.95367 1.19209 1.49012
1.86265 2.32831 2.91038 3.63798 5.336 6.013 6.777 7.639 8.609 9.703 10.935
12.325 13.89 15.655 17.644 19.886 22.412 25.26 28.469 32.086 36.162 40.756
45.934 51.77 58.347 65.76 74.114 83.53 94.142 123.037

DJ CON 933.381

DK CON 50.

PAYDEPTH ALL

40*5025.

**\$ RESULTS PROP NULL Units: Dimensionless

**\$ RESULTS PROP Minimum Value: 1 Maximum Value: 1

**\$ 0 = NULL block, 1 = Active block

NULL CON 1.

**\$ RESULTS PROP PINCHOUTARRAY Units: Dimensionless

**\$ RESULTS PROP Minimum Value: 1 Maximum Value: 1

**\$ 0 = PINCHED block, 1 = Active block

PINCHOUTARRAY CON 1.

RESULTS SECTION GRID

RESULTS SPEC 'Grid Top'

RESULTS SPEC SPECNOTCALCVAL 0

RESULTS SPEC REGION 'All Layers (Whole Grid)'

RESULTS SPEC REGIONTYPE 0

RESULTS SPEC LAYERNUMB 0

RESULTS SPEC PORTYPE 1

RESULTS SPEC CON 5000

RESULTS SPEC STOP

RESULTS SPEC 'Grid Thickness'

RESULTS SPEC SPECNOTCALCVAL 0

RESULTS SPEC REGION 'Layer 1 - Whole layer'

RESULTS SPEC REGIONTYPE 1

RESULTS SPEC LAYERNUMB 1

RESULTS SPEC PORTYPE 1

RESULTS SPEC CON 50

RESULTS SPEC STOP

RESULTS SECTION NETPAY

RESULTS SECTION NETGROSS

RESULTS SECTION POR

RESULTS SPEC 'Porosity'

RESULTS SPEC SPECNOTCALCVAL 0

RESULTS SPEC REGION 'Layer 1 - Whole layer'

RESULTS SPEC REGIONTYPE 1

RESULTS SPEC LAYERNUMB 1

RESULTS SPEC PORTYPE 1

RESULTS SPEC CON 0.13

RESULTS SPEC STOP

**\$ RESULTS PROP POR Units: Dimensionless

**\$ RESULTS PROP Minimum Value: 1E-005 Maximum Value: 0.13

POR IVAR

1.E-05 39*0.13

RESULTS SECTION PERMS

**\$ RESULTS PROP PERMI Units: md

**\$ RESULTS PROP Minimum Value: 0.15 Maximum Value: 50
 PERMI IVAR
 50.39*0.15

**\$ RESULTS PROP PERMJ Units: md
 **\$ RESULTS PROP Minimum Value: 0.15 Maximum Value: 50
 PERMJ EQUALSI

**\$ RESULTS PROP PERMK Units: md
 **\$ RESULTS PROP Minimum Value: 0.015 Maximum Value: 5
 PERMK EQUALSI * 0.1
 RESULTS SECTION TRANS
 RESULTS SECTION FRACS
 RESULTS SECTION GRIDNONARRAYS
 CPOR MATRIX 4.E-06
 PRPOR MATRIX 3900.

RESULTS SECTION VOLMOD
 RESULTS SECTION SECTORLEASE

RESULTS SECTION ROCKCOMPACTION
 RESULTS SECTION GRIDOTHER
 RESULTS SECTION MODEL

*MODEL *PR
 *NC 7 7
 *COMPNAME 'N2 toC1' 'CO2toC2' 'C3' 'IC4' 'IC5'
 'FC6' 'C07+'
 *HCFLAG 0 0 0 0 0
 0 0
 *VISCOR *HZYT
 *VISCOEFF 0.1023
 0.023364
 0.058533
 -0.040758
 0.0093324
 *MIXVC 1
 *TRES 335.
 *PCRIT 44.144387 51.146860 41.900000 36.000000 33.400000
 32.460000 24.332452
 *TCRIT 183.18372 305.23612 369.80000 408.10000 460.40000
 507.50000 645.02130
 *AC 0.011529 0.118905 0.152000 0.176000 0.227000
 0.275040 0.465523
 *VCRIT 0.097937 0.138552 0.203000 0.263000 0.306000
 0.344000 0.545848
 *MW 17.36317 32.36457 44.09700 58.12400 72.15100
 86.00000 148.00000
 *PCHOR 73.02957 103.06191 150.30000 181.50000 225.00000
 250.10000 418.45120
 *SG 0.337820 0.407517 0.507000 0.563000 0.625000
 0.690000 0.804400
 *TB -265.41940 -124.54780 -43.69000 10.67000 82.13000

```

146.93000 365.83300
*VISVC 0.097952 0.139111 0.203000 0.263000 0.306000
0.344000 0.545848
*VSHIFT 0.000000 0.000000 0.000000 0.000000 0.000000
0.000000 0.000000
*OMEGA .535635310 .457235530 .457235530 .457235530 .457235530
.457235530 .470494520
*OMEGB .093360000 .077796074 .077796074 .077796074 .077796074
.077796074 .079301035
*PVC3 1.2
*BIN
0.0020028
0.008794 0.002427
0.0160603 0.0068098 0.0011166
0.0212738 0.0103789 0.0028007 0.0003821
0.0257777 0.0136371 0.0046198 0.0012003 0.0002283
0.0473763 0.0305853 0.0161021 0.0088252 0.0055585 0.003543
*PHASEID *DEN
*CW 3.6E-06
*REFPW 3900.
*VISW 0.3049
*ENTHCOEF
-5.0416143E+00 5.3051511E-01 -2.5336856E-04 3.7274761E-07 -1.3592071E-10
1.7419063E-14
1.5153820E-01 2.4697290E-01 -1.9238674E-05 2.5696370E-07 -1.1553971E-10
1.6744980E-14
-1.2230100E+00 1.7973300E-01 6.6458000E-05 2.5099800E-07 -1.2474610E-10
1.8935090E-14
1.3286600E+01 3.6637000E-02 3.4963100E-04 5.3610000E-09 -2.9811100E-11
5.4866200E-15
2.7623420E+01 -3.1504000E-02 4.6988400E-04 -9.8283000E-08 1.0298500E-11
-2.9485000E-16
0.0000000E+00 -1.6543460E-02 4.1169070E-04 -5.7742760E-08 0.0000000E+00
0.0000000E+00
0.0000000E+00 -5.2396317E-02 4.2731831E-04 -6.5494995E-08 0.0000000E+00
0.0000000E+00 **$ ModelBuilder passed through this Keyword

```

RESULTS SECTION MODELARRAYS

RESULTS SECTION ROCKFLUID

```
**-----ROCK FLUID-----
```

*ROCKFLUID

*RPT 1 *DRAINAGE

*SWT

```

0.160000 0.000000 0.740000 50.000000
0.200000 0.002000 0.680000 32.000000
0.240000 0.010000 0.620000 21.000000
0.280000 0.020000 0.562000 15.500000
0.320000 0.033000 0.505000 12.000000

```


0.360000 0.049000 0.450000 9.200000
 0.400000 0.066000 0.400000 7.000000
 0.440000 0.090000 0.348000 5.300000
 0.480000 0.119000 0.300000 4.200000
 0.520000 0.150000 0.260000 3.400000
 0.560000 0.186000 0.222000 2.700000
 0.600000 0.227000 0.187000 2.100000
 0.640000 0.277000 0.156000 1.700000
 0.680000 0.330000 0.126000 1.300000
 0.720000 0.390000 0.100000 1.000000
 0.760000 0.462000 0.078000 0.700000
 0.800000 0.540000 0.058000 0.500000
 0.840000 0.620000 0.040000 0.400000
 0.880000 0.710000 0.026000 0.300000
 0.920000 0.800000 0.013000 0.200000
 0.960000 0.900000 0.005000 0.100000
 0.995000 1.000000 0.000000 0.000000

*SGT

0.005000 0.000000 0.740000 0.000000
 0.040000 0.005000 0.650000 0.000000
 0.080000 0.013000 0.513000 0.000000
 0.120000 0.026000 0.400000 0.000000
 0.160000 0.040000 0.315000 0.000000
 0.200000 0.058000 0.250000 0.000000
 0.240000 0.078000 0.196000 0.000000
 0.280000 0.100000 0.150000 0.000000
 0.320000 0.126000 0.112000 0.000000
 0.360000 0.156000 0.082000 0.000000
 0.400000 0.187000 0.060000 0.000000
 0.440000 0.222000 0.040000 0.000000
 0.480000 0.260000 0.024000 0.000000
 0.520000 0.300000 0.012000 0.000000
 0.560000 0.348000 0.005000 0.000000
 0.600000 0.400000 0.000000 0.000000
 0.640000 0.450000 0.000000 0.000000
 0.680000 0.505000 0.000000 0.000000
 0.720000 0.562000 0.000000 0.000000
 0.760000 0.620000 0.000000 0.000000
 0.800000 0.680000 0.000000 0.000000
 0.840000 0.740000 0.000000 0.000000

*KROIL *STONE2 *SWSG

RESULTS SECTION ROCKARRAYS

RESULTS SECTION INIT

**-----INITIAL CONDITION---

*INITIAL

*VERTICAL *BLOCK_CENTER *COMP

*NREGIONS 1

*REFDEPTH 5000.

*REFPRES 3900.

*DWOC 7500.
 *CDEPTH 5000.
 *ZDEPTH
 7500. 0.5141 0.1373 0.0759 0.0638 0.0431 0.0592 0.1066
 *SEPARATOR
 624.7 100
 94.7 80
 14.7 75

RESULTS SECTION INITARRAYS

RESULTS SECTION NUMERICAL

**-----NUMERICAL-----

*NUMERICAL

*DTMAX 365.

*DTMIN 0.01

*ITERMAX 200

*NORM *PRESS 145.04

*NORM *GMOLAR 0.15

*NORM *SATUR 0.15

*CONVERGE *PRESS 0.514884

RESULTS SECTION NUMARRAYS

RESULTS SECTION GBKEYWORDS

RUN

DATE 1986 01 01

DTWELL 5.

AIMWELL WELLNN

*DTMAX 1.

*DTMIN 1.E-05

**\$ RESULTS PROP AIMSET Units: Dimensionless

**\$ RESULTS PROP Minimum Value: 1 Maximum Value: 1

AIMSET CON 1.

WELL 1 'PROD'

CYCLPROD 'PROD'

OPERATE MIN BHP 1000. CONT

GEOMETRY K 0.25 0.37 1. 1.39

PERF GEO 'PROD'

1 1 1 1. OPEN FLOW-TO 'SURFACE'

DATE 1986 01 02

DATE 1986 01 03

DATE 1986 01 04

.
.
.

TIME 3652

TIME 5478

TIME 8000

STOP

***** TERMINATE SIMULATION *****

RESULTS SECTION WELLDATA

RESULTS SECTION PERFS

E.3 CMG data file for 2-D case study ($x_e/x_f=2$)

RESULTS SIMULATOR GEM

RESULTS SECTION INOUT

*TITLE1 'SPE3 modified to specify drawdown'

*INUNIT *FIELD

*INTERRUPT *INTERACTIVE

*RANGECHECK *ON

*XDR *ON

*MAXERROR 20

*WRST *TIME

*WPRN *WELL *TIME

*WPRN *GRID *TIME

*WPRN *ITER *BRIEF

*WSRF *WELL 1

*WSRF *GRID 10

*DIARY *CHANGES

*OUTPRN *WELL *ALL

*OUTPRN *GRID ADS 'C1' SG SO PRES SW

*OUTPRN *RES *ALL

*OUTSRF *GRID PRES SO SG SW RHO0 RHO1 SIG VISO

*OUTSRF *RES *ALL

*DIM *MDDD 3000 **\$ ModelBuilder passed through this Keyword

RESULTS XOFFSET 0.

RESULTS YOFFSET 0.

RESULTS ROTATION 0

RESULTS AXES-DIRECTIONS 1. -1. 1.

GRID VARI 20 11 1

KDIR DOWN

DI IVAR

11*44.4467 7*50. 55. 61.6905

DJ JVAR

10. 1. 2. 4. 8. 16. 32. 64. 128. 256. 417.381

DK CON 200.

DTOP

220*5000.

**\$ RESULTS PROP NULL Units: Dimensionless

**\$ RESULTS PROP Minimum Value: 1 Maximum Value: 1

**\$ 0 = NULL block, 1 = Active block

NULL CON 1.

**\$ RESULTS PROP PINCHOUTARRAY Units: Dimensionless

**\$ RESULTS PROP Minimum Value: 1 Maximum Value: 1

**\$ 0 = PINCHED block, 1 = Active block

PINCHOUTARRAY CON 1.

RESULTS SECTION GRID

RESULTS SPEC 'Grid Top'

RESULTS SPEC SPECNOTCALCVAL 0

RESULTS SPEC REGION 'Layer 1 - Whole layer'

RESULTS SPEC REGIONTYPE 1

RESULTS SPEC LAYERNUMB 1

RESULTS SPEC PORTYPE 1

RESULTS SPEC CON 5000

RESULTS SPEC STOP

RESULTS SPEC 'Grid Thickness'

RESULTS SPEC SPECNOTCALCVAL 0

RESULTS SPEC REGION 'Layer 1 - Whole layer'

RESULTS SPEC REGIONTYPE 1

RESULTS SPEC LAYERNUMB 1

RESULTS SPEC PORTYPE 1

RESULTS SPEC CON 200

RESULTS SPEC STOP

RESULTS SECTION NETPAY

RESULTS SECTION NETGROSS

RESULTS SECTION POR

RESULTS SPEC 'Porosity'

RESULTS SPEC SPECNOTCALCVAL 0

RESULTS SPEC REGION 'All Layers (Whole Grid)'

RESULTS SPEC REGIONTYPE 0

RESULTS SPEC LAYERNUMB 0

RESULTS SPEC PORTYPE 1

RESULTS SPEC CON 0.13

RESULTS SPEC STOP

**\$ RESULTS PROP POR Units: Dimensionless

**\$ RESULTS PROP Minimum Value: 0.0325 Maximum Value: 0.13

POR CON 0.13

MOD 1:1 1:1 1:1 / 4

2:20 1:1 1:1 / 2

1:1 2:11 1:1 / 2

RESULTS SECTION PERMS

RESULTS SPEC 'Permeability K'

RESULTS SPEC SPECNOTCALCVAL 0

RESULTS SPEC REGION 'All Layers (Whole Grid)'

RESULTS SPEC REGIONTYPE 0

RESULTS SPEC LAYERNUMB 0

RESULTS SPEC PORTYPE 1

RESULTS SPEC CON 0.003

RESULTS SPEC STOP

RESULTS SPEC 'Permeability I'

RESULTS SPEC SPECNOTCALCVAL 0

RESULTS SPEC REGION 'All Layers (Whole Grid)'

RESULTS SPEC REGIONTYPE 0

RESULTS SPEC LAYERNUMB 0

RESULTS SPEC PORTYPE 1

RESULTS SPEC CON 0.15

RESULTS SPEC STOP

RESULTS SPEC 'Permeability J'

RESULTS SPEC SPECNOTCALCVAL 0

RESULTS SPEC REGION 'All Layers (Whole Grid)'

RESULTS SPEC REGIONTYPE 0

RESULTS SPEC LAYERNUMB 0

RESULTS SPEC PORTYPE 1

RESULTS SPEC CON 0.15

RESULTS SPEC STOP

**\$ RESULTS PROP PERMI Units: md

**\$ RESULTS PROP Minimum Value: 0.015 Maximum Value: 50

PERMI CON 0.03

MOD 1:11 1:1 1:1 = 50

12:20 1:1 1:1 / 2

**\$ RESULTS PROP PERMJ Units: md

**\$ RESULTS PROP Minimum Value: 0.015 Maximum Value: 100

PERMJ CON 0.03

MOD 1:1 1:1 1:1 = 50

2:11 1:1 1:1 = 100

1:1 2:11 1:1 / 2

**\$ RESULTS PROP PERMK Units: md

**\$ RESULTS PROP Minimum Value: 0.003 Maximum Value: 0.003

PERMK CON 0.003

RESULTS SECTION TRANS

RESULTS SECTION FRACS

RESULTS SECTION GRIDNONARRAYS

CPOR MATRIX 4.E-06

PRPOR MATRIX 3900.

RESULTS SECTION VOLMOD
RESULTS SECTION SECTORLEASE

RESULTS SECTION ROCKCOMPACTION
RESULTS SECTION GRIDOTHER
RESULTS SECTION MODEL

```

*MODEL      *PR
*NC          10 10
*COMPNAME   'C1'  'C2'  'C3'  'C4'  'C5'
            'C6'  'C7-9' 'C10-11' 'C12-14' 'C15+'
*HCFLAG     0    0    0    0    0
            0    0    0    0    0
*TRES       200.
*PCRIT      40.000000 48.200000 42.010000 37.470000 33.310000
            29.920000 26.253000 23.184000 19.987000 12.554400
*TCRIT      194.44600 305.43000 369.90000 425.20000 469.60000
            507.90000 573.45000 637.79000 685.75000 748.33100
*AC         0.013000 0.098600 0.152400 0.201000 0.253900
            0.300700 0.361300 0.450100 0.533900 0.724400
*VCRIT      0.099000 0.148000 0.200000 0.255000 0.311000
            0.368000 0.465700 0.569400 0.690100 0.964800
*MW         16.04300 30.07000 44.09700 58.12400 72.15100
            86.17800 114.43000 144.83000 177.78000 253.63000
*VSHIFT     -0.217010 0.000000 0.000000 0.000000 0.000000
            0.000000 0.258450 0.205220 0.164540 0.094711
*BIN
  0.0
  0.0  0.0
  0.0  0.0  0.0
  0.0  0.0  0.0  0.0
  0.0  0.0  0.0  0.0  0.0
  0.0  0.0  0.0  0.0  0.0  0.0
  0.0
  0.0  0.0  0.0  0.0  0.0  0.0
  0.0  0.0
  0.2466  0.0  0.0  0.0  0.0  0.0
  0.0  0.0  0.0
*PHASEID    *GAS
*PSAT       3500.
*RHOW       1587.757
*CW         3.6E-06
*REFPW      3900.
*VISW       0.3049

```

RESULTS SECTION MODELARRAYS
RESULTS SECTION ROCKFLUID

```

**-----ROCK FLUID-----
*ROCKFLUID
*RPT 1 *DRAINAGE
*SWT

```

0.160000 0.000000 0.740000 50.000000
 0.200000 0.002000 0.680000 32.000000
 0.240000 0.010000 0.620000 21.000000
 0.280000 0.020000 0.562000 15.500000
 0.320000 0.033000 0.505000 12.000000
 0.360000 0.049000 0.450000 9.200000
 0.400000 0.066000 0.400000 7.000000
 0.440000 0.090000 0.348000 5.300000
 0.480000 0.119000 0.300000 4.200000
 0.520000 0.150000 0.260000 3.400000
 0.560000 0.186000 0.222000 2.700000
 0.600000 0.227000 0.187000 2.100000
 0.640000 0.277000 0.156000 1.700000
 0.680000 0.330000 0.126000 1.300000
 0.720000 0.390000 0.100000 1.000000
 0.760000 0.462000 0.078000 0.700000
 0.800000 0.540000 0.058000 0.500000
 0.840000 0.620000 0.040000 0.400000
 0.880000 0.710000 0.026000 0.300000
 0.920000 0.800000 0.013000 0.200000
 0.960000 0.900000 0.005000 0.100000
 0.995000 1.000000 0.000000 0.000000

*SGT

0.005000 0.000000 0.740000 0.000000
 0.040000 0.005000 0.650000 0.000000
 0.080000 0.013000 0.513000 0.000000
 0.120000 0.026000 0.400000 0.000000
 0.160000 0.040000 0.315000 0.000000
 0.200000 0.058000 0.250000 0.000000
 0.240000 0.078000 0.196000 0.000000
 0.280000 0.100000 0.150000 0.000000
 0.320000 0.126000 0.112000 0.000000
 0.360000 0.156000 0.082000 0.000000
 0.400000 0.187000 0.060000 0.000000
 0.440000 0.222000 0.040000 0.000000
 0.480000 0.260000 0.024000 0.000000
 0.520000 0.300000 0.012000 0.000000
 0.560000 0.348000 0.005000 0.000000
 0.600000 0.400000 0.000000 0.000000
 0.640000 0.450000 0.000000 0.000000
 0.680000 0.505000 0.000000 0.000000
 0.720000 0.562000 0.000000 0.000000
 0.760000 0.620000 0.000000 0.000000
 0.800000 0.680000 0.000000 0.000000
 0.840000 0.740000 0.000000 0.000000

*KROIL *STONE2 *SWSG
 RESULTS SECTION ROCKARRAYS
 RESULTS SECTION INIT

**-----INITIAL CONDITION---

*INITIAL

*VERTICAL *BLOCK_CENTER *COMP

```

*NREGIONS 1
*REFDEPTH 5000.
*REFPRES 3900.
*DWOC 7500.
*ZDEPTH
      7500. 0.6793 0.099 0.0591 0.0517 0.0269 0.0181 0.0399 0.0122 0.008 0.0058
*SEPARATOR
  815      80
   65      80
  14.7     60

```

```

RESULTS SECTION INITARRAYS
RESULTS SECTION NUMERICAL

```

```

**-----NUMERICAL-----
*NUMERICAL
*DTMAX 365.
*DTMIN 1.E-05
*ITERMAX 100
*NORM *PRESS 145.04
*NORM *GMOLAR 0.15
*NORM *SATUR 0.15
*CONVERGE *PRESS 0.514884

```

```

RESULTS SECTION NUMARRAYS
RESULTS SECTION GBKEYWORDS
RUN
DATE 1986 01 01

```

```
DTWELL 5.
```

```
AIMWELL WELLNN
```

```
*DTMAX 1.
```

```
*DTMIN 1.E-05
```

```

WELL 1 'PROD'
PRODUCER 'PROD'
OPERATE MIN BHP 1000. CONT

```

```

GEOMETRY K 0.2083333 0.37 1. 0.
PERF GEO 'PROD'
      1 1 1. OPEN FLOW-TO 'SURFACE'

```

```
OPEN 'PROD'
```

```

DATE 1986 01 02
DATE 1986 01 03

```

```

.
.
.

```


TIME 3652

TIME 5478

STOP

***** TERMINATE SIMULATION *****

RESULTS SECTION WELLDATA

RESULTS SECTION PERFS

VITA

Name: REZA ROSTAMI RAVARI

Permanent Address: No. 177, Alley No. 7, Shahid Rajaei St.
Kerman, Iran, 76146-43664

E-mail: rostamir1000@yahoo.com

Education: M.S., Petroleum Engineering,
Texas A&M University
College Station, August 2004

B.S., Chemical Engineering
Sharif University of Technology
Tehran, Iran, September 2000